# Convection Induced Temperature Change in GATE

by
Pamela G. Grub

P.I. William M. Gray

Department of Atmospheric Science
Colorado State University
Fort Collins, Colorado

NSF ATM 78-01640
NSF (RANN) ENV 77-10229

Colorado State University

Department of Atmospheric Science

Paper No. 305

# CONVECTION INDUCED TEMPERATURE CHANGE IN GATE

By

Pamela G. Grube

Preparation of this report
has been financially supported by
the National Science Foundation
Grant No. ATM 78-01640
Grant No. ENV 77-10229

Department of Atmospheric Science
Colorado State University
Fort Collins, Colorado

February, 1979

Atmospheric Science No. 305

ABSTRACT

An analysis is made of GATE B-array short time resolution (3-6 hours) upper tropospheric temperature and moisture changes. Convective patterns are examined to determine how deep-cumulus clouds are related to such upper level changes. Thermodynamic characteristics of a raining area are compared to those of a non-raining area. Information is obtained from the B-array rawinsonde, rain gauge, and weather radar products.

It appears that tropospheric warming ($\partial T/\partial t$) at individual locations is not directly related to the magnitude of condensation energy release. It is dependent on the magnitude of the cloud's return flow subsidence which occurs adjacent or between the convective elements or at large distances from the convection. Average tropospheric temperature changes in convective regions are quite small. The diurnal variation in temperature found in both the convective and non-convective regimes dominates meso-scale averaged temperature changes. When vertically integrated, the direct effect of an individual convective element is to slightly cool the local environment where the cloud existed. It is only in upper levels (principally 500-200 mb) that convection has an overall warming effect. A compositing of upper level GATE warming events shows these locations to be partially ringed by convective elements.

The final two chapters of this report (by W. Fingerhut and W. Gray) further discuss the magnitude and time-scales of cumulus warming events and how cumulus warming may be related to tropical cyclone genesis.

TABLE OF CONTENTS


| | | Page |
|---|---|---|
| 1. | INTRODUCTION | 1 |
| 2. | DATA AND ANALYSIS METHODS | 4 |
| | 2.1 Data Sources | 4 |
| | 2.2 Data Characteristics | 4 |
| | 2.3 Computation of Parameter Deviations | 10 |
| | 2.4 Compositing Techniques | 10 |
| 3. | TEMPERATURE AND MOISTURE DIFFERENCES BETWEEN RAINING AND NON-RAINING ENVIRONMENTS | 11 |
| | 3.1 Determination of Cases | 11 |
| | 3.2 Six-hourly Time Changes | 14 |
| | 3.3 Comparison of Rain and No Rain Temperature Profiles | 21 |
| | 3.4 Rain Minus No Rain Thickness Calculations | 23 |
| | 3.5 Comparison of Rain and No Rain Vertical Motion Profiles | 26 |
| | 3.6 Net Kinetic Energy Generation in the Rain Environment | 28 |
| 4. | RAWINSONDE ANALYSIS OF UPPER TROPOSPHERIC TEMPERATURE ANOMALIES | 35 |
| | 4.1 Determination of Warming, Cooling and Rainfall Cases. | 36 |
| | 4.2 Characteristics of Warming, Cooling and Rainfall Cases. | 47 |
| | 4.3 Rawinsonde Composites | 57 |
| 5. | AREAL PORTRAYAL OF CONVECTIVE EVENTS AS DETERMINED BY RADAR COMPOSITES. | 67 |
| 6. | CONCLUSIONS | 81 |
| 7. | NUMERICAL MODELING EXPERIMENTS | 85 |
| 8. | GENERAL DISCUSSION OF CUMULUS HEATING | 94 |
| ACKNOWLEDGEMENTS | | 110 |
| BIBLIOGRAPHY | | 111 |
| APPENDIX A - UPPER-AIR DATA: DESCRIPTIONS AND COMPARISONS | | 115 |
| APPENDIX B - AREA COVERAGE OF SATELLITE DATA COLLECTED IN SUPPORT OF GATE | | 125 |
| APPENDIX C - MASS-BALANCING OF WIND DATA | | 127 |

# 1. INTRODUCTION

The GATE experiment produced rawinsonde and other data sets of time and space scale resolution heretofore unrivalled. The main purpose of such fine resolution was to resolve the internal structure of tropical cloud clusters and observe how they affect the circulation in their immediate environment. Another aim was to determine how cumulus convection acts as an energy transformation mechanism in the tropical atmosphere so that mathematical models of the tropical atmosphere can be realistically formulated. This study was conducted as a step toward achieving such understanding. The small time and space scale resolution data of the B-array has been used to examine how cumulus clouds alter the sensible temperature of the tropical atmosphere and balance the radiational cooling which is continually occurring.

This study involves the analysis of two sets of data stratifications. The first set consists of a comparison of raining environments with non-raining environments. It is shown that temperature changes occurring on the B-scale are dominated by a diurnal temperature variation. The second set is based on individual soundings which measured large upper level temperature changes in excess of the mean diurnal temperature changes. These warming and cooling events occur over a time interval less than 3-6 hours. Rawinsonde, rain gauge, radar and satellite data have all been combined in the analysis. The primary goal of the study has been to determine how cumulus convection acts to alter the sensible and latent energy gains and losses in the tropical atmosphere.

The troposphere is radiatively cooling at a daily rate of about $1\text{-}2^{o}C$. This cooling is roughly balanced by convective processes. Yet

how do clouds actually warm the troposphere or cause up-moist and compensating down-dry motions? In the past a number of convective models have been formulated on the premise that cumulus cloud updrafts are warmer than their surroundings, and subsequently warm the environment by direct diffusion of sensible heat from their sides. Additional evidence is gathered to show that this general view is invalid. It has also been hypothesized by some modellers that sensible temperature gain can be directly related to low level moisture convergence or upward vertical velocity. This concept appears to be unsubstantiated in the data examined here. The results of this study indicate that cumuli warm at upper levels through mechanically forced subsidence. It will be shown that the vertically integrated local effect (< 50 km) of raining convection is actually one of slightly cooling the immediate environment. Cumulus convection results in a large amount of low level downdraft and evaporative cooling, which more than offsets any direct diffusional warming by the clouds.

Upper level warming and cooling occur frequently, and often on the same day within the same cluster environments. Although both events are normally associated with some degree of convection, individual warming soundings occur adjacent to the convectively active regions, and not within them as the cooling soundings do.

The hypothesis for indirect cloud heating asserts that latent heat released by cumulus convection is locally converted to potential energy gain, with the resulting subsidence warming occurring at some distance from the cumulus activity. The results of this study indicate that in certain instances a portion of the cloud warming from active convection may occur at a radius as small as $1^{o}$ latitude or less. This happens

with an appropriate orientation of convective elements; that is, one in which the meso-scale cloud orientation and upper flow environment act to inhibit outflow from the Cb elements and cause an enhancement of local subsidence. This convective warming process appears to be substantiated by the radar composite echo patterns associated with the upper level warming events, which show deep convection partially ringing a clear area.

## 2. DATA AND ANALYSIS METHODS

### 2.1 Data Sources

The primary data sources utilized in this study were the B-scale rawinsonde network (Fig. 1), and hourly precipitation data derived from digital radar reflectivities at the Center for Experiment Design and Data Analysis (CEDDA). Also used were shipboard rain gauge measurements, and navigated digital satellite imagery from the Synchronous Meteorological Satellite (SMS-1).

### 2.2 Data Characteristics

Rawinsonde Network. The GATE data set has better temporal and spatial resolution than that of any previous tropical experiment. A map of the GATE A/B and B-scales as they looked during Phase I (Julian Days 179-197) is shown in Fig. 1. The stationing of ships for the other two phases (Julian Days 209-228, and Julian Days 242-262, respectively) was similar, except that during Phase III there were a few additional ships added to create a C-scale with finer spatial resolution than the A/B and B-scales. The GATE network was designed such that the B-scale lies in the path of cloud clusters tracking their way southwestward from continental Africa.

For the purpose of analysis, each day is divided into 8 time segments, centered on the nominal rawinsonde launch times of 00Z, 03Z, 06Z, 09Z, 12Z, 15Z, 18Z and 21Z. A flight launched within the window -1 to +2 hours of nominal launch time is considered to belong to that segment. Rawinsondes were typically launched during GATE at 6-hourly intervals, with three hourly soundings during intensive observational periods.

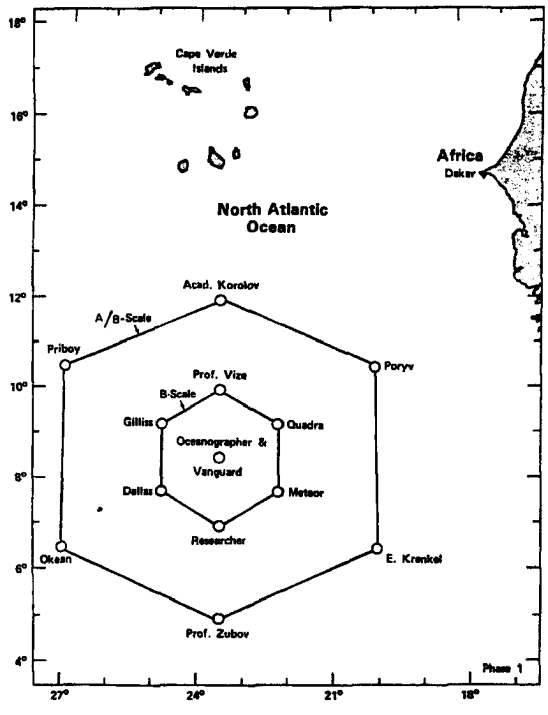


Fig. 1. GATE A/B and B-scale arrays as they looked during Phase I.

Magnetic tapes containing the GATE Processed and Validated Rawinsonde Data and the accompanying set of Change Records were used as they were received from the Convection Subprogram Data Center (CSDC) of CEDDA. The Change Records are suggestions for deletion or replacement of data contained on the original data tapes. To eliminate the use of unrealistic and spurious data values all these changes were implemented.

There is an element of internal inconsistency within the GATE rawinsonde network, in that VIZ-sondes were used by the United States, Canada, France, and Germany, whereas RKZ-sondes were used by the Soviet Union. Noted differences in the data reported by these different systems have been documented (NOAA Technical Report EDS 20; Reeves and Esbensen, 1977; Esbensen and Ooyama, 1977; Reeves, 1977; and Reynolds, 1977), and are described in Appendix A.

Radar Coverage. The eight ships equipped with weather radars during GATE were the Oceanographer, Researcher, Gilliss, Quadra, Meteor, Prof. Vize, Acad. Korolov and Prof. Zubov. National affiliation and other information regarding these radars can be found in Table 1. The displays from the four C-band radars, aboard the Oceanographer, Researcher, Gilliss and Quadra can be positioned to within an accuracy of 3 minutes of latitude ($\sim$ 7.8 km or 4.2 n mi), and although the four X-band radars aboard the Meteor, Prof. Vize, Prof. Zubov and Acad. Korolov cannot be positioned as accurately as the C-band radars, the errors still do not exceed 6 minutes of latitude ($\sim$ 15.7 km or 8.5 n mi).

In this study, only the C-band digital reflectivity data was used in the form of estimates derived by the CSDC, and placed in 4 x 4 km data bins filling a 100 x 100 cartesian master array.

> "The hourly accumulations were derived by trapezoidal integration of the five 15-minute observations, which were nominally available at T (initial time), (T-15 min), (T-30 min), (T-45 min) and (T-60 min). Occasionally, one or more of the five observations were missing; albeit, hourly integrated values were still calculated if data were available for two or more of the 5 times, and if all times in the hourly interval were within 30 minutes of at least one of the existing observations"[1].

The actual data covers a circle of approximately 204 km in radius centered at $8^{\circ}$ 30'N latitude and $23^{\circ}$ 30'W longitude (Fig. 2). The final estimates were obtained by combining data from two or more of the C-band radars after corrections for biases and attenuation effects were applied to data from the individual radars. For Phases I and II of GATE, only the radar sets from the Oceanographer and Researcher were used to derive the hourly precipitation estimates. They were used

[1] From documentation for GATE hourly radar data, p. 4.

TABLE 1

Assigned positions of ships equipped with weather radars.

| Ship | Country | Normal Useful Range | Wavelength | Lat. N. | Long. W. | Phase I | Phase II | Phase III |
|---|---|---|---|---|---|---|---|---|
| Oceanographer | USA | 232 km (125 n mi) | 5.3 cm | 8°30' | 23°30' | X | X | |
| | | | | 7°45' | 22°12' | | | X |
| Researcher | USA | 232 km (125 n mi) | 5.3 cm | 7°00' | 23°30' | X | X | X |
| Gillis | USA | 250 km (135 n mi) | 5.3 cm | 9°15' | 24°48' | X | X | X |
| Quadra | Canada | 200 km (108 n mi) | 5.3 cm | 9°15' | 22°12' | X | X | |
| | | | | 9°00' | 22°40' | | | X |
| Meteor | FRG | 150-200 km (81-108 n mi) | 3.2 cm | 7°45' | 22°12' | X | X | |
| | | | | 8°30' | 23°30' | | | X |
| Prof. Vize | USSR | 150 km (81 n mi) | 3.2 cm | 10°10' | 23°30' | X | | |
| | | | | 8°30' | 23°30' | | X | X |
| Acad. Korolov | USSR | 100 km (54 n mi) | 3.2 cm | 12°00' | 23°30' | X | X | X |
| Prof. Zubov | USSR | 100 km (54 n mi) | 3.2 cm | 5°00' | 23°30' | X | X | X |

(This table is composed from Tables 1, 3 and 4 of the GATE International Meteorological Radar Atlas)

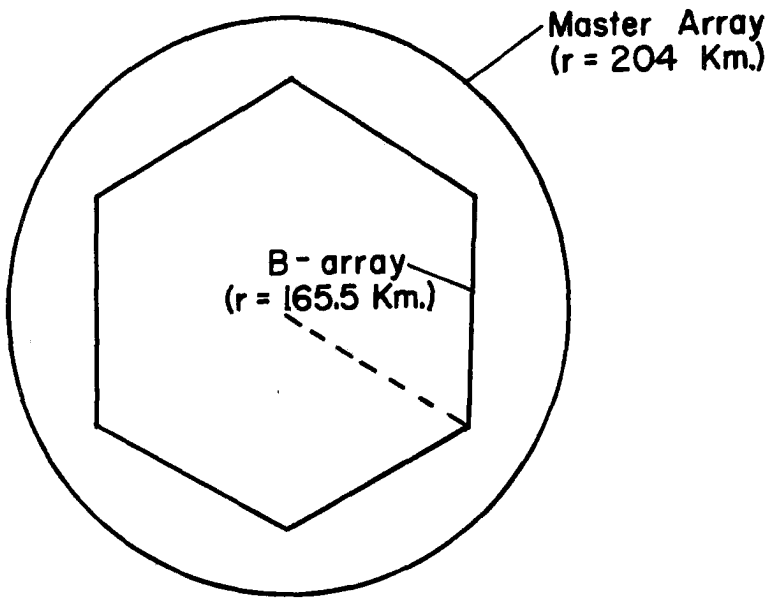


Fig. 2. Area coverage of radar master array with respect to the B-array ship network.

because of data availability and the fact that the Oceanographer was stationed near the center of the GATE network during the first two phases where its radar was able to cover the complete master array. To cover the master array during Phase III, data from all four radars were merged[2] when available.

Ship Rain Gauge Data. The B-scale shipboard rain gauge measurements used for this research were from siphon gauges, mounted on the masts of four of the US ships, the Researcher, the Gilliss, the

[2]The merging process was somewhat different for Phase III than for Phases I and II. For Phase III, the non-zero rainfall amounts (mm) for the common data bins falling inside the master array from the various radars were averaged. For Phases I and II, all non-zero rainfall rates from the Oceanographer were taken alone as the best estimates. Researcher estimates were substituted only for common data bins within the master array where the Oceanographer values were zero and the Researcher estimates were non-zero. This merging process recovered data that were missed by the Oceanographer radar in a sector forward of the ship that resulted from obstruction of the radar beam by the ship's superstructure. The Oceanographer's "dead" sector was normally located in areas covered by the Researcher radar.

Dallas, and the Oceanographer, and from a standard 8-in rain gauge located amidships on the deck of the NASA ship Vanguard. Rainfall that passed through a siphon gauge was collected at the base of the mast and manually recorded in standard WMO marine logs.

The five US gauges were read only once every 6 hours, whereas the Russian ship gauges were read every three hours, and the Canadian ship Quadra and the FRG ship Meteor reported hourly. However, it should be noted that start and stop times of observed precipitation were also given by the US ships in addition to the 6-hourly reports.

Satellite Data. The earth synchronous meteorological satellite (SMS-1) was positioned over the Atlantic at approximately 45°W longitude throughout GATE, and primarily in support of GATE. The imaging sensor onboard the SMS is a Visible and Infrared Spin Scan Radiometer (VISSR), which is a 2-channel instrument sensitive to both the visible (.5-.7μ) and infrared (10.5-12.5μ) portions of the spectrum. The image resolution on the earth's surface at the sub-satellite point was 0.5 n mi for the visible data, and 4.0 n mi for the infrared data. More detailed information on areal coverage of this satellite data can be found in Appendix B. The basic imaging frequency was one image every 30 minutes throughout the day. Between 1900 and 0800 GMT, only full disk IR data was available. In this investigation, magnetic tapes containing the GATE satellite data in digital form at hourly intervals were used. The images on these tapes have been previously navigated to an accuracy of 4 mi (Smith and Vonder Haar, 1976). The data were displayed on the All Digital Video Imaging System for Atmospheric Research (ADVISAR) at Colorado State University for analysis of convective patterns.

## 2.3 Computation of Parameter Deviations

Because of the small temperature gradients found in the tropics, and also because of ship to ship differences in temperature measurements (particularly the difference between the US VIZ-sondes and the Soviet sondes), it was necessary to work with temperature deviations rather than with absolute temperatures. These deviations were calculated by taking the difference between a particular temperature value and the mean for that ship and that phase. This allows elimination of the individual ship biases and is more meaningful than the T value alone.

## 2.4 Compositing Techniques

Since the upper level temperature changes which form the primary topic of this paper are a recurring feature of the GATE experiment, and because of the instrumental biases and problems with the upper air data obtained during GATE[3], (see Appendix A), it was decided to consider groups of cases rather than individual case studies. Therefore, compositing or averaging techniques were adopted and applied to the data sets. This should allow the underlying physical mechanisms producing the upper level temperature changes to be quantitatively treated.

---

[3] As stated by Esbensen and Ooyama (1977), "With correction of major biases, the CSDC data set should provide a good instantaneous description of the structure of large amplitude disturbances with space and time scales greater than 200 km and 2 days respectively. More detailed analysis will require compositing, or more detailed correction procedures. In particular, the merging of high frequency wind data from the various platforms remains a major problem."

## 3. TEMPERATURE AND MOISTURE DIFFERENCES BETWEEN RAINING AND NON-RAINING ENVIRONMENTS

To determine what average effect convection has on the surrounding environment, rawinsonde temperature and moisture values were averaged across the B-array, level by level, for 6-hourly time periods. This was done for two distinct data classes, Rain or enhanced conditions (40 of the most convective cases) and No Rain or suppressed conditions (40 of the least convective cases). Each of these two classes of convective phenomena was divided into four 6-hourly time stratifications of 10 cases each. 20 soundings are contained in each separate time stratification. Tables 2 and 3 give the dates, times and 6-hourly rainfall amounts for these cases as determined by the CSDC radar estimates.

### 3.1 Determination of Cases

The individual soundings for the Rain and No Rain data sets were selected based on radar rainfall estimates:

1) Rain Cases. These were chosen by considering the radar master array precipitation values in 6-hourly time blocks: 00-06Z, 06-12Z, 12-18Z and 18-00Z. The ten heaviest 00-06Z rainfall events were composited to form one Rain stratification, then the ten heaviest rain cases in the 06-12Z period were composited to form the next stratification, and similarly for the 12-18Z and 18-00Z periods.

2) No Rain Cases. B-scale observations were similarly composited for the ten least convective cases in the same 6-hourly time intervals.

B-scale area averaged values were calculated for the following parameters:

T = temperature ($^{o}$C)

$\Delta$T = temperature deviation values ($^{o}$C) calculated by subtracting from each temperature value, the phase mean temperature for that ship.

TABLE 2

Six-hourly rain case stratifications. Rainfall radar accumulations (mm/6hr) are B-scale area averaged estimates (set obtained from the CSDC in the fall 1977).

RAIN CASES

| | 00-06Z | | | 06-12Z | | | 12-18Z | | | 18-00Z | | |
|---|---|---|---|---|---|---|---|---|---|---|---|---|
| Case No. | Date | J.D. | Rainfall (mm/6hr) | Date | J.D. | Rainfall (mm/6hr) | Date | J.D. | Rainfall (mm/6hr) | Date | J.D. | Rainfall (mm/6hr) |
| 1 | July 2 | 183 | 5.39 | June 29 | 180 | 3.50 | June 29 | 180 | 6.66 | July 1 | 182 | 3.52 |
| 2 | July 7 | 188 | 5.27 | July 7 | 188 | 9.77 | July 7 | 188 | 21.92 | July 2 | 183 | 4.83 |
| 3 | July 8 | 189 | 2.37 | July 8 | 189 | 4.46 | July 8 | 189 | 10.73 | July 7 | 188 | 13.58 |
| 4 | July 15 | 196 | 3.70 | July 15 | 196 | 5.07 | July 13 | 194 | 6.76 | July 13 | 194 | 12.93 |
| 5 | Aug 13 | 225 | 4.27 | Aug 8 | 220 | 5.71 | Sept 2 | 245 | 11.75 | Aug 5 | 217 | 4.93 |
| 6 | Sept 5 | 248 | 6.89 | Aug 10 | 222 | 10.16 | Sept 5 | 248 | 7.38 | Sept 2 | 245 | 11.71 |
| 7 | Sept 14 | 257 | 8.95 | Sept 5 | 248 | 7.96 | Sept 9 | 252 | 7.48 | Sept 4 | 247 | 9.10 |
| 8 | Sept 15 | 258 | 3.96 | Sept 14 | 257 | 4.35 | Sept 12 | 255 | 9.96 | Sept 13 | 256 | 9.31 |
| 9 | Sept 16 | 259 | 7.06 | Sept 16 | 259 | 7.99 | Sept 14 | 257 | 5.33 | Sept 14 | 257 | 8.15 |
| 10 | Sept 17 | 260 | 5.00 | Sept 17 | 260 | 5.06 | Sept 16 | 259 | 6.27 | Sept 16 | 259 | 5.62 |
| Average | | | 5.29 | | | 6.40 | | | 9.42 | | | 8.37 |

TABLE 3

Same as Table 2, except for No Rain Cases.

NO RAIN CASES

| Case No. | 00-06Z | | | 06-12Z | | | 12-18Z | | | 18-00Z | | |
|---|---|---|---|---|---|---|---|---|---|---|---|---|
| | Date | J.D. | Rainfall (mm/6hr) | Date | J.D. | Rainfall (mm/6hr) | Date | J.D. | Rainfall (mm/6hr) | Date | J.D. | Rainfall (mm/6hr) |
| 1 | July 4 | 185 | .46 | July 5 | 186 | .14 | July 3 | 184 | .15 | July 3 | 184 | .44 |
| 2 | July 6 | 187 | .06 | July 6 | 187 | .21 | July 6 | 187 | .20 | July 9 | 190 | .05 |
| 3 | July 10 | 191 | .04 | July 10 | 191 | .00 | July 10 | 191 | .00 | July 10 | 191 | .00 |
| 4 | July 11 | 192 | .00 | July 11 | 192 | .03 | July 11 | 192 | .09 | July 11 | 192 | .15 |
| 5 | July 12 | 193 | .04 | Aug 9 | 221 | .12 | July 12 | 193 | .35 | July 12 | 193 | .50 |
| 6 | Aug 7 | 219 | .16 | Aug 11 | 223 | .03 | Aug 11 | 223 | .00 | July 31 | 212 | .67 |
| 7 | Aug 11 | 223 | .02 | Aug 14 | 226 | .39 | Aug 14 | 226 | .16 | Aug 6 | 218 | .76 |
| 8 | Aug 15 | 227 | .20 | Aug 15 | 227 | .09 | Aug 15 | 227 | .39 | Aug 11 | 223 | .10 |
| 9 | Sept 1 | 244 | .14 | Sept 1 | 244 | .12 | Sept 1 | 244 | .39 | Aug 14 | 226 | .11 |
| 10 | Sept 11 | 254 | .05 | Sept 11 | 254 | .07 | Sept 3 | 246 | .39 | Sept 8 | 251 | .33 |
| Average | | | .12 | | | .12 | | | .21 | | | .31 |

$q$ = specific humidity (g/kg)

$\Delta q$ = moisture deviation values calculated by subtracting from each specific humidity value, the phase mean specific humidity for that ship (g/kg)

$s$ = dry static energy ($^{o}K$)

$u,v$ = east-west and north-south components of the wind (m/s)

$V_r$ = radial wind (m/s)

Div = mass divergence ($s^{-1}$) } non mass-balanced, and mass-balanced[4]

Omega = ($\omega$) vertical velocity (mb/day) }

3.2 Six-hourly Time Changes

Figures 3a-d show Rain vs. No Rain comparisons of 6-hourly temperature changes. Viewed one at a time these graphs show that, with the exception of values above 200 mb, there is very little difference between Rain Case 6-hourly temperature changes and No Rain Case 6-hourly temperature changes. However, by following from one graph to the next, it can be seen that both cases display a similar diurnal shift in temperature which is significantly larger than the Rain and No Rain temperature differences. These same diurnal changes can be observed in Fig. 4 which shows diurnal plots of Rain Case and No Rain Case 6-hourly temperature changes integrated through the layers 500-200 mb and surface to 200 mb, respectively. It can be seen that the diurnal variation is large and dominates the average B-scale temperature change for both the Rain and No Rain Cases; this change has little dependence on whether or not the sonde is penetrating a raining environment. If the convection were directly producing a large mean temperature change in the environment, significant difference between the Rain and No Rain environment

[4]Appendix C discusses the mass-balancing procedures.

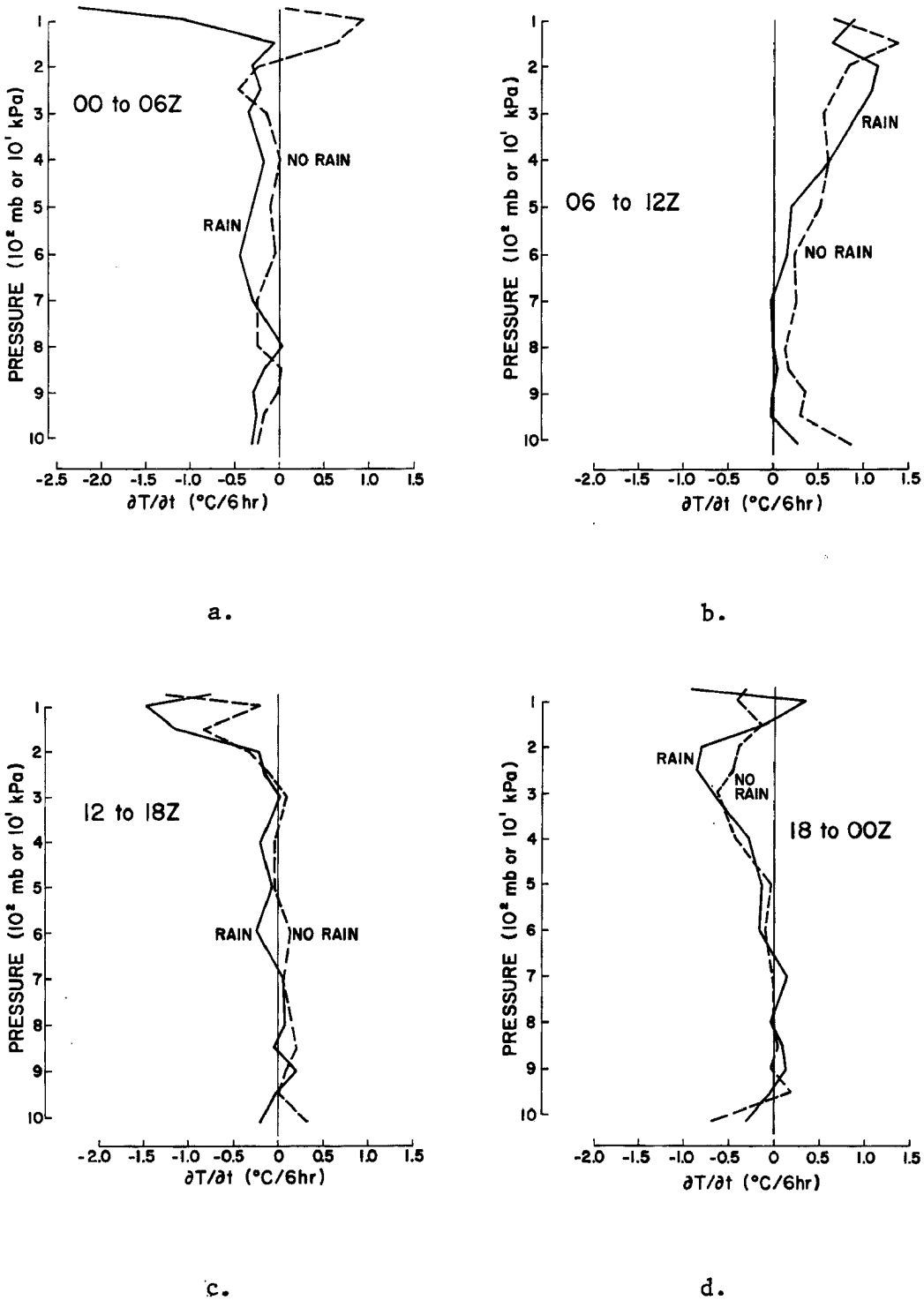


Fig. 3a-d. Rain vs. No Rain comparisons of 6-hourly temperature changes.

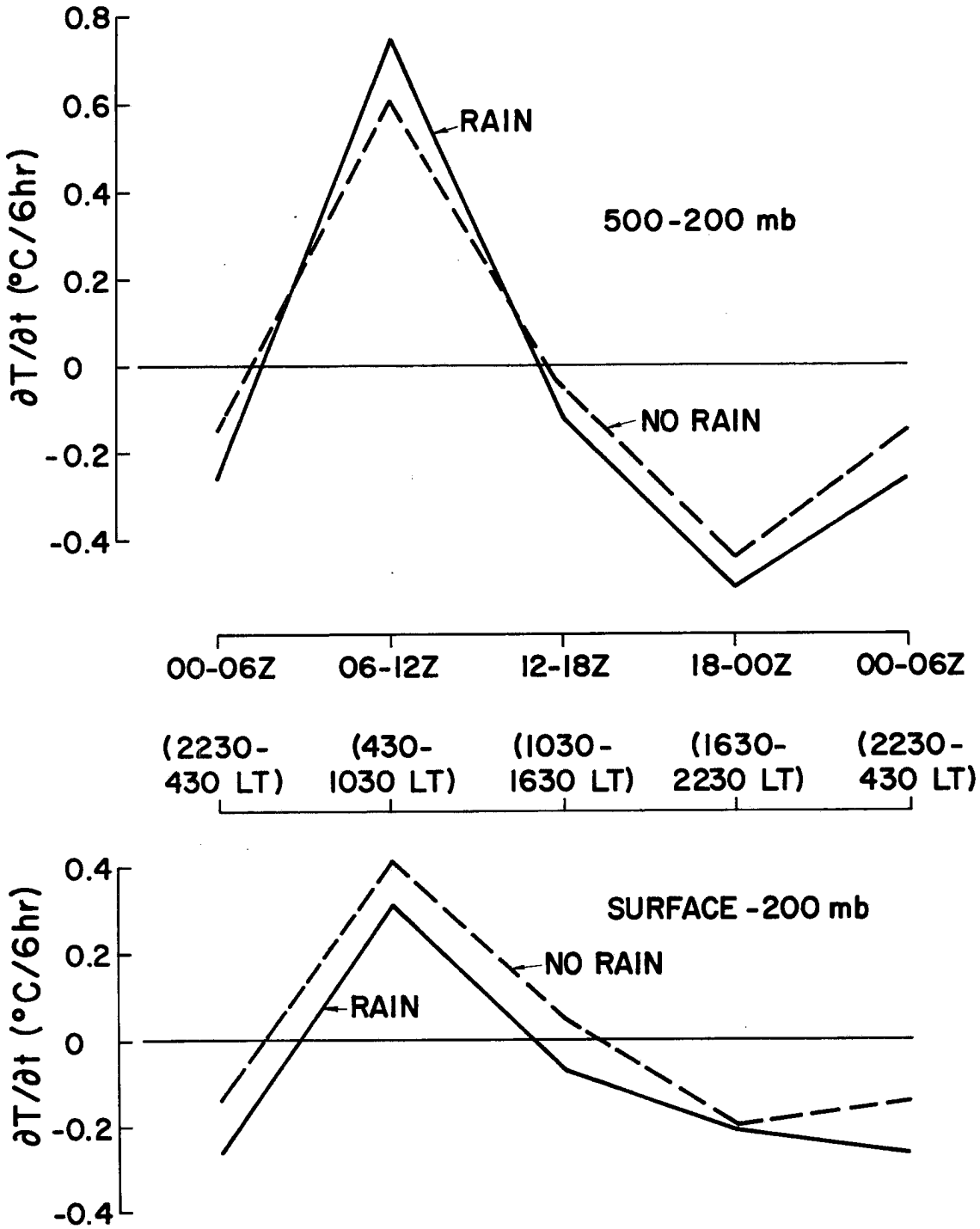


Fig. 4. Diurnal plots of Rain Case and No Rain Case 6-hourly temperature changes.

$\frac{\partial T}{\partial t}$ would be found, irrespective of the diurnal temperature change in both. Since this is not the case, it appears that the convection is not producing much warming of the environment. The diurnal warming of Fig. 4 is a feature which GATE has in common with other tropical data sets, as indicated in Fig. 5. [See Dewart (1978) for a more detailed discussion of the diurnal effects in GATE and Foltz (1976) for an explanation of the diurnal temperature changes in other regions.]

Figures 6a-d and 7 show the corresponding comparisons for 6-hourly moisture changes. These indicate more of a Rain vs. No Rain difference than do the temperature changes. The Rain Cases show a general moistening above 700 mb at all time periods, and a general drying below 700 mb. This is likely due to the effects of convective downdrafts drying out the lower levels and convective updrafts carrying moisture aloft. This pattern of drying below 700 mb is least distinct in the 00-06Z case, because (as indicated in Table 2) the Rain Case atmosphere was least convective at this time and fewer downdrafts were likely occurring. For the No Rain Cases moisture changes occur in a more vertically uniform fashion. Figure 6 indicates that slight drying out of the entire atmospheric column occurs in the evening during the intervals 00-06Z and 06-12Z, and a general moistening occurs during the afternoon. The slight nighttime drying is likely indicative of enhanced diurnal subsidence which occurs in response to the greater nighttime radiative cooling accompanying a non-convective regime. The daytime moistening, then, in keeping with the former argument, is likely due to less daytime radiative cooling, which would require less of a balancing subsidence warming and drying. This is supported by the observation that low level convergence and upward vertical motion almost always were found

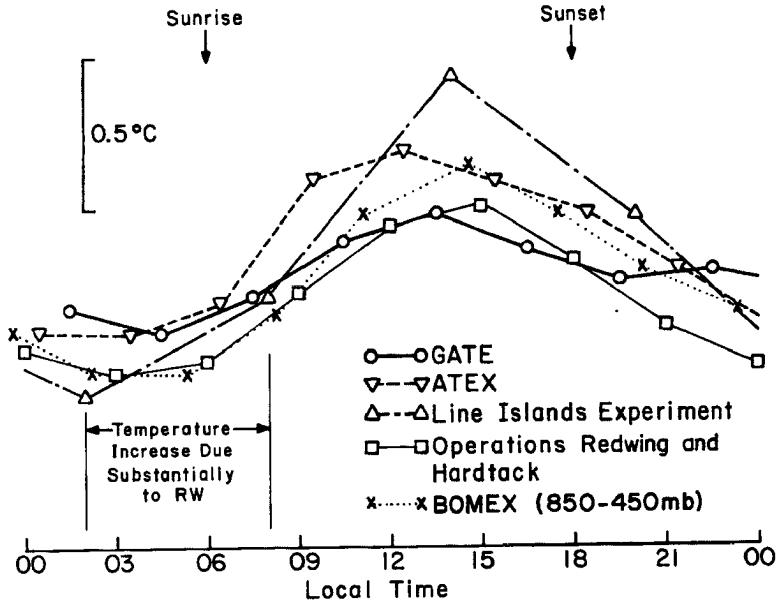


a.

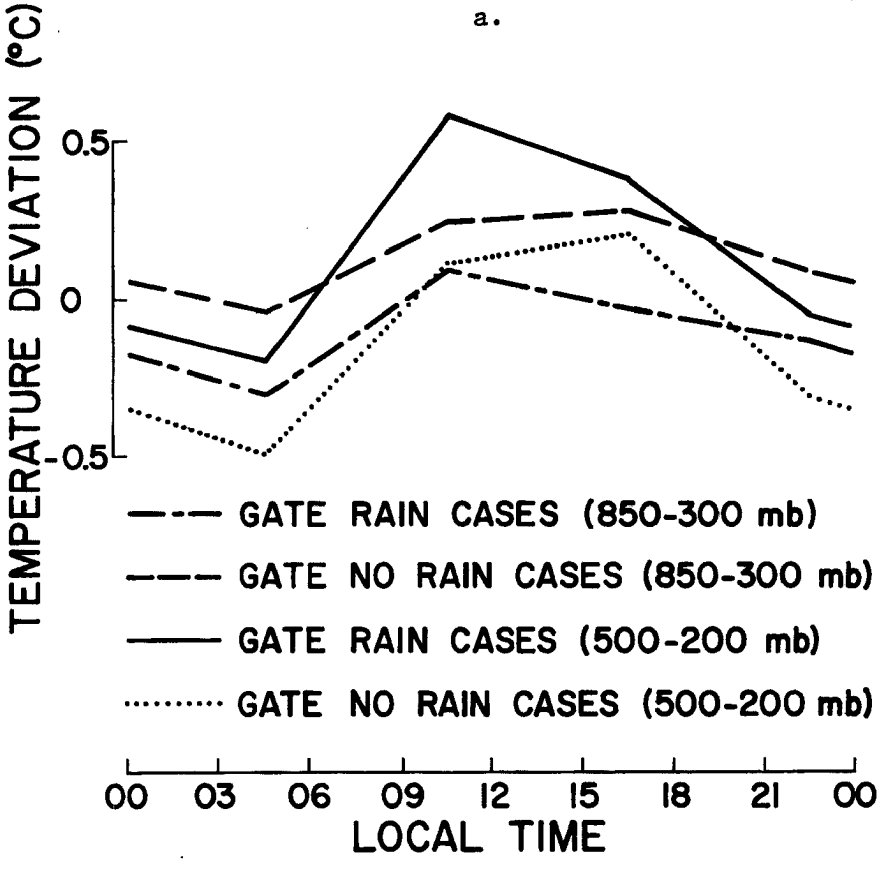


b.

Fig. 5a-b. a) Diurnal temperature variation of the 850-300 mb layer for special tropical experiments (from Foltz, 1976). b) Diurnal temperature variation of the 850-300 mb and 500-200 mb layer for GATE Rain and No Rain Cases.

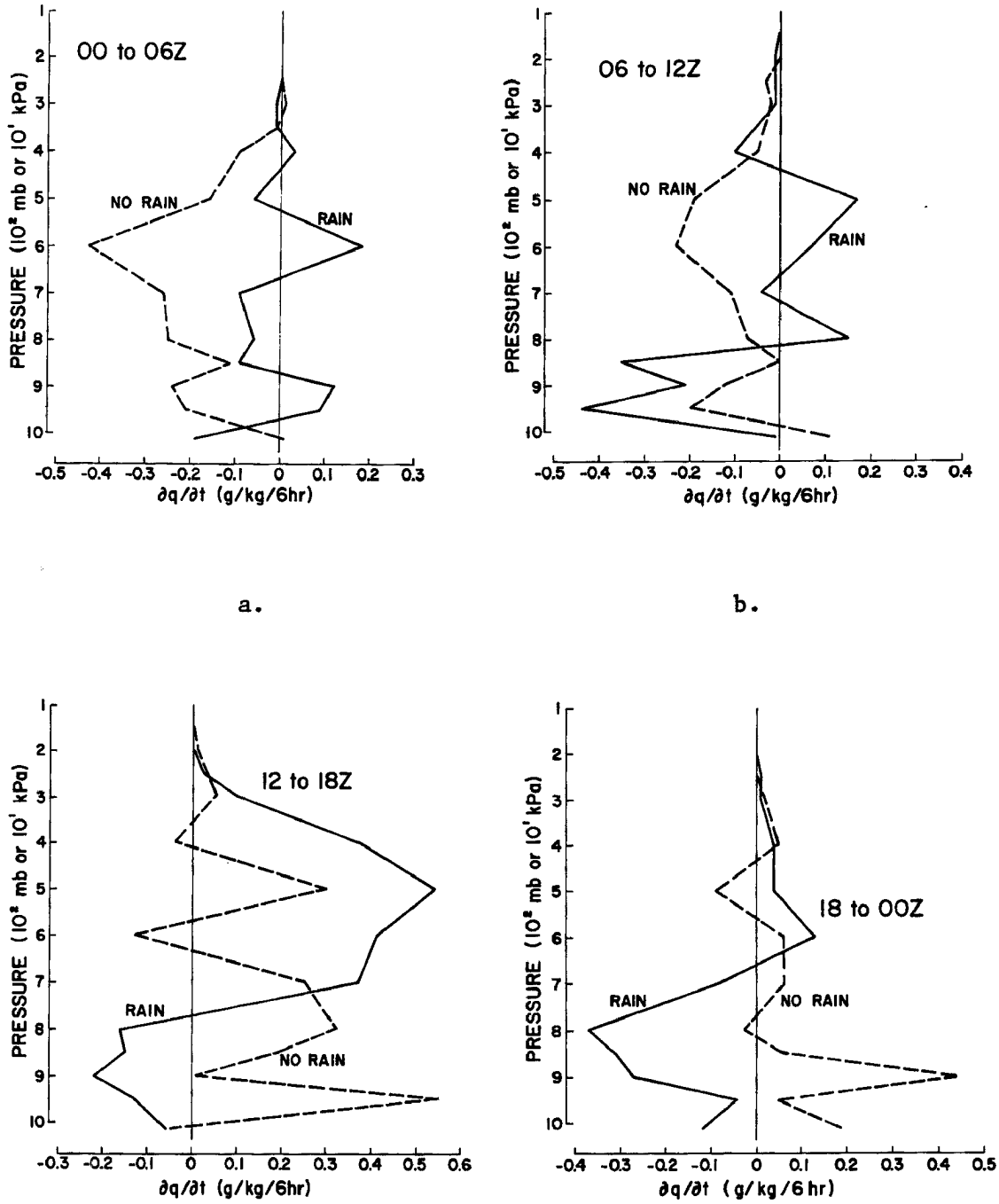


Fig. 6a-d. Rain vs. No Rain 6-hourly moisture changes.

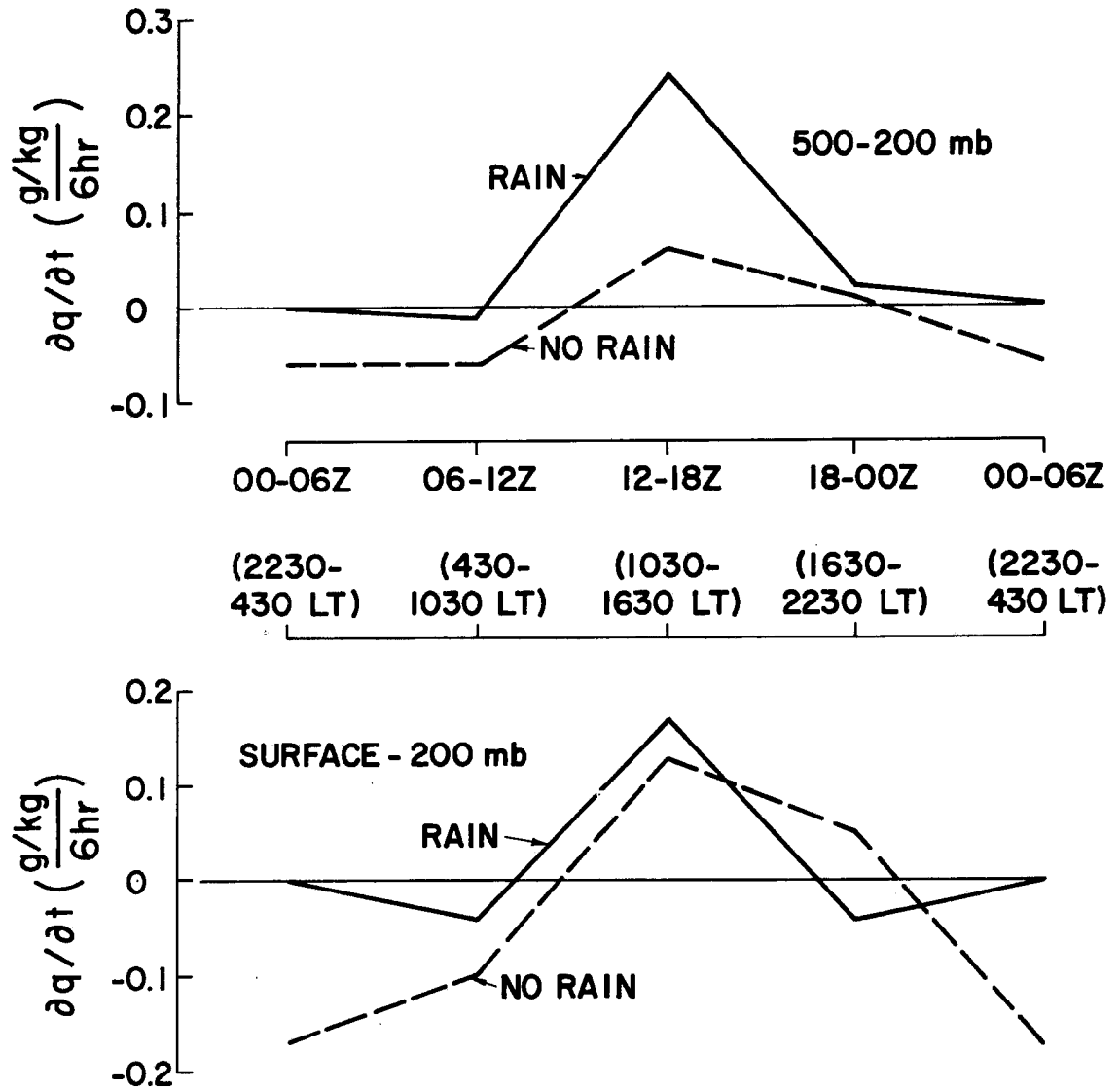


Fig. 7. Diurnal plots of Rain Case and No Rain Case 6-hourly moisture changes.

during the daytime in GATE, even in the ridges and suppressed areas. By noting the vertically integrated daily effect in both rain regimes and non-rain regimes it can be seen that atmospheric moisture storage is small. Neither regime shows significant moistening or drying of the troposphere.

3.3 Comparison of Rain and No Rain Temperature Profiles

Figures 8a-d are plots of 6-hourly average temperature deviations (all values subtracted from the phase mean for the particular ship from which the individual sounding was launched). As such, they do not represent time rates of change, but rather indicate temperature changes from the mean for the cases and time periods under consideration. It should be noted from these graphs that the vertical temperature deviation trends appear to be nearly mirror images, i.e., when the Rain Case values become warmer with height, the No Rain Case values become cooler, and vice versa, indicating that opposing mechanisms are at work producing these two contrasting profiles. The Rain Cases are typically cool in low levels due to convective downdrafts and evaporation. They then become warmer with height up to about 400-200 mb where they reverse their trend and again become cool. The warming which occurs from 500-250 mb is believed to be primarily produced by Cb return flow mass subsidence. At these altitudes, the moisture content of the air is not sufficiently high for evaporative cooling to exceed subsidence warming. In the presence of Cb return-flow subsidence, the upper troposphere will always warm more than evaporation can cool. The cooling above 200 mb in the Rain Cases is believed to result from Cb cloud overshoot and enhanced radiative cooling off the tops of the clouds. Relative to the Rain Cases, then, the No Rain Cases are warmer in low levels due to the absence of convective downdrafts and evaporative processes, and cooler in upper levels (500-250 mb) because of the lack of Cb-induced return-flow subsidence. Although these opposing temperature trends of the Rain and No Rain curves with respect to each other remain fairly constant throughout the day, both curves undergo a rather sizeable temperature shift from

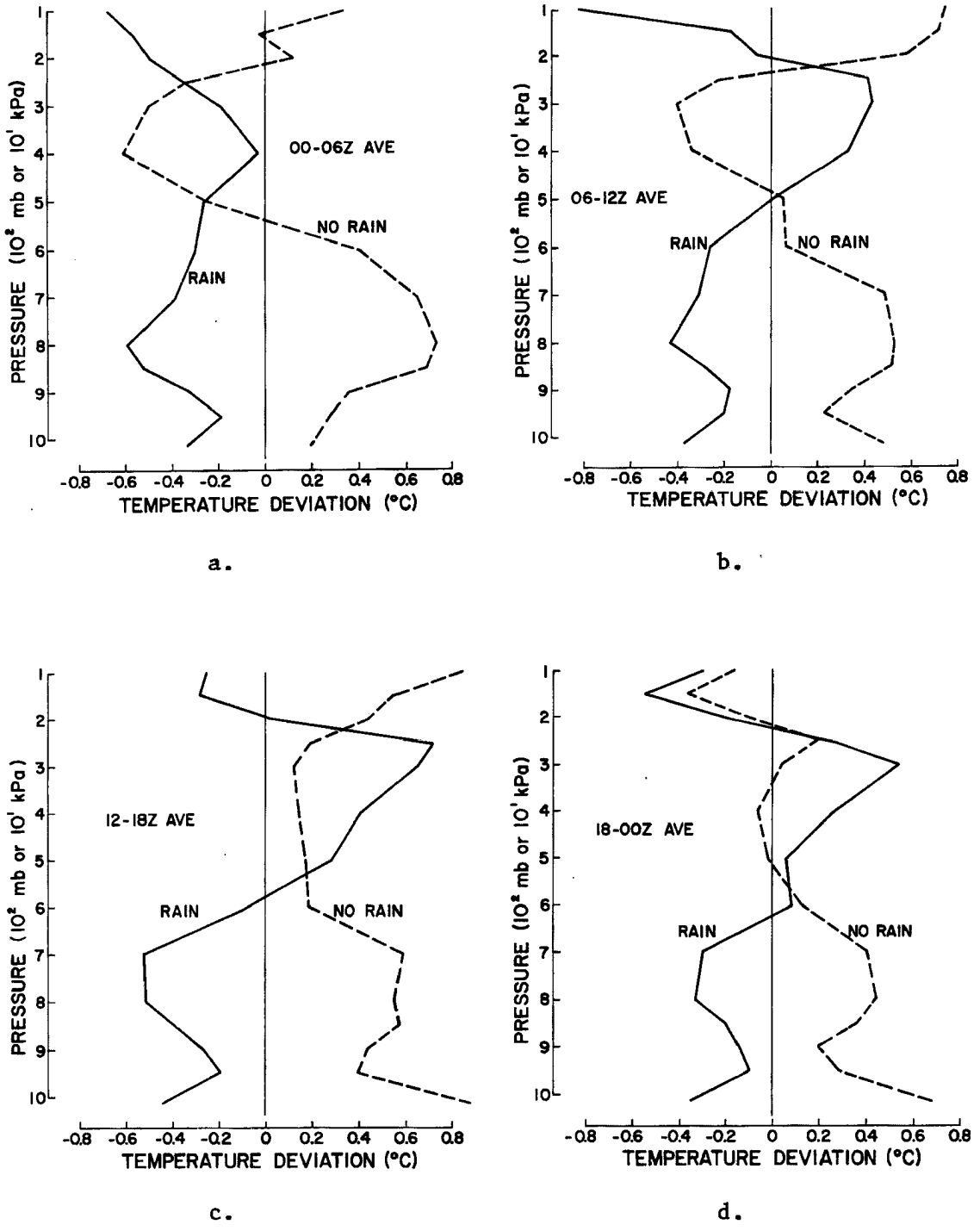


Fig. 8a-d. Average temperature deviations for 6-hourly time intervals. (Deviation taken from phase mean for the particular ship from which a sounding is launched in B-array.)

time period to time period, due to solar radiation effects. This shows again that diurnal changes in temperature are dominant over all other temperature changes occurring. This points out the importance of distinguishing time of day when discussing temperature structure. One cannot compare temperature measurements taken at different times of day unless the large diurnal ranges are first accounted for.

When the vertical temperature deviation profiles for the No Rain Cases are subtracted from the corresponding Rain Case deviation profiles, the vertical profiles of Fig. 9 result . (A number of researchers have obtained similar temperature profiles in association with convective vs. non-convective regions.) The uniformity of the four time periods represented on this graph demonstrates that while the Rain and No Rain temperature deviations both experience large diurnal changes, the Rain minus No Rain temperature differences are nearly independent of the time of day. It can also be seen that rain environments are cold core with respect to their surroundings in low layers, but warm core in upper layers; and indirect circulation characterizes the lower layers, while a direct circulation exists in upper levels. These vertical differences in temperature deviation demonstrate the large importance (when referring to the temperature structure of a system) of designating the particular layer of concern, as well as the time of day.

### 3.4 Rain Minus No Rain Thickness Calculations

Thicknesses can be calculated from the Rain minus No Rain layer mean temperature deviation differences (Fig. 10). Virtual temperature corrections for Rain minus No Rain temperature differences are as follows:

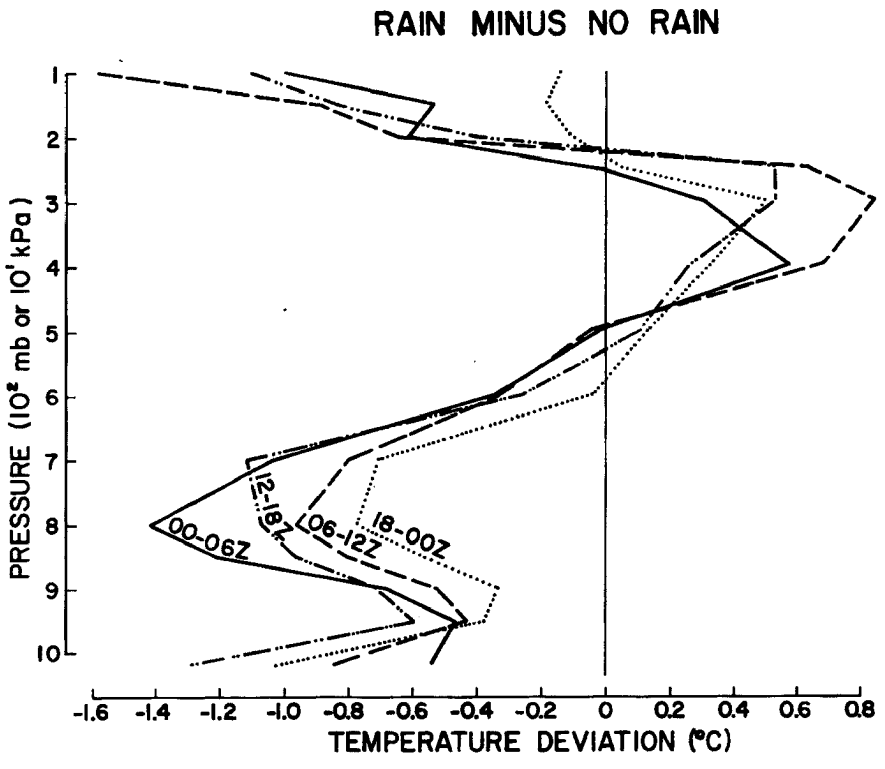


Fig. 9. Rain minus No Rain temperature deviation differences for various time stratifications.

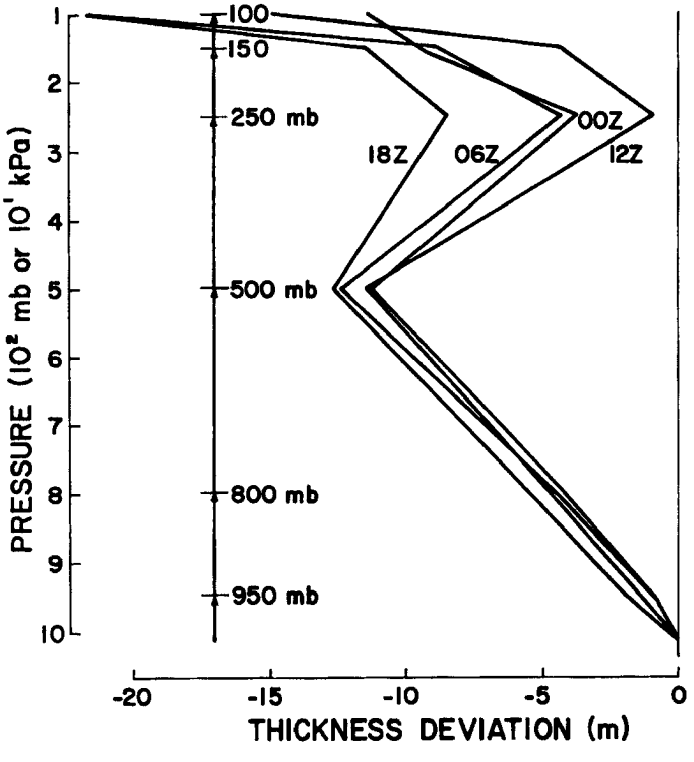


Fig. 10. Rain minus No Rain thickness difference for various time stratifications (integrated upward from the surface).

| Pressure (mb) | °C |
|---|---|
| 100 | 0 |
| 200 | 0 |
| 300 | .02 |
| 400 | .09 |
| 500 | .07 |
| 600 | .11 |
| 700 | .14 |
| 800 | .07 |
| 900 | .07 |
| 975 | .05 |
| Sfc | -.03 |

These corrections were not applied because the vertically integrated thickness difference resulting is only about 3 m. Computations show the thickness difference between Rain and No Rain Cases to be increasing up to about 500 mb, decreasing to about 250 mb (because of the upper level warming accompanying the Rain Cases), then again increasing above about 250 mb. The resulting overall average thickness difference between Rain and No Rain environments at the top of the troposphere is only about 18 m, the Rain Case thickness being less. Between the surface and 250 mb it is only 4 m. In lieu of the large amount of condensation energy released, it is quite significant that not more of a systematic thickness difference is observed between the Rain and No Rain Cases. Thus, when considering integrations through the troposphere, the temperature differences and therefore the thickness differences are so small that it does not appear relevant to speak about a warm-core or cold-core system. In a vertically averaged sense, the systems are nearly neutral. If a Rain environment cannot be said to be either warmer or cooler than a No Rain environment in the vertical average, then it is not possible for a convective system to be producing a significant surface pressure fall which would enhance the circulation and intensify the system.

3.5 Comparison of Rain and No Rain Vertical Motion Profiles

The B-scale vertical motion ($\omega$) profiles (Figs. 11 and 12) for the Rain and No Rain Cases were calculated using $2V_r/r$, where $V_r$ is the average radial wind. They appear as might have been expected; much greater low level convergence and upward vertical velocity ($-\omega$) accompany the raining environment. With the Rain Cases this upward vertical motion is a maximum from 12-18Z and a minimum from 00-06Z, an expected result in view of the fact that the daily maximum in GATE rainfall occurs during the afternoon. [The diurnal variation of GATE convection has been previously discussed in reports by Gray and Jacobson (1977), McBride and Gray (1978), Dewart (1978), and Frank (1978).] These are relative comparisons. When dealing with absolute vertical velocity values on the B-scale in GATE, difficulties arise because of the quality of the wind data (see Appendix A) and the wind correction values which often need to be applied in order to achieve mass-balance. The large wind corrections required in turn lead to a sensitivity in the vertical velocity ($\omega$) calculation to the type of mass-balancing scheme employed. Figure 11 shows the results of applying a mass-balancing factor that remains constant with height, while in Fig. 12, a correction factor which increases linearly with height has been applied (see Appendix C). It is seen that by using a mass-balancing correction factor that increases with height, a subsidence ($+\omega$) profile can be obtained at all No Rain time periods except 00-06Z (Fig. 12), whereas with a constant mass-balancing factor, all No Rain time periods show small upward vertical motion. The differences in these two sets of vertical motion profiles become important when performing budget calculations. When a "q" (moisture) budget is made for the Rain and No Rain Cases, the resulting

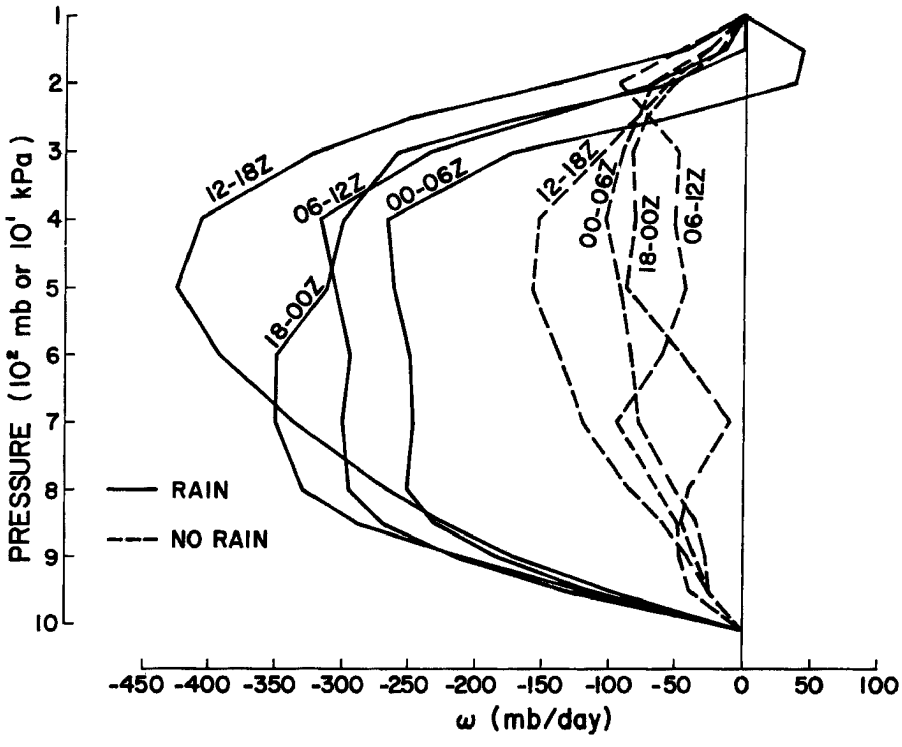


Fig. 11. Vertical motion profiles for Rain and No Rain time stratifications, calculated using a mass-balancing correction constant with height.

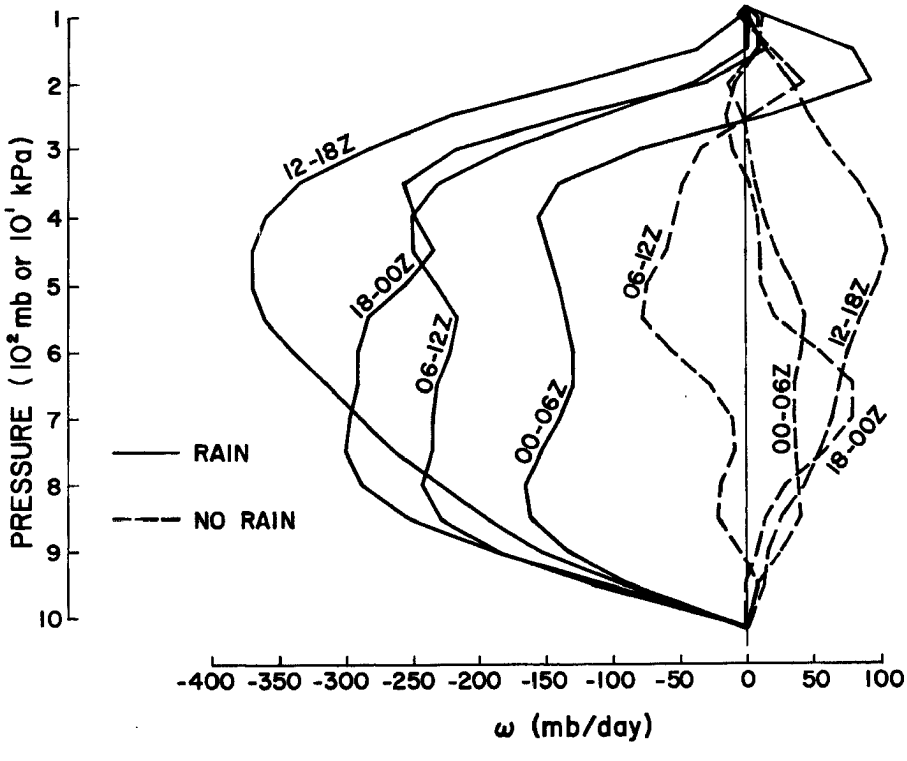


Fig. 12. Same as Fig. 11, except using a mass-balancing correction increasing linearly with height.

rainfall is higher than measured by the radar measurements (Table 4). Although these rainfall discrepancies are due in part to the unreliability of the B-scale winds as explained above and described in more detail in Appendix A, there is also reason to believe that the radar estimates may be low for light and moderate precipitation. [Further discussion of the possible underestimation of rain by radar can be found in Dewart (1978) and Frank (1978).] Budget calculations tend to indicate as much as 50% more rainfall than indicated by the combined radar-satellite data.

3.6 Net Kinetic Energy Generation in the Rain Environment

Figures 13a and b show vertical plots of temperature deviation multiplied by the mean vertical velocity ($T'\bar{\omega}$) for the various Rain Case time stratifications. For Fig. 13a, the value was computed using a mass-balancing factor constant with height, and for Fig. 13b the vertical velocity was computed with the mass-balancing factor increasing linearly with height (see Section 3.5 and Appendix C). The corrected temperature deviations were calculated as shown in Table 5. The initial temperature deviations are those computed from ship phase means. The mean GATE diurnal deviations were then subtracted from these to give the final temperature deviations. The diurnal temperature changes constitute a large contribution to the temperature deviations measured at a particular time [an investigation of diurnal effects in GATE has been made by Dewart (1978) and Frank (1978) - see also Figs. 4 and 5] and thus must be subtracted out in order to obtain only the effects of convection. Although the two sets of $\bar{\omega}$ profiles differ somewhat in magnitude (Figs. 11 and 12), there remains very little difference

TABLE 4

6-hourly rainfall amounts as derived from moisture budget calculations and estimated from hourly radar values.

B-scale Rainfall Comparison ($g/cm^2$ per 6 hr)

| | Rain | | | | No Rain | | | |
|---|---|---|---|---|---|---|---|---|
| | 00-06Z | 06-12Z | 12-18Z | 18-00Z | 00-06Z | 06-12Z | 12-18Z | 18-00Z |
| Radar Estimates | .53 | .64 | .94 | .84 | .01 | .01 | .02 | .03 |
| Budget Cal.* | 1.06 | 1.27 | 1.23 | 1.37 | .48 | .41 | .37 | .22 |
| Budget Cal.** | .67 | 1.03 | 1.04 | 1.18 | .08 | .05 | .18 | -.08 |

* A mass-balancing correction constant with height was applied to the wind values.

** A mass-balancing correction increasing linearly with height was applied to the wind data.

between the curves plotted in Fig. 13a and those of Fig. 13b, indicating that the $T'\bar{\omega}$ profiles mainly reflect the T' values used.

Vertical integrations of the $T'\bar{\omega}$ values are shown in Table 5. The vertical integrals of the 06-12Z and 18-00Z time periods indicate a slight direct circulation (upward motion with positive T'), whereas the 00-06Z and 12-18Z time periods show a slight indirect circulation (upward motion with negative T'). However, when all four time periods are averaged over an entire day, the resultant direct and indirect circulations nearly cancel themselves out. Thus, there appears to be no significant B-array generation of kinetic energy by the raining regime over that of the no-rain environment, even though the rain environment is characterized by a large upward vertical velocity and positive mesoscale temperature deviation in the upper troposphere.

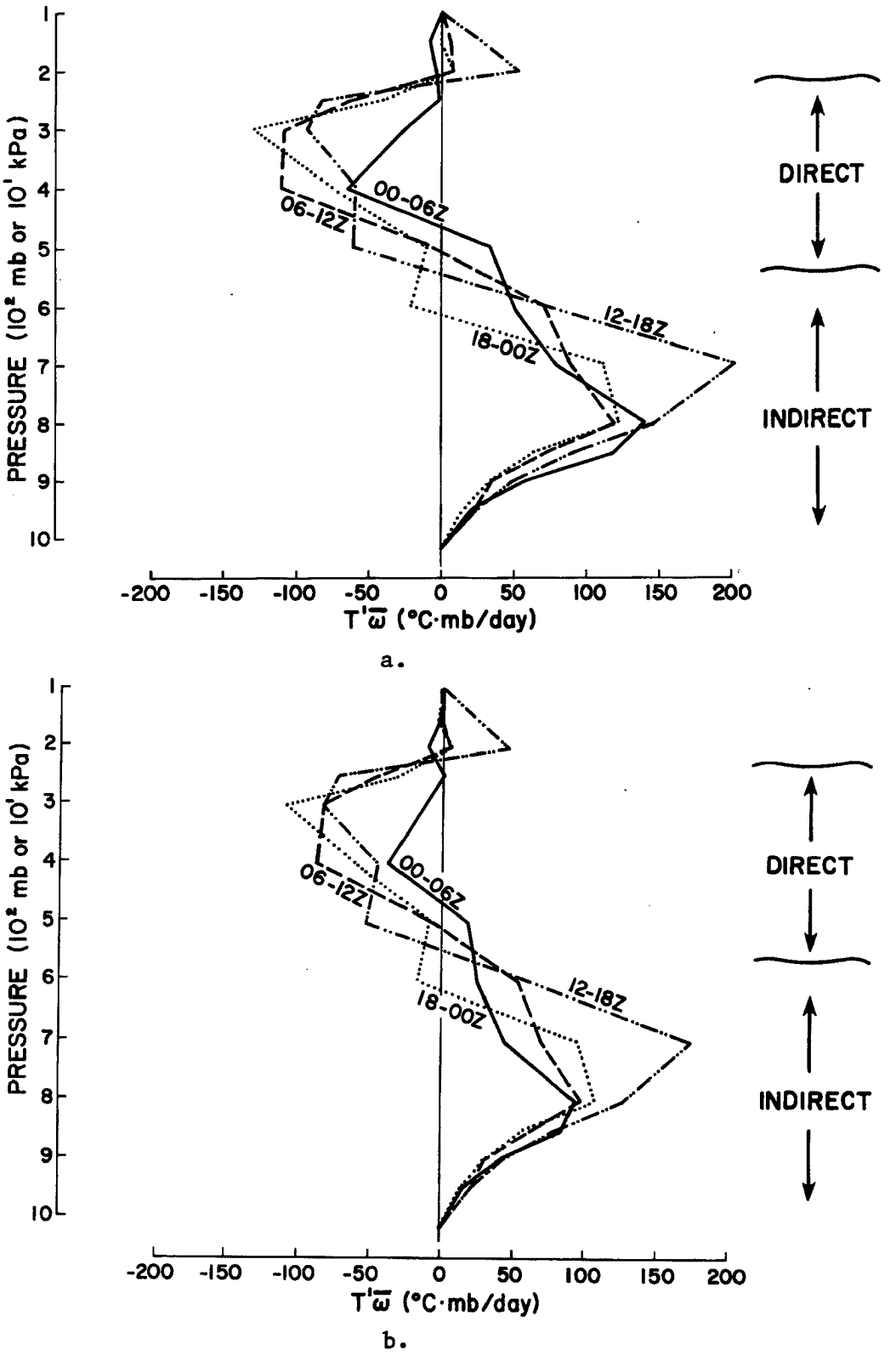


Fig. 13a-b. Vertical plots of $T'\bar{\omega}$ for the Rain Case. a) Mass-balancing factor constant with height; b) mass-balancing factor increasing linearly with height.

TABLE 5

RAIN CASE $T'\overline{\omega}$.

| Pres. (mb) | 00-06Z Initial Temp. Dev. | − Diurnal Temp. Dev. | = Corr. Temp. Dev. | x ω(mb/day) (Vert. Motion) | = T'ω (°C mb/day) | 06-12Z Initial Temp. Dev. | − Diurnal Temp. Dev. | = Corr. Temp. Dev. | x ω(mb/day) (Vert. Motion) | = T'ω (°C mb/day) |
|---|---|---|---|---|---|---|---|---|---|---|
| Surf. | -.35 | -.23 | -.12 | 0.00 | 0.00 | -.37 | -.06 | -.32 | 0.00 | 0.00 |
| 950 | -.20 | -.02 | -.18 | -118.36 | 20.71 | -.20 | -.03 | -.18 | -132.68 | 23.22 |
| 900 | -.33 | -.02 | -.31 | -184.72 | 57.26 | -.18 | -.02 | -.16 | -216.73 | 34.68 |
| 850 | -.53 | -.01 | -.52 | -230.15 | 118.53 | -.29 | -.02 | -.27 | -271.03 | 73.18 |
| 800 | -.60 | -.04 | -.56 | -250.80 | 140.45 | -.44 | -.04 | -.40 | -293.93 | 117.57 |
| 700 | -.39 | -.07 | -.32 | -247.27 | 79.13 | -.31 | -.02 | -.30 | -300.12 | 88.54 |
| 600 | -.31 | -.11 | -.20 | -248.81 | 49.76 | -.26 | -.02 | -.24 | -294.27 | 70.62 |
| 500 | -.27 | -.14 | -.13 | -261.55 | 34.00 | .01 | -.02 | .03 | -304.59 | -7.61 |
| 400 | -.04 | -.28 | .25 | -266.38 | -65.26 | .34 | -.01 | .35 | -316.78 | -110.87 |
| 300 | -.20 | -.35 | .16 | -170.50 | -26.43 | .44 | -.03 | .47 | -232.80 | -108.25 |
| 250 | -.35 | -.39 | .04 | -56.45 | -2.26 | .42 | -.01 | .42 | -151.79 | -63.75 |
| 200 | -.50 | -.39 | -.11 | 37.73 | -4.15 | -.07 | .06 | -.13 | -67.53 | 8.44 |
| 150 | -.57 | -.38 | -.20 | 42.93 | -8.37 | -.18 | .21 | -.39 | -16.27 | 6.26 |
| 100 | -.68 | -.30 | -.38 | -.08 | .03 | -.84 | .22 | -1.05 | -.05 | .05 |
| Integrated Sum - Mass Weighted | | | | | 24.45 | | | | | -20.01 |

TABLE 5 (cont'd)

RAIN CASE $T'\bar{\omega}$.

| Pres. (mb) | 12-18Z Initial Temp. Dev. | − Diurnal Temp. Dev. | = Corr. Temp. Dev. | × ω(mb/day) (Vert. Motion) | = $T'\omega$ ($^{o}$C mb/day) | 18-00Z Initial Temp. Dev. | − Diurnal Temp. Dev. | = Corr. Temp. Dev. | × ω(mb/day) (Vert. Motion) | = $T'\omega$ ($^{o}$C mb/day) |
|---|---|---|---|---|---|---|---|---|---|---|
| Surf. | -.44 | .23 | -.67 | 0.00 | 0.00 | -.35 | .06 | -.41 | 0.00 | 0.00 |
| 950 | -.20 | .02 | -.22 | -101.61 | 21.85 | -.10 | .03 | -.13 | -122.61 | 15.33 |
| 900 | -.27 | .02 | -.29 | -172.16 | 49.93 | -.14 | .02 | -.16 | -213.83 | 34.21 |
| 850 | -.39 | .02 | -.41 | -222.93 | 91.40 | -.20 | .03 | -.23 | -288.65 | 64.95 |
| 800 | -.52 | .04 | -.56 | -265.41 | 147.30 | -.33 | .04 | -.37 | -330.47 | 122.27 |
| 700 | -.53 | .08 | -.60 | -336.30 | 201.78 | -.30 | .02 | -.32 | -350.03 | 112.01 |
| 600 | -.08 | .11 | -.19 | -391.86 | 72.49 | .09 | .03 | .06 | -349.20 | -20.95 |
| 500 | .29 | .14 | .15 | -422.60 | -61.28 | .06 | .03 | .04 | -312.49 | -10.94 |
| 400 | .41 | .29 | .13 | -407.01 | -50.88 | .27 | .02 | .25 | -300.16 | -75.04 |
| 300 | .65 | .36 | .29 | -320.47 | -92.94 | .54 | .04 | .50 | -260.04 | -130.02 |
| 250 | .72 | .39 | .33 | -249.28 | -82.26 | .25 | .01 | .24 | -164.41 | -39.46 |
| 200 | .03 | .40 | -.37 | -143.48 | 53.09 | -.21 | -.05 | -.16 | -54.68 | 8.75 |
| 150 | -.29 | .37 | -.65 | -43.96 | 28.57 | -.55 | -.22 | -.33 | -1.41 | .47 |
| 100 | -.26 | .24 | -.49 | -.04 | .02 | -.30 | -.28 | .02 | -.04 | -.00 |
| Integrated Sum - Mass Weighted | | | | | 24.50 | | | | | -26.20 |

A similar result is obtained by calculating kinetic energy generation using a deviation vertical velocity $\omega'$ (deviation of Rain Case vertical motion values from the B-array GATE mean $\bar{\omega}$ profile shown in Fig. 14). Vertically integrated $\overline{T'\omega'}$ values and the associated daily kinetic energy changes are shown by 6-hourly time period in Table 6. Since the GATE mean kinetic energy is on the order of $25 \times 10^4 cm^2/s^2/day$, these changes represent only a small percentage of the mean kinetic energy within the B-array. When averaged over a day, the Rain Case data show a net kinetic energy generation of $-2.1 \times 10^4 cm^2/s^2/day$, an amount which would result in a very small wind speed change (approximately .2-.3 m/s).

Those who have previously envisaged tropical rain areas as regions of meso-scale KE generation due to positive correlation between meso-scale upward vertical motion and meso-scale temperature deviation are likely incorrect in such an assessment. It appears that KE generation is not significant on the meso-scale. It should be noted that this holds only for the spatial scale under consideration. Some KE generation no doubt does result from favorable $\omega'$ and $T'$ correlation in individual clouds and also over the macro-scale tropical region encompassed by the ITCZ with its upward warming circulation and the associated Hadley circulation subsidence area with its cooler air. Tropical convective environments are known to display modest momentum and KE fields despite large amounts of condensation energy release and vertical motion.

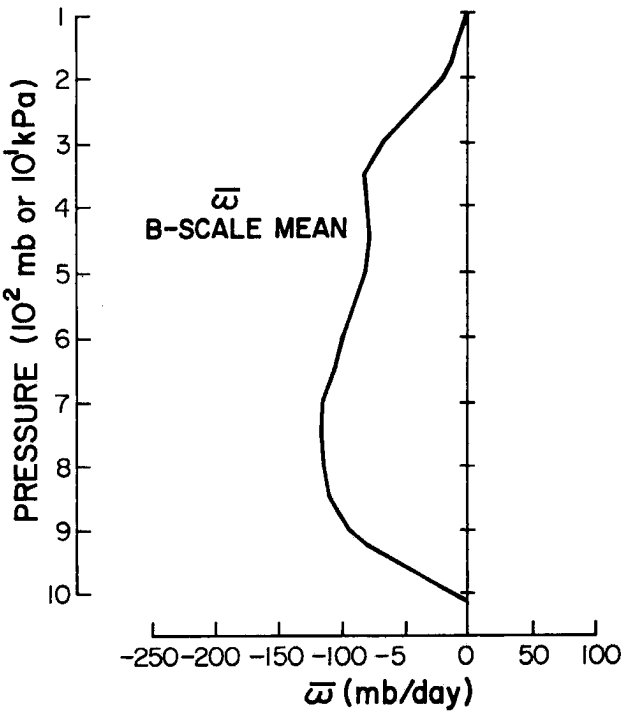


Fig. 14. GATE B-array mean $\bar{\omega}$ profile.

TABLE 6

RAIN CASE $\overline{T'\omega'}$

| | 00-06Z | 06-12Z | 12-18Z | 18-00Z | Daily Ave. |
|---|---|---|---|---|---|
| $\overline{T'\omega'}$ ($^{o}$C mb/day) Integrated Sum (surface to 100mb) - mass-weighted | 8.3 | -19.9 | 8.8 | -23.5 | -6.6 |
| Resulting $\frac{\partial KE}{\partial t}$ ($cm^2/s^2$/day) | $2.7x10^4$ | $-6.4x10^4$ | $2.8x10^4$ | $-7.5x10^4$ | $-2.1x10^4$ |
| Approx. resulting mean tropospheric wind speed change m/s per day | +0.3 | -0.6 | +0.3 | -0.7 | -0.2 |

## 4. RAWINSONDE ANALYSIS OF UPPER TROPOSPHERIC TEMPERATURE ANOMALIES

In order to better document how cumulus clouds warm the troposphere it is necessary to have an adequate means of detecting and recording atmospheric temperature changes, which in the tropics are generally quite small. The rawinsonde was the principal instrument used to measure temperature during GATE. Although instrumental aircraft flights provided some additional temperature information, radiosonde data afforded much more vertical resolution and also simultaneous coverage over an entire network of stations. (See Appendix A for a discussion of rawinsonde data quality.)

Since GATE radiosondes were launched at time intervals of 3-6 hours, anomalous upper level temperature changes with such a time resolution could be discerned. $\frac{\partial T}{\partial t}$ values were obtained by subtracting each sounding from the subsequent sounding, after having first subtracted out the GATE mean diurnal temperature deviations (see Table 7) for those times. With the temperature contamination due to diurnal radiative and diurnal subsidence influences subtracted out of all the data, it is believed that the values remaining represent temperature changes produced mainly by local convective influences. To discover more about how these temperature changes might be related to the presence of convection, radar and rawinsonde data were positioned around soundings with rain, and around soundings showing anomalous upper level temperature changes. Average echo distributions as well as average temperature and moisture patterns for the various situations were then compared.

TABLE 7

GATE mean diurnal temperature deviations from the daily mean. For local time subtract 1½ hours from Z time values shown.

B-scale

| P(mb) | 00Z | 03Z | 06Z | 09Z | 12Z | 15Z | 18Z | 21Z |
|---|---|---|---|---|---|---|---|---|
| Surf | -.12 | -.32 | -.34 | -.11 | +.23 | +.43 | +.23 | -.08 |
| 950 | +.06 | -.02 | -.10 | -.12 | +.05 | +.28 | -.01 | +.15 |
| 900 | +.05 | +.10 | -.08 | -.12 | +.05 | +.22 | -.01 | +.14 |
| 850 | +.07 | +.01 | -.09 | -.19 | +.06 | +.10 | -.02 | +.12 |
| 800 | +.06 | -.06 | -.13 | -.18 | +.06 | +.11 | +.02 | +.10 |
| 700 | -.02 | -.09 | -.12 | -.14 | +.09 | +.09 | +.06 | +.05 |
| 600 | -.05 | +.01 | -.16 | -.23 | +.12 | +.19 | +.10 | +.04 |
| 500 | -.04 | -.06 | -.23 | -.01 | +.19 | +.27 | +.09 | +.14 |
| 400 | -.21 | -.27 | -.35 | +.07 | +.33 | +.51 | +.24 | +.05 |
| 300 | -.26 | -.43 | -.44 | -.05 | +.38 | +.71 | +.34 | -.09 |
| 250 | -.30 | -.39 | -.47 | +.11 | +.46 | +.66 | +.32 | -.14 |
| 200 | -.37 | -.49 | -.41 | +.12 | +.53 | +.66 | +.27 | -.33 |
| 150 | -.47 | -.34 | -.28 | +.39 | +.70 | +.38 | +.03 | -.55 |
| 100 | -.31 | -.25 | -.29 | +.63 | +.72 | +.10 | -.25 | +.01 |
| 75 | -.49 | -.78 | -.58 | +1.02 | +.67 | +.71 | +.10 | -.78 |

4.1 Determination of Warming, Cooling and Rainfall Cases

The data set described here is based on individual soundings which demonstrate a specific feature observed at a point location. Categorization of sonde data resulted in the following cases:

1) Warming Case - instances where a positive $\frac{\partial T}{\partial t}$ of $\geq .7^{\circ}C$ per 3-6 hours was observed in the vertical column from 500-200 mb.

2) Cooling Case - instances where a negative $\frac{\partial T}{\partial t}$ of $\geq 1.0^{\circ}C$ per 3-6 hours was observed in the vertical column from 500-200 mb.

3) Rainfall Case - where it was determined from shipboard rain gauges that rain was falling on a particular ship coincident with the ascent of a rawinsonde from that ship.

The Warming Cases and Cooling Cases were further sub-divided into Non-squall and Squall events (see Table 8 for a list of Squall days), because these two categories differ so greatly in cloud organization and speed of rain propagation through the B-scale network. The convection associated with Non-squall Cases is much more steady-state when compared with the rapidly moving Squall Cases. Time stratifications were then developed based on the sounding times for the Rainfall, Warming and Cooling Cases. These include 3-6 hours before the event (PRE), the time of the event itself (0) and 3-6 hours after the event (POST). For the Rainfall Case, these times are 2-3½ hours before the rainfall (BEFORE RAIN), the sounding time when rain is falling at the ship (DURING RAIN) and 2-3½ hours after the rainfall (AFTER RAIN). (See Table 9 for a listing of all these case types, and Tables 10-12 for a listing of all the soundings comprising these cases.)

TABLE 8

Squall Days in GATE

| Julian Day |
|---|
| 179 |
| 221-222 |
| 247 |
| 254 |
| 255 |
| 259 |

As can be seen from Tables 10 and 11 there are considerably fewer upper level cooling (30) than warming (73) cases. This is partly a result of the cooling soundings which were eliminated due to the fact that they show cooling throughout the entire vertical column. They were not included because they do not satisfy hydrostatic constraints,

TABLE 9

Listing of Warming and Cooling Data Stratifications

1) Rainfall Case

   a. Prior to Rainfall
   b. During Rainfall
   c. After Rainfall

2) Warming Case - Non-Squall

   a. Pre-Warming
   b. Warming
   c. Post-Warming

   Warming Case - Squall

   a. Pre-Warming
   b. Warming
   c. Post-Warming

3) Cooling Case - Non-Squall

   a. Pre-Cooling
   b. Cooling
   c. Post-Cooling

   Cooling Case - Squall

   a. Pre-Cooling
   b. Cooling
   c. Post-Cooling

---

and are therefore physically unrealistic. For example, with 3-hourly temperature changes such as those measured by the Dallas between the Day 225, 2106Z sounding and the Day 226, 0010Z sounding there was a mean column cooling of 1.1$^{o}$C which should result in a hydrostatic thickness change equivalent to about 9 mb. This magnitude of pressure decrease was never observed. It is likely that such soundings were launched in or near areas of drizzle or thick cloud, such that the radiosonde became wet. Subsequent evaporation from the sonde would then cause a continuous reading of particularly large cooling

TABLE 10

List of Warming Case soundings for three time stratifications. Pre-warming and Post-warming refer to 3-6 hours prior to and following the warming event, respectively.

SQUALL CASES

| Pre-Warming | | | Warming | | | Post-Warming | | |
|---|---|---|---|---|---|---|---|---|
| Ship | J.D. | Time (Z) | Ship | J.D. | Time (Z) | Ship | J.D. | Time (Z) |
| Quadra | 221 | 1500 | Quadra | 221 | 2105 | Quadra | 222 | 0005 |
| Vanguard | 222 | 0301 | Vanguard | 222 | 0538 | Vanguard | 222 | 0840 |
| Gilliss | 222 | 0557 | Gilliss | 222 | 1153 | Gilliss | 222 | 1439 |
| Oceanographer | 222 | 1206 | Oceanographer | 222 | 1501 | Oceanographer | 222 | 1800 |
| Oceanographer | 247 | 1205 | Oceanographer | 247 | 1802 | Oceanographer | 247 | 2103 |
| Vanguard | 247 | 1432 | Vanguard | 247 | 2027 | Vanguard | 247 | 2332 |
| Quadra | 254 | 1204 | Quadra | 254 | 1501 | Quadra | 254 | 1801 |
| Oceanographer | 254 | 1801 | Oceanographer | 254 | 2216 | Oceanographer | 255 | 0037 |
| Dallas | 255 | 0258 | Dallas | 255 | 0605 | Dallas | 255 | 0908 |
| Vanguard | 255 | 1136 | Vanguard | 255 | 1425 | Vanguard | 255 | 1731 |
| Dallas | 255 | 2058 | Dallas | 256 | 0001 | Dallas | 256 | 0301 |
| Oceanographer | 259 | 0903 | Oceanographer | 259 | 1202 | Oceanographer | 259 | 1506 |
| Oceanographer | 259 | 1506 | Oceanographer | 259 | 1813 | Oceanographer | 259 | 2111 |

NON-SQUALL CASES

| | | | | | | | | |
|---|---|---|---|---|---|---|---|---|
| Meteor | 180 | 0558 | Meteor | 180 | 1159 | Meteor | 180 | 1805 |
| Quadra | 181 | 0559 | Quadra | 181 | 1202 | Quadra | 181 | 1801 |
| Vize | 181 | 1130 | Vize | 181 | 1730 | Vize | 182 | 0148 |
| Researcher | 182 | 2043 | Researcher | 182 | 2343 | Researcher | 183 | 0304 |
| Vize | 183 | 0648 | Vize | 183 | 1130 | Vize | 183 | 1730 |
| Vanguard | 187 | 2352 | Vanguard | 188 | 0553 | Vanguard | 188 | 1156 |
| Dallas | 188 | 1201 | Dallas | 188 | 1508 | Dallas | 188 | 1756 |

TABLE 10 (cont'd)

NON-SQUALL CASES

| Pre-Warming | | | Warming | | | Post-Warming | | |
|---|---|---|---|---|---|---|---|---|
| Ship | J.D. | Time (Z) | Ship | J.D. | Time (Z) | Ship | J.D. | Time (Z) |
| Quadra | 188 | 1204 | Quadra | 188 | 1800 | Quadra | 188 | 2107 |
| Dallas | 189 | 0006 | Dallas | 189 | 0544 | Dallas | 189 | 0843 |
| Vize | 191 | 0530 | Vize | 191 | 1130 | Vize | 191 | 1736 |
| Meteor | 191 | 0901 | Meteor | 191 | 1203 | Meteor | 191 | 1454 |
| Quadra | 192 | 0004 | Quadra | 192 | 0604 | Quadra | 192 | 1203 |
| Dallas | 194 | 0604 | Dallas | 194 | 0857 | Dallas | 194 | 1209 |
| Quadra | 194 | 1202 | Quadra | 194 | 1801 | Quadra | 194 | 2121 |
| Dallas | 194 | 2059 | Dallas | 195 | 0011 | Dallas | 195 | 0259 |
| Meteor | 195 | 0253 | Meteor | 195 | 0628 | Meteor | 195 | 0858 |
| Vize | 196 | 2354 | Vize | 197 | 0230 | Vize | 197 | 0612 |
| | | | Researcher | 197 | 0556 | Researcher | 197 | 1151 |
| Meteor | 209 | 2354 | Meteor | 210 | 0557 | Meteor | 210 | 0902 |
| Dallas | 215 | 0026 | Dallas | 215 | 0606 | Dallas | 215 | 0907 |
| Dallas | 215 | 0907 | Dallas | 215 | 1202 | Dallas | 215 | 1806 |
| Meteor | 216 | 0309 | Meteor | 216 | 0642 | Meteor | 216 | 0902 |
| Dallas | 217 | 0016 | Dallas | 217 | 0305 | Dallas | 217 | 0601 |
| Dallas | 217 | 0601 | Dallas | 217 | 0905 | Dallas | 217 | 1515 |
| Vanguard | 219 | 0612 | Vanguard | 219 | 1132 | Vanguard | 219 | 1728 |
| Meteor | 220 | 0301 | Meteor | 220 | 0610 | | | |
| Meteor | 220 | 0900 | Meteor | 220 | 1200 | | | |
| Meteor | 220 | 1806 | Meteor | 220 | 2107 | Meteor | 221 | 0017 |
| Quadra | 223 | 0002 | Quadra | 223 | 0301 | Quadra | 223 | 0603 |
| Gilliss | 223 | 1146 | Gilliss | 223 | 1755 | Gilliss | 223 | 2325 |
| Vize | 226 | 0230 | Vize | 226 | 0700 | Vize | 226 | 0830 |
| Vize | 226 | 1430 | Vize | 226 | 1730 | Vize | 226 | 2030 |
| Gilliss | 227 | 0224 | Gilliss | 227 | 0554 | Gilliss | 227 | 0841 |
| Meteor | 242 | 2122 | Meteor | 243 | 0301 | | | |

TABLE 10 (cont'd)

NON-SQUALL CASES

| Pre-Warming | | | Warming | | | Post-Warming | | |
|---|---|---|---|---|---|---|---|---|
| Ship | J.D. | Time (Z) | Ship | J.D. | Time (Z) | Ship | J.D. | Time (Z) |
| Researcher | 244 | 0246 | Researcher | 244 | 0538 | Researcher | 244 | 0848 |
| Vanguard | 244 | 1729 | Vanguard | 244 | 2034 | Vanguard | 244 | 2332 |
| Researcher | 245 | 0551 | Researcher | 245 | 0853 | Researcher | 245 | 1152 |
| Researcher | 245 | 2356 | Researcher | 246 | 0257 | Researcher | 246 | 0552 |
| Researcher | 246 | 0552 | Researcher | 246 | 1155 | Researcher | 246 | 1751 |
| Oceanographer | 246 | 1205 | Oceanographer | 246 | 1501 | Oceanographer | 246 | 1803 |
| Dallas | 246 | 1503 | Dallas | 246 | 1800 | Dallas | 246 | 2058 |
| Quadra | 246 | 1503 | Quadra | 246 | 1800 | Quadra | 246 | 2103 |
| Quadra | 248 | 0002 | Quadra | 248 | 0311 | Quadra | 248 | 0606 |
| Oceanographer | 248 | 1205 | Oceanographer | 248 | 1521 | Oceanographer | 248 | 1800 |
| Oceanographer | 249 | 0601 | Oceanographer | 249 | 0907 | Oceanographer | 249 | 1212 |
| Meteor | 249 | 0602 | Meteor | 249 | 1207 | Meteor | 249 | 1459 |
| Oceanographer | 250 | 0007 | Oceanographer | 250 | 0300 | Oceanographer | 250 | 0610 |
| Dallas | 250 | 2100 | Dallas | 251 | 0000 | Dallas | 251 | 0304 |
| Oceanographer | 250 | 2101 | Oceanographer | 251 | 0005 | Oceanographer | 251 | 0603 |
| Meteor | 251 | 0004 | Meteor | 251 | 0558 | Meteor | 251 | 0857 |
| Meteor | 251 | 1510 | Meteor | 251 | 2113 | Meteor | 252 | 0006 |
| Vize | 252 | 0718 | Vize | 252 | 1136 | Vize | 252 | 1730 |
| Oceanographer | 253 | 0602 | Oceanographer | 253 | 0913 | Oceanographer | 253 | 1203 |
| Meteor | 253 | 1453 | Meteor | 253 | 1800 | Meteor | 253 | 2057 |
| Quadra | 256 | 0530 | Quadra | 256 | 0906 | Quadra | 256 | 1200 |
| Vanguard | 256 | 1436 | Vanguard | 256 | 1734 | Vanguard | 256 | 2037 |
| Quadra | 256 | 2103 | Quadra | 257 | 0016 | Quadra | 257 | 0302 |
| Researcher | 258 | 1149 | Researcher | 258 | 1757 | Researcher | 259 | 0001 |
| Vanguard | 258 | 1428 | Vanguard | 258 | 1725 | Vanguard | 258 | 2007 |
| Meteor | 260 | 0002 | Meteor | 260 | 0301 | Meteor | 260 | 0856 |

TABLE 11

List of Cooling Case soundings for three time stratifications. Pre-cooling and Post-cooling refer to 3-6 hours prior to and following the cooling event, respectively.

SQUALL CASES

| Pre-Cooling | | | Cooling | | | Post-Cooling | | |
|---|---|---|---|---|---|---|---|---|
| Ship | J.D. | Time (Z) | Ship | J.D. | Time (Z) | Ship | J.D. | Time (Z) |
| Oceanographer | 179 | 0009 | Oceanographer | 179 | 0600 | Oceanographer | 179 | 0912 |
| Quadra | 221 | 2105 | Quadra | 222 | 0005 | Quadra | 222 | 0306 |
| Vize | 222 | 0530 | Vize | 222 | 0912 | Vize | 222 | 1130 |
| Oceanographer | 222 | 0858 | Oceanographer | 222 | 1206 | Oceanographer | 222 | 1501 |
| Researcher | 222 | 1157 | Researcher | 222 | 1453 | Researcher | 222 | 1801 |
| Oceanographer | 222 | 1501 | Oceanographer | 222 | 1800 | Oceanographer | 222 | 2108 |
| | | | Researcher | 222 | 2045 | Researcher | 222 | 2346 |
| Vize | 254 | 0830 | Vize | 254 | 1136 | Vize | 254 | 1430 |
| Vize | 258 | 2336 | Vize | 259 | 0230 | Vize | 259 | 0530 |
| Vanguard | 258 | 2331 | Vanguard | 259 | 0523 | Vanguard | 259 | 0818 |
| Oceanographer | 259 | 1202 | Oceanographer | 259 | 1506 | Oceanographer | 259 | 1813 |

NON-SQUALL CASES

| | | | | | | | | |
|---|---|---|---|---|---|---|---|---|
| Meteor | 180 | 0019 | Meteor | 180 | 0558 | Meteor | 180 | 1159 |
| Dallas | 188 | 1508 | Dallas | 188 | 1756 | Dallas | 188 | 2053 |
| Meteor | 191 | 0559 | Meteor | 191 | 0901 | Meteor | 191 | 1203 |
| Vize | 194 | 2036 | Vize | 194 | 2336 | Vize | 195 | 0230 |
| Quadra | 196 | 1205 | Quadra | 196 | 1804 | Quadra | 197 | 0000 |
| Oceanographer | 210 | 2353 | Oceanographer | 211 | 0557 | Oceanographer | 211 | 1159 |
| Dallas | 216 | 2125 | Dallas | 217 | 0016 | Dallas | 217 | 0305 |
| Dallas | 217 | 0305 | Dallas | 217 | 0601 | Dallas | 217 | 0905 |
| Meteor | 220 | 2107 | Meteor | 221 | 0017 | Meteor | 221 | 0338 |
| Vize | 223 | 0236 | Vize | 223 | 0712 | Vize | 223 | 1300 |
| Meteor | 224 | 2104 | Meteor | 224 | 2355 | Meteor | 225 | 0304 |

TABLE 11 (cont'd)

NON-SQUALL CASES

| Pre-Cooling | | | Cooling | | | Post-Cooling | | |
|---|---|---|---|---|---|---|---|---|
| Ship | J.D. | Time (Z) | Ship | J.D. | Time (Z) | Ship | J.D. | Time (Z) |
| Researcher | 242 | 1153 | Researcher | 242 | 1743 | Researcher | 242 | 2046 |
| Quadra | 243 | 1517 | Quadra | 243 | 1809 | Quadra | 243 | 2100 |
| Vanguard | 244 | 2034 | Vanguard | 244 | 2332 | Vanguard | 245 | 0241 |
| Researcher | 246 | 0257 | Researcher | 246 | 0552 | Researcher | 246 | 1155 |
| Quadra | 246 | 0302 | Quadra | 246 | 0601 | Quadra | 246 | 0902 |
| Quadra | 252 | 0005 | Quadra | 252 | 0301 | Quadra | 252 | 0600 |
| Meteor | 253 | 0004 | Meteor | 253 | 0304 | Meteor | 253 | 0558 |
| Dallas | 253 | 1804 | Dallas | 253 | 2101 | Dallas | 254 | 0012 |

TABLE 12

List of Rainfall Case soundings for three time stratifications. Before Rain Events and After Rain Events encompass 2-3½ hours prior to and following the rainfall, respectively. The During Rain Events stratification is comprised of more soundings than the other two stratifications because rain frequently continues at a ship for more than one sounding period.

| Before Rain Events | | | During Rain Events | | | After Rain Events | | |
|---|---|---|---|---|---|---|---|---|
| Ship | J.D. | Time (Z) | Ship | J.D. | Time (Z) | Ship | J.D. | Time (Z) |
| Oceanographer | 181 | 1828 | Researcher | 179 | 0008 | Quadra | 183 | 0929 |
| Researcher | 182 | 0858 | Researcher | 179 | 0103 | Quadra | 183 | 2100 |
| Oceanographer | 183 | 0310 | Researcher | 179 | 0600 | Krenkel | 185 | 0848 |
| Quadra | 183 | 0304 | Researcher | 179 | 1206 | Krenkel | 187 | 1448 |
| Dallas | 183 | 0843 | Researcher | 180 | 1747 | Krenkel | 189 | 1154 |
| Researcher | 189 | 0851 | Researcher | 180 | 2348 | Zubov | 191 | 1130 |
| Gilliss | 195 | 0605 | Vanguard | 181 | 2045 | Okean | 193 | 0300 |
| Vanguard | 210 | 1133 | Researcher | 182 | 1205 | Zubov | 193 | 1430 |
| Dallas | 211 | 0005 | Researcher | 182 | 1451 | Okean | 194 | 0000 |
| Vize | 212 | 2330 | Researcher | 183 | 0304 | Quadra | 194 | 1202 |
| Dallas | 213 | 0613 | Oceanographer | 183 | 0849 | Okean | 194 | 1500 |
| Quadra | 213 | 1503 | Vanguard | 183 | 0848 | Vanguard | 194 | 1750 |
| Vize | 213 | 1430 | Oceanographer | 183 | 1210 | Dallas | 195 | 0906 |
| Vanguard | 214 | 0530 | Dallas | 183 | 1506 | Priboy | 195 | 1430 |
| Vize | 214 | 1730 | Quadra | 183 | 1800 | Vize | 195 | 1736 |
| Dallas | 217 | 0305 | Researcher | 183 | 2056 | Poryv | 196 | 0600 |
| Vanguard | 217 | 2329 | Researcher | 186 | 1754 | Zubov | 196 | 2330 |
| Gilliss | 242 | 1805 | Vanguard | 189 | 0003 | Quadra | 210 | 1803 |
| Researcher | 245 | 1450 | Vanguard | 189 | 1755 | Quadra | 212 | 1202 |
| Dallas | 248 | 0900 | Quadra | 194 | 1500 | Vize | 213 | 0830 |
| Quadra | 252 | 0900 | Dallas | 194 | 1817 | Krenkel | 213 | 2330 |
| Vanguard | 252 | 1130 | Dallas | 195 | 0011 | Gilliss | 221 | 0249 |
| Oceanographer | 254 | 1503 | Dallas | 195 | 0259 | Oceanographer | 222 | 0858 |
| Vanguard | 256 | 1436 | Gilliss | 195 | 1207 | Oceanographer | 242 | 0559 |

TABLE 12 (cont'd)

| Before Rain Events | | | During Rain Events | | | After Rain Events | | |
|---|---|---|---|---|---|---|---|---|
| Ship | J.D. | Time (Z) | Ship | J.D. | Time (Z) | Ship | J.D. | Time (Z) |
| Vize | 257 | 1130 | Gilliss | 195 | 1804 | Gilliss | 242 | 2344 |
| Oceanographer | 259 | 0315 | Oceanographer | 196 | 0259 | Okean | 245 | 1730 |
| Vanguard | 259 | 1723 | Researcher | 209 | 0552 | Korolov | 246 | 0230 |
| Quadra | 260 | 1204 | Dallas | 209 | 0605 | Oceanographer | 247 | 2103 |
| Oceanographer | 262 | 0900 | Researcher | 209 | 0853 | Dallas | 248 | 1809 |
| | | | Dallas | 211 | 1803 | Korolov | 249 | 1130 |
| | | | Vize | 213 | 0536 | Quadra | 252 | 1512 |
| | | | Dallas | 213 | 0914 | Oceanographer | 255 | 0306 |
| | | | Vanguard | 213 | 1442 | Dallas | 255 | 1800 |
| | | | Dallas | 213 | 1803 | Oceanographer | 255 | 1804 |
| | | | Dallas | 214 | 0611 | Oceanographer | 259 | 2111 |
| | | | Quadra | 214 | 1805 | Gillis | 260 | 1811 |
| | | | Oceanographer | 214 | 2113 | Quadra | 260 | 1803 |
| | | | Dallas | 217 | 0905 | | | |
| | | | Vanguard | 218 | 0543 | | | |
| | | | Gilliss | 218 | 1149 | | | |
| | | | Gilliss | 220 | 1759 | | | |
| | | | Vanguard | 221 | 2036 | | | |
| | | | Vanguard | 224 | 2338 | | | |
| | | | Vanguard | 225 | 1744 | | | |
| | | | Oceanographer | 242 | 0036 | | | |
| | | | Oceanographer | 242 | 0259 | | | |
| | | | Researcher | 245 | 1747 | | | |
| | | | Gilliss | 248 | 0936 | | | |
| | | | Dallas | 248 | 1501 | | | |
| | | | Quadra | 248 | 1501 | | | |
| | | | Oceanographer | 249 | 0601 | | | |
| | | | Quadra | 252 | 1201 | | | |
| | | | Vanguard | 252 | 1730 | | | |

TABLE 12 (cont'd)

| Before Rain Events | | | During Rain Events | | | After Rain Events | | |
|---|---|---|---|---|---|---|---|---|
| Ship | J.D. | Time (Z) | Ship | J.D. | Time (Z) | Ship | J.D. | Time (Z) |
| | | | Oceanographer | 254 | 2216 | | | |
| | | | Researcher | 254 | 2357 | | | |
| | | | Dallas | 255 | 0908 | | | |
| | | | Dallas | 255 | 1235 | | | |
| | | | Oceanographer | 255 | 1513 | | | |
| | | | Quadra | 256 | 0530 | | | |
| | | | Quadra | 256 | 0906 | | | |
| | | | Quadra | 256 | 1200 | | | |
| | | | Dallas | 256 | 1501 | | | |
| | | | Quadra | 256 | 1524 | | | |
| | | | Vanguard | 256 | 1734 | | | |
| | | | Dallas | 256 | 2102 | | | |
| | | | Vanguard | 256 | 2037 | | | |
| | | | Dallas | 257 | 0300 | | | |
| | | | Meteor | 257 | 0302 | | | |
| | | | Gilliss | 257 | 1514 | | | |
| | | | Meteor | 257 | 1816 | | | |
| | | | Vanguard | 257 | 2326 | | | |
| | | | Oceanographer | 259 | 0600 | | | |
| | | | Meteor | 259 | 0906 | | | |
| | | | Researcher | 259 | 1152 | | | |
| | | | Oceanographer | 259 | 1202 | | | |
| | | | Researcher | 259 | 1812 | | | |
| | | | Gilliss | 260 | 1455 | | | |
| | | | Quadra | 260 | 1502 | | | |
| | | | Quadra | 262 | 0901 | | | |

unrepresentative of the surrounding air. Another example which likely experienced this effect is the Researcher, 248, 0849Z sounding. When compared to the previous 0617Z sounding, a cooling of between 0.6 to 2.6°C was reported at nearly every vertical level. And, in fact, the rainfall accompanying this reported cooling was a light rain and drizzle.

## 4.2 Characteristics of Warming, Cooling and Rainfall Cases

Table 13 and Figs. 15, 16 and 17 demonstrate a rather significant result obtained from this investigation. From Table 13 it can be seen that not only are 67% of all the days in GATE Warming Case days, but 75% of the Cooling Case days are also Warming Case days, indicating that these events occur on a quite frequent basis, and neither event takes place in an environment exclusive of the other. Cooling and Warming Cases often occur simultaneously at different locations within the same environment, and it can be further concluded that this environment is most frequently a convective one, since only 11% of the individual Warming and Cooling Cases were characterized by no echo or too little echo to be significant. The pre-warming state in Fig. 16 is observed to be cool, and similarly, the pre-cooling environment in Fig. 17 is observed to be warm. The fact that most Warming and Cooling Cases demonstrate this 3-6 hourly temperature trend is likely a result of the case selection procedure, since only the largest 3-6 hourly warming and cooling events were chosen. These would frequently be the ones which had gone from measurements of very warm temperatures at one time period to measurements of very cool temperatures the next, or vice-versa. Based on modelling results of W. Fingerhut (Chapter 7) it is not believed likely that these warming and cooling events are of 3-6 hour duration, but

TABLE 13

Days of Warming and Cooling Cases

| Cooling Days | | | Warming Days | | | Days in Common | | |
|---|---|---|---|---|---|---|---|---|
| Phase I | Phase II | Phase III | Phase I | Phase II | Phase III | Phase I | Phase II | Phase III |
| 179 | 211 | 242 | 180 | 210 | 243 | 180 | 217 | 243 |
| 180 | 217 | 243 | 181 | 215 | 244 | 188 | 220 | 244 |
| 188 | 220 | 244 | 182 | 216 | 245 | 191 | 222 | 246 |
| 191 | 222 | 246 | 183 | 217 | 246 | 194 | 223 | 252 |
| 194 | 223 | 252 | 188 | 219 | 247 | | | 253 |
| 196 | 225 | 253 | 189 | 220 | 248 | | | 254 |
| | | 254 | 191 | 221 | 249 | | | 259 |
| | | 259 | 192 | 222 | 250 | | | |
| | | | 194 | 223 | 251 | | | |
| | | | 195 | 226 | 252 | | | |
| | | | 197 | 227 | 253 | | | |
| | | | | | 254 | | | |
| | | | | | 255 | | | |
| | | | | | 256 | | | |
| | | | | | 257 | | | |
| | | | | | 258 | | | |
| | | | | | 259 | | | |
| | | | | | 260 | | | |

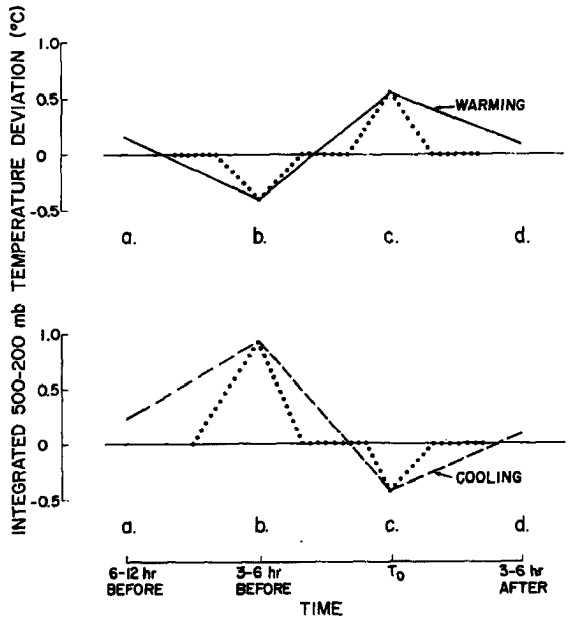


Fig. 15. Mean temperature deviations associated with the time sequence of warming (——) and cooling (- - -) events (500-200 mb). An interpretation of how warming and cooling may actually occur, as deduced from numerical modeling results (· · ·).

instead last closer to one hour. Therefore, one sonde could be launched so that it ascends through an anomalously cool region, while the sonde launched 3-6 hours later from the same platform may ascend into a particularly warm area. In view of an hour long time frame, the observed 3-6 hourly changes in temperature deviation can be interpreted as short ($\sim$ 1 hour) concentrated (10-100 km) temperature increases and decreases separated in time by a period of relatively neutral temperature structure. See the alternate temperature change lines in Fig. 15. If this interpretation is a valid one, then the measured 3-6 hour temperature changes of from $1^{\circ}$ to $2^{\circ}$C may be overestimates of the actual warming and cooling amounts, which are likely closer to $.5^{\circ}$ to $1.5^{\circ}$C. Thus, upper limits can be placed on the time and space scales of upper level warming and cooling events, but they cannot be completely resolved

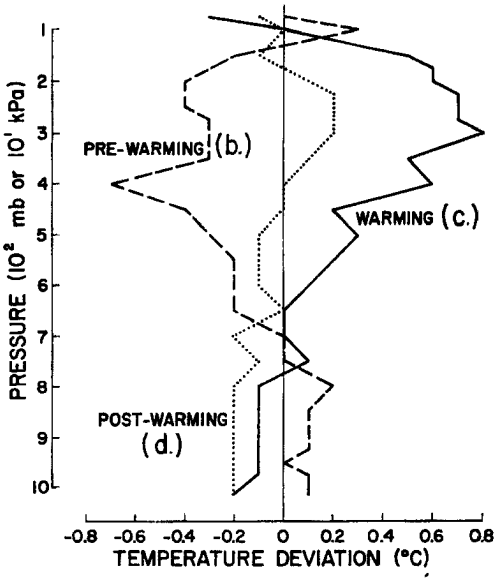


Fig. 16. Average temperature deviation profiles for the various Warming Case time stratifications. Pre-warming and Post-warming refer to 3-6 hours before and after the warming event, respectively. Letters refer to those in Fig. 15.

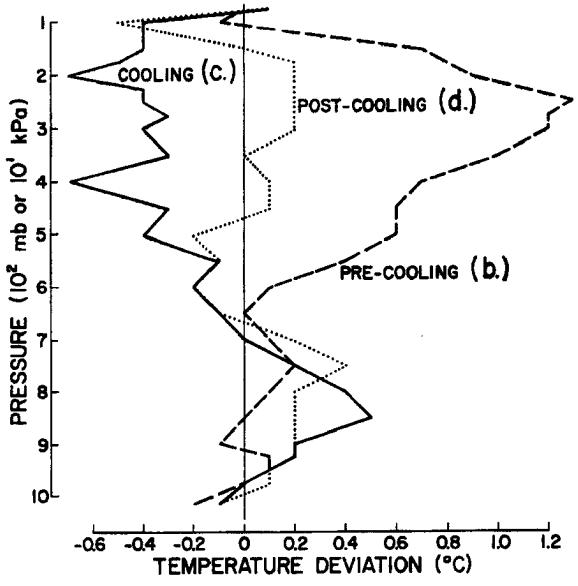


Fig. 17. Same as Fig. 16, except for the Cooling Case.

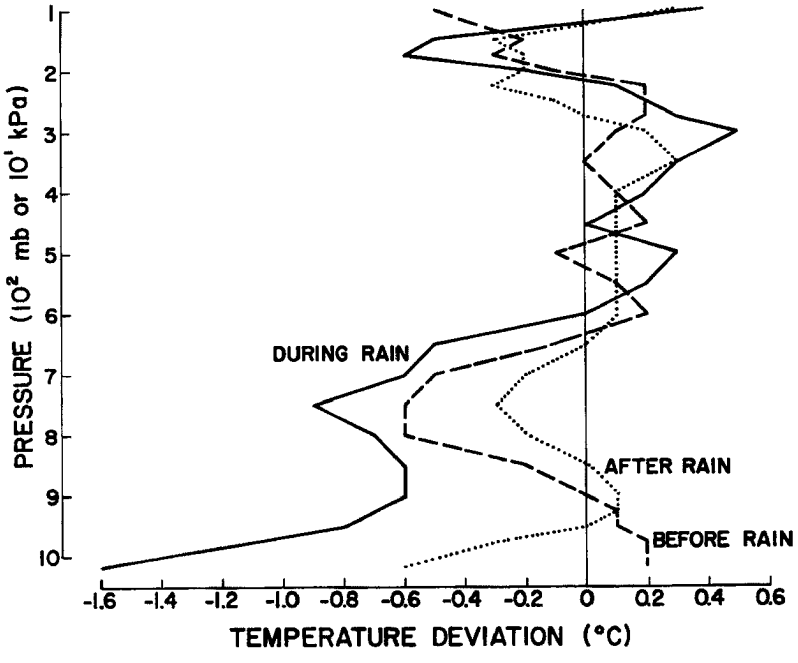


Fig. 18. Same as Fig. 16, except for the Rainfall Case. Before Rain and After Rain refer to 2-3½ hours prior to and following a rain event, respectively.

by the B-scale rawinsonde network. However, since these warming and cooling time intervals are considerably shorter than the time scale of passage of a cloud cluster through the B-array, the 3-6 hour interval observations of both warming and cooling do indicate that cooling and warming mechanisms are both at work within the same convective system.

To obtain an average picture of what the atmosphere looks like at the actual Warming, Cooling and Rainfall Case sounding locations, all soundings comprising a particular case were averaged. This compositing at a point location yields a profile of the mean vertical structure at a particular site. Figures 16 and 17 show the average temperature deviation profiles for the various warming and cooling time stratifications. For comparison the temperature deviations of the Rainfall Cases are shown in Fig. 18. Figure 18 demonstrates once again the typical temperature profile which accompanies a raining environment, generally cool except for the layer between about 500-250 mb. The large degree of upper level warming and cooling in Figs. 16 and 17 should be noted for comparison. Temperature anomalies at upper levels prior to warming and cooling appear large, as are the 3-6 hour temperature changes which follow. By contrast, warming and cooling changes at lower levels are significantly smaller.

A similar graph for the Rainfall Case moisture profile (Fig. 19) shows a generally moist environment with downdraft drying in lowest levels. The cooling environment (not shown) is moist at all levels while the warming environment can be said to be neither moist nor dry. Subsidence accompanying the warming should result in drying; that a net drying is not observed by the rawinsonde is likely due to the convective environment in which warming events take place and the time lag of the

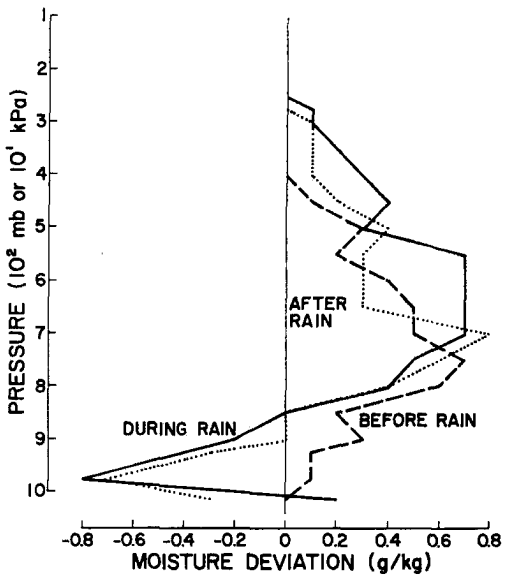


Fig. 19. Average moisture deviation profile for the various Rainfall Case time stratifications. Before Rain and After Rain refer to 2-3½ hours prior to and following a rain event, respectively.

sounding to the subsidence events. A convective environment is characterized by a good deal of cumulus moisture diffusion and evaporation which would act to cancel the subsidence drying.

An examination by W. M. Gray (1975) of all middle level U.S. aircraft observations within and around the GATE B-array showed that there were many cases of middle level humidity decrease of 10-30% accompanying cloud-scale (10-100 km) 0.5° to 1.5°C warming events. Such observations of middle level warming appear to support the rawinsonde measurements of temperature deviation. As with the rawinsonde data, temperature anomalies of greater than 1½°C were seldom encountered at these levels.

The two types of positive temperature anomaly discussed thus far are 1) the B-scale (100-500 km) area upper level positive temperature anomaly occurring in the presence of meso-scale convection (described in Chapter 3) and 2) the smaller time (3-6 hours or less) and space

(10-100 km) scale upper level warming events. For comparison, both types are shown on the same graph in Fig. 20. It is believed that the larger scale (100-500 km) warmer temperatures occurring in the rain areas result from an accumulation and rapid spreading out of the smaller cloud scale (10-100 km) subsidence events.

Radiation values reported by Cox and Griffith (1978) indicate that radiationally produced daytime temperature changes for a disturbed environment are of the order of $-0.1^{\circ}C/3$ hr. Such temperature changes are too small to account for the observed magnitude of warming especially in view of the fact that GATE mean diurnal temperature effects have been subtracted out. In addition, it is interesting to note that about 50 percent of warming events occur at night (see Fig. 21). Sample advection calculations indicate that this term would also have a negligible affect on 3-6 hour temperature changes. Across the GATE B and A/B-scale networks, no systematic temperature gradient has been observed which could lead to the general advective temperature changes discussed here. Even if there are systematic temperature gradients across the B-array, these would likely not lead to horizontal temperature advection changes as variable and sharp as the ones discussed here. Once such gradients have been established, however, small scale local temperature advection likely does play a role.

Temperature Equation. The general equation for temperature change at upper levels can be written as:

$$\frac{\partial T}{\partial t} = - V \cdot \nabla T + \omega(\Gamma_d - \Gamma_a) + L(c-e) + Q_R \qquad (1)$$

(a) (b) (c) (d) (e)

where conventional symbols have been used (i.e., Yanai et al., 1973) and all quantities are defined for this scale. If both the advection (term b) and radiation (term e) terms are dismissed as being small in comparison with these special warming and cooling events, then only terms involved with vertical motion or convective processes (terms c + d) remain for producing the observed local changes in temperature (term a). In the net terms (c) and (d) very closely balance each other. In convective conditions, term (c) in upper levels is slightly greater than term (d). The opposite is typically the case in lower layers.

The convective terms can be more carefully examined by breaking them up into rising and sinking motion, thus:

$$\omega_u(\Gamma_d-\Gamma_a) + \omega_d(\Gamma_d-\Gamma_a) + Lc - Le, \text{ or} \qquad (2)$$

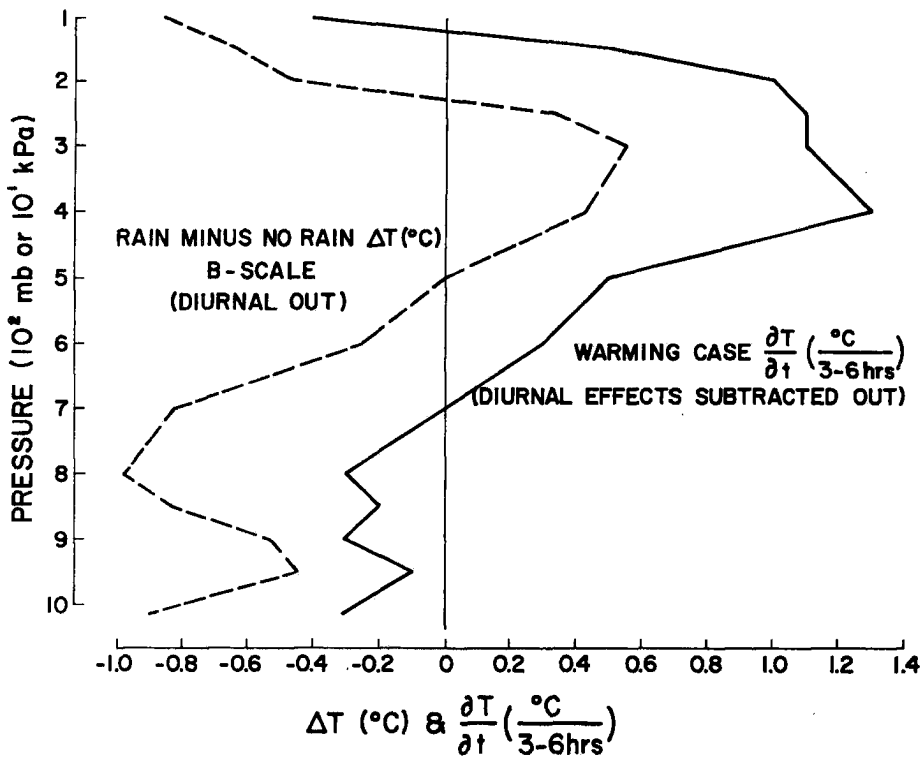


Fig. 20. Comparison in vertical profile form of B-scale averaged Rain Case minus No Rain Case warming amounts (all time periods averaged), and average Warming Case local temperature changes.

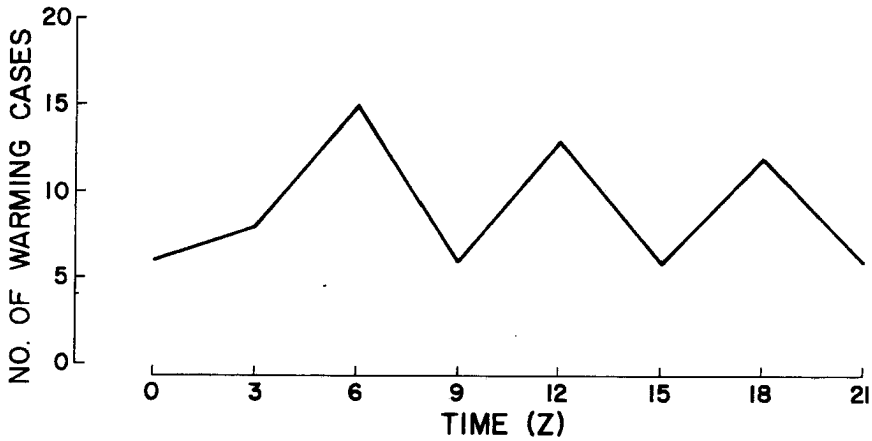


Fig. 21. Number of warming cases occurring at different times of day. Fewer cases at 3, 9, 15 and 21Z are a result of fewer soundings launched at these times.

$$\omega_u(\Gamma_d-\Gamma_a) + Lc + \omega_d(\Gamma_d-\Gamma_a) - Le \qquad (3)$$

(w) (x) (y) (z)

(rising motion) (sinking motion)

where subscript u stands for upward motion and d stands for downward motion. For rising motion in cumulus clouds, terms (w) and (x) are of opposite sign. The observational information of this paper indicates that they almost exactly cancel each other when integrated over the lifetime of the convective events. The net contribution of upward vertical motion to the observed warming and cooling is considered to be quite small. Term (y) is slightly larger than term (z) in the upper troposphere and is believed to be responsible for most of the upper level positive temperature anomaly associated with rain events. Because negative temperature deviations are typically observed at lower levels as a result of convective evaporation processes, it appears that term (y) is slightly smaller than term (z) for these situations. There are places and times when the data show this general trend to be reversed, and

upper level cooling [term (z) > term (y)] and low level warming [term (y) > term (z)] are present. Upper level cooling can occur due to residual liquid water at upper levels without compensating subsidence, or forced upward vertical motion associated with layered convection. Low level warming would be caused by subsidence at low levels without compensating evaporation.

The concept of subsidence as a means of warming has been discussed by Gray (1972, 1973), Yanai, Esbensen and Chu (1973), Betts (1973) and many others. Latent heat of condensation is utilized primarily in allowing air parcels to rise without cooling. Most condensation heat energy is converted to potential energy. Potential energy is exported from the individual convective system in its outflow levels. When the air later subsides, the cumulus warming is finally realized in an indirect fashion.

It is conjectured that the cases of upper level cooling included in this study were brought about for the most part by evaporation and perhaps in some situations by a forced vertical uplift [such as that proposed by Houze (1977) (based on Brown's (1974) numerical model) to explain the large percentages of anvil cloud precipitation observed in the 4-5 Sept. 1974 GATE squall line system.] It would be unreasonable to suppose that most of these cooling events could be due to layer uplifting, because most of the roughly 200 mb/day mean upward vertical motion associated with a cloud cluster is due to vertical motion occurring within individual cumulus and Cb elements. The data does not allow a direct correlation to be made between moisture changes and cooling events, although cooling generally does take place when the environment is convective.

4.3 Rawinsonde Composites

To learn something about the area surrounding these observations of rain at a ship and of anomalous upper level temperature changes from individual ship soundings, rawinsonde compositing was performed.

Composite Technique. Following the philosophy and general technique outlined in previous reports (see Williams and Gray (1973), Ruprecht and Gray (1976), George and Gray (1976), Frank (1976) and Zehr (1976)), a cylindrical grid divided into octants of 45° each was employed. The grid center was positioned at the location of the ship associated with the rainfall, warming or cooling sounding. For application to the GATE network, the cylinder was of 3.25° radius extending from the surface to 75 mb, and was marked off into 3 radial bands or "belts", chosen to make optimal use of the available sonde data. The horizontal grid is shown in Fig. 22. Belt #2 roughly corresponds to the size of the B-scale, (radius .75-2.00° latitude) and Belt #3 to the A/B-scale (2.00-3.25°). All available soundings surrounding a location measuring rainfall or anomalous temperature change fall into one of the 24 grid boxes. All the soundings in a particular box are averaged, and the 8 boxes in a particular belt are again averaged to get a mean value for that belt. In the case of wind data, an average radial wind ($V_r$) is calculated within a specific radius for each of the 8 octants, these $V_r$ values are mass balanced in the vertical, and from this a mass-balanced divergence profile is constructed. (See Appendix C regarding mass balancing techniques.)

Balloon Corrections. Rawinsonde balloon ascent from the surface to about 100 mb requires about 30-45 minutes and frequently results in a substantial drift of the balloon from the geographical position of

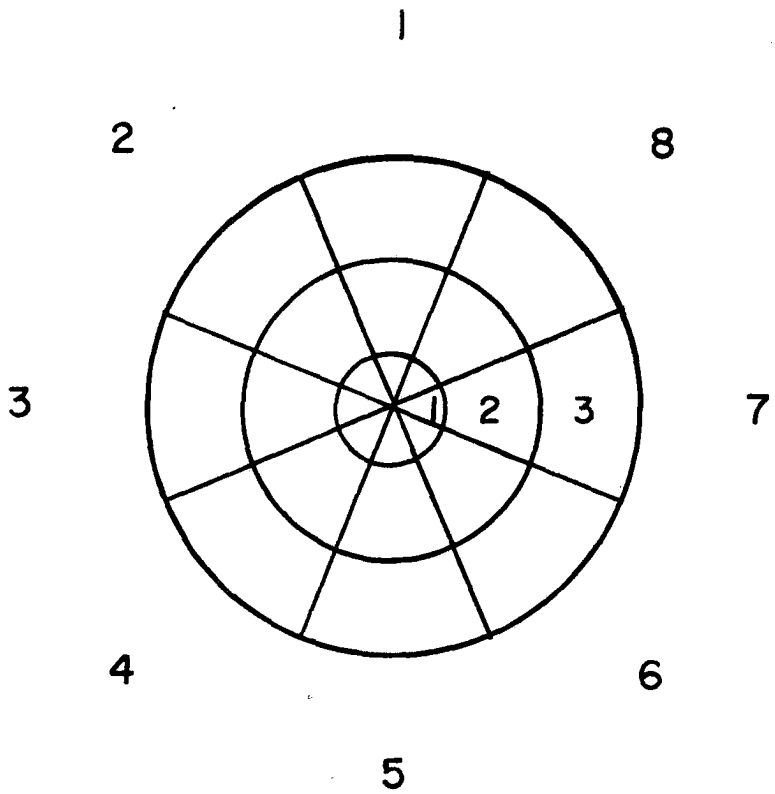


| Belt No. | Radius (°Lat.) |
|---|---|
| 1 | 0-.75 |
| 2 | .75-2.00 |
| 3 | 2.00-3.25 |

Fig. 22. Horizontal grid for rawinsonde composites.

its launch. These Δx (change in the east-west direction) and Δy (change in the north-south direction) correction values are a standard part of the rawinsonde data output, and were used in the belt compositing to assign the sondes to their proper box. They were also used in determining the center positions for the rawinsonde composites and for the radar composites described in a later section. For locating the exact upper level warming and cooling positions, the Δx and Δy corrections at 300 mb are taken as representative of upper tropospheric balloon drift.

Composite Results. Results of the rawinsonde composites are shown in Figs. 23-25 for temperature and Figs. 26-28 for moisture. Only composite results out to Belt #2 were used in these analyses because Belt #2 (annulus of radius .75-2.00°, with average radius 1.5°)

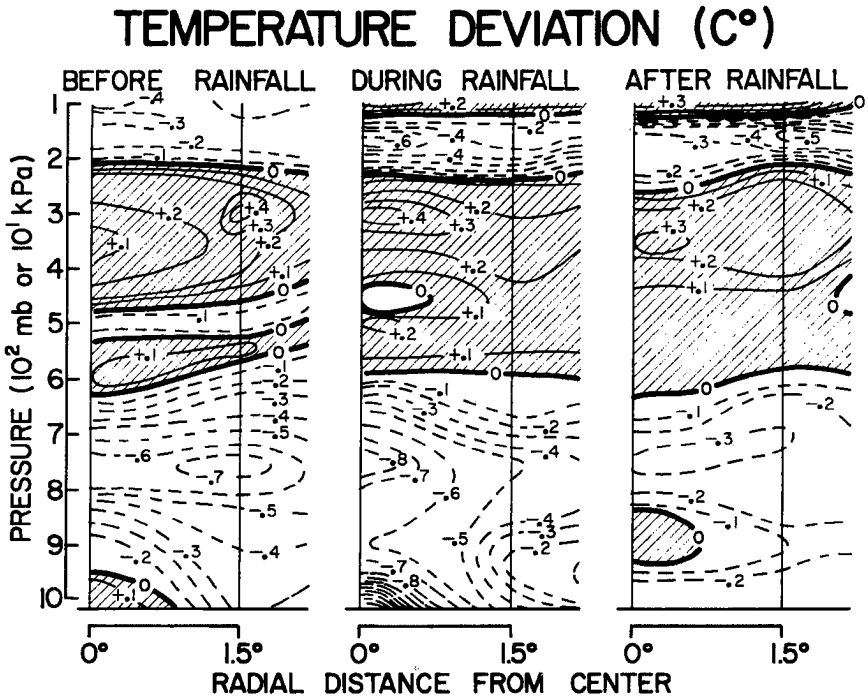


Fig. 23. Vertical cross-sections of Rainfall Case rawinsonde composite temperature deviations out to 2.00° radius. Before Rain and After Rain refer to 2-3½ hours prior to and following a rain event, respectively (contoured from belt averages).

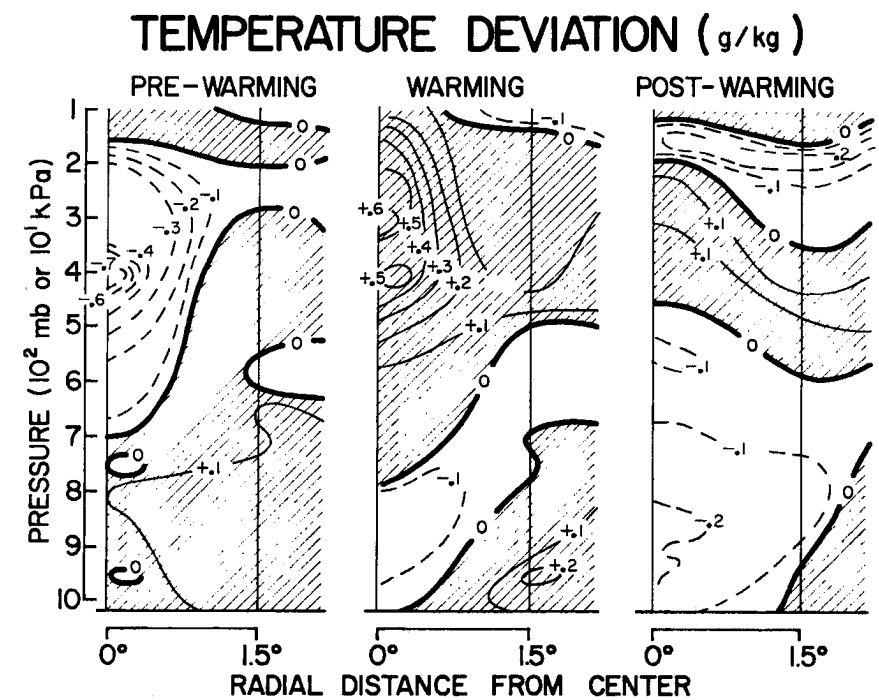


Fig. 24. Same as Fig. 23, except for the Warming Case. Pre-warming and Post-warming refer to 3-6 hours before and after the warming event, respectively.

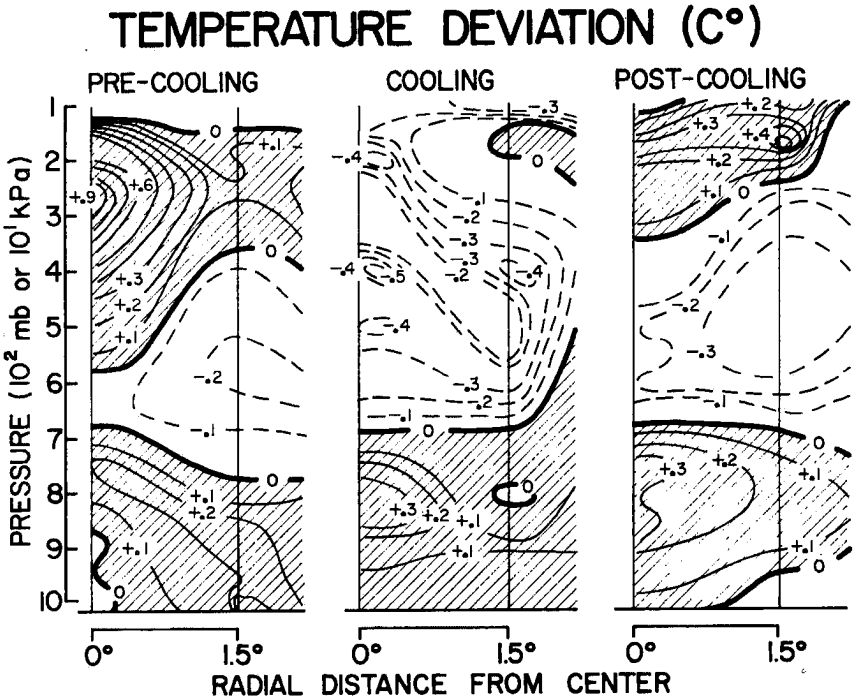


Fig. 25. Same as Fig. 24, except for the Cooling Case.

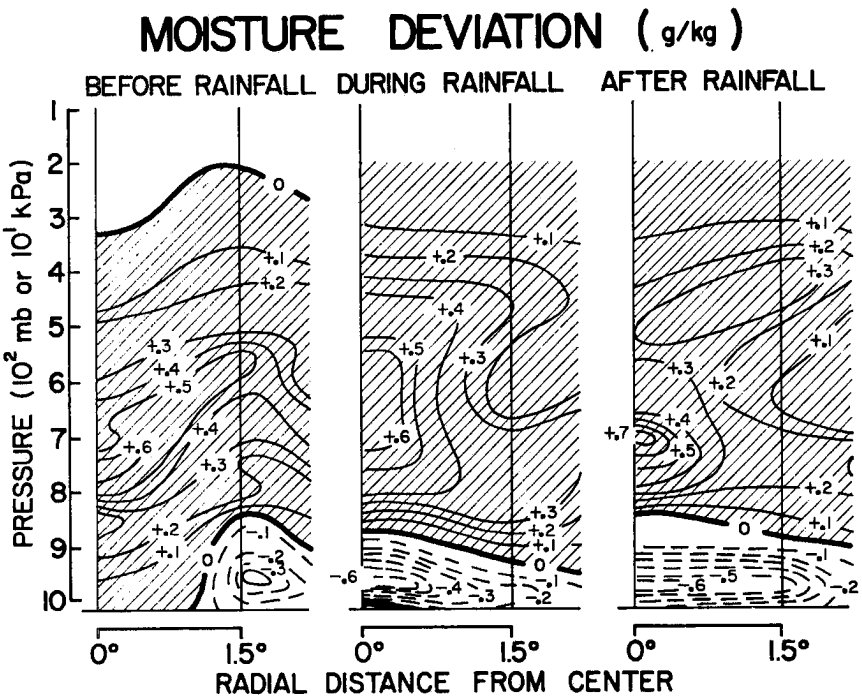


Fig. 26. Vertical cross-sections of Rainfall Case rawinsonde composite moisture deviations out to 2.00° radius. Before Rain and After Rain refer to 2-3½ hours prior to and following a rain event, respectively.

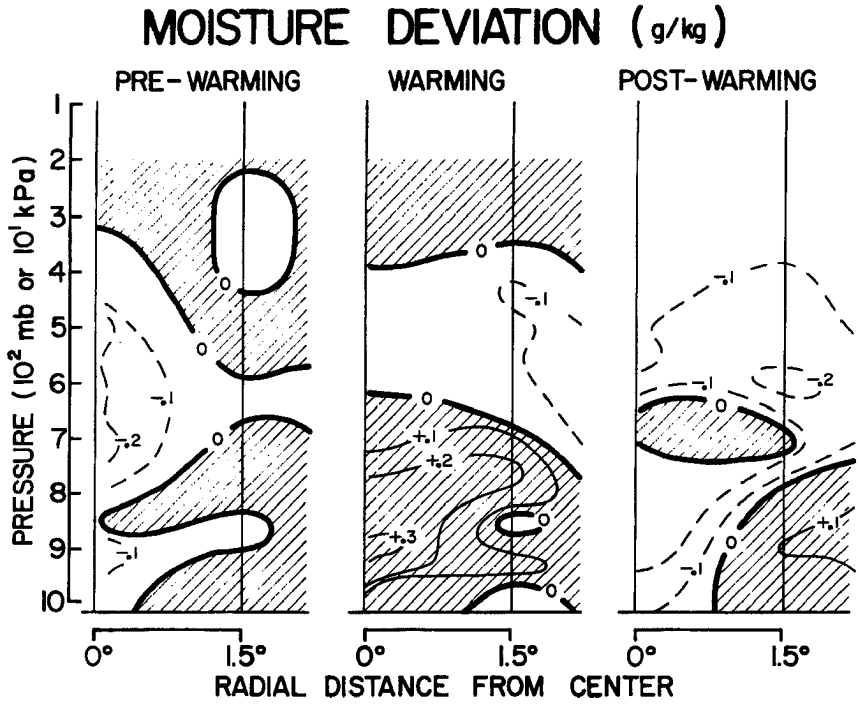


Fig. 27. Same as Fig. 26, except for the Warming Case. Pre-warming and Post-warming refer to 3-6 hours before and after the warming event, respectively.

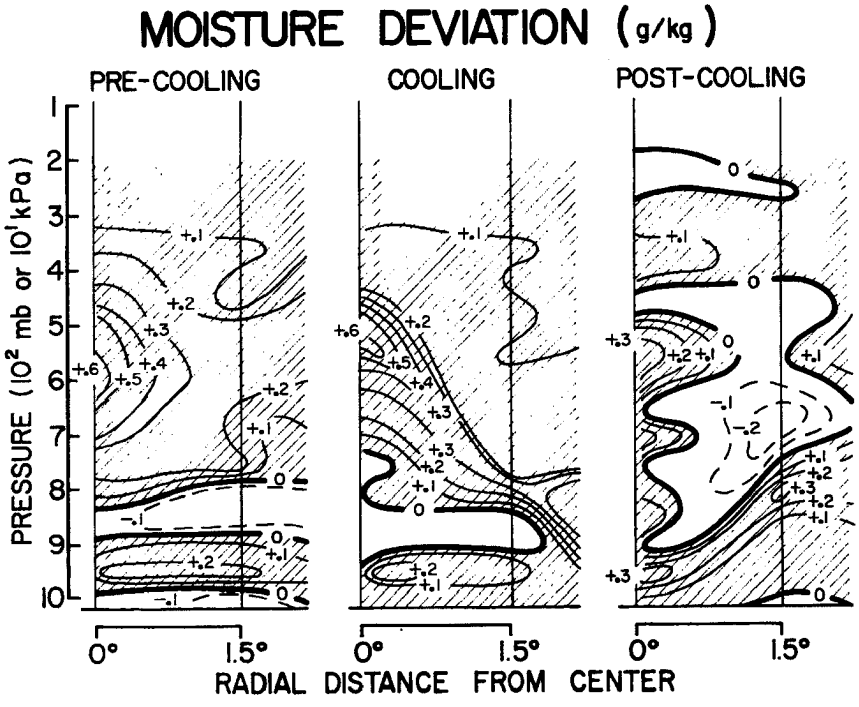


Fig. 28. Same as Fig. 27, except for the Cooling Case.

corresponds to the limits of the B-scale area. Belt #1 extends from the center of the composite to .75°, but due to the fixed separation distance between ships, most of the sondes included in this belt were situated at the center of the grid (0°), with very few scattered in the range 0-.75° radius (average radius .5°). The Rainfall Case as shown in Figs. 23 and 26 is cool at low levels and at the outflow level, warm in-between and generally moist out to an average radius of 1.5° with low level downdraft drying experienced in close proximity to the rainfall. Note that warming is shown occurring in the layer 500-200 mb at all 3 time stratifications, and out to a radius of at least 2°. This warm feature is hypothesized to be the result of the spreading out and weakening of the more concentrated smaller scale warming events (Fig. 24). The Warming Case temperature cross sections when compared with those for the Cooling Case, indicate that the warming occurs higher in the troposphere than the cooling. This would be expected if the cooling events are being produced by evaporation, because the moisture content of the air above about 300 mb is inappreciable and thus does not contribute to evaporative cooling. Subsidence at upper levels always results in warming. The fact that a positive upper level temperature anomaly is not observed at the second radial band (.75-2.00° radius), shows again that the warming events are confined in size to 100 km or less.

It can be seen from the Cooling Case moisture deviation cross sections, that the considerable moistness present at the cooling sites extends out to 2.00°. However, the Warming Case cross-sections appear to indicate no distinct drying effect. Again, this is likely due to obliteration of subsidence drying effects by residual moisture evaporation and moisture ventilation.

The same rawinsonde composite temperature information for the Warming and Cooling Case data is plotted by belt in a graphical format instead of in cross section format in Figs. 29 and 30. According to Fig. 29, the warming occurrences would appear to be confined within an area smaller than the .75-2.00° radial belt. Note that in Fig. 30 the overshoot cooling which occurs at about 100 mb with the Pre-cooling and Cooling stratifications does not appear with the Post-cooling stratification. This would indicate that the convection is no longer active, and likely has dissipated somewhat or moved away from the cooling site.

The composite vertical velocity calculations for the 0-2.00° radius (Fig. 31) indicate subsidence profiles for the Warming Cases and upward motion for the Cooling Cases, while the Rain Cases show the expected strong upward motion. Vertical velocities for all 3 time stratifications have been averaged for each case to produce these profiles. These wind-derived composites for the Warming and Cooling Cases represent values from all the ships in the B-array, while the Rainfall Case composite contains values from both the A/B and B-array ships. Grouping together and averaging the various wind measurement systems has likely introduced some inaccuracies in the divergence and vertical velocity calculations for the Rainfall Case, and the B-scale winds used in the Warming and Cooling Cases are known to be unreliable (see Appendix A). Therefore, the absolute magnitudes of these calculations cannot be considered accurate. For instance, the magnitude of downward motion calculated for the Warming Case is too large to be realistic. The Cooling Case divergence values are probably least accurate because of the smaller number of soundings in this composite average. Nevertheless,

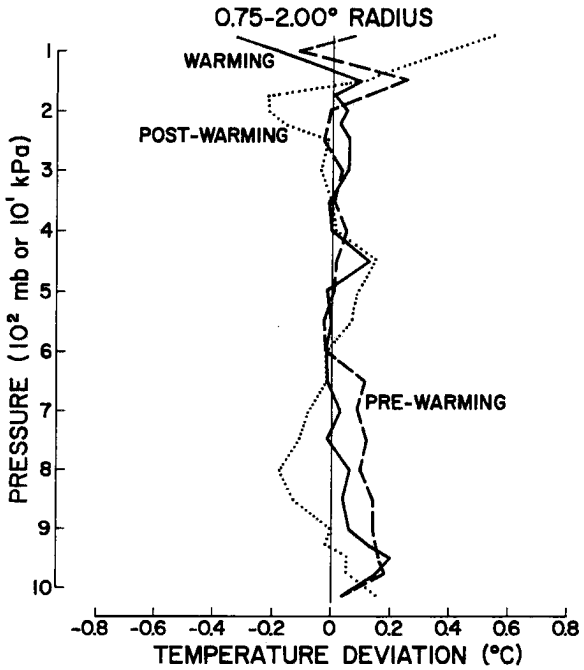


Fig. 29. Temperature deviation vertical profiles for the Warming Case time stratifications. Values are for the composite band centered on 1.5° radius.

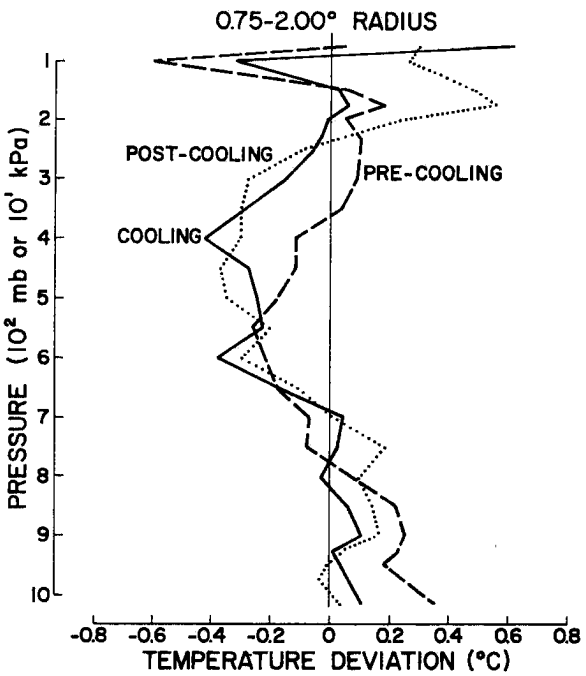


Fig. 30. Same as Fig. 29, except for the Cooling Case.

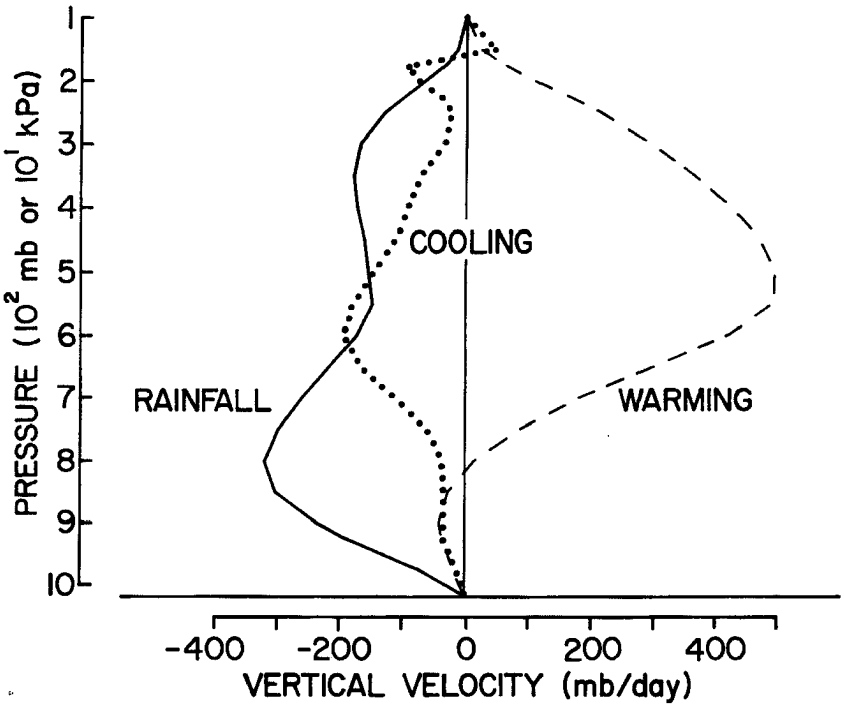


Fig. 31. Vertical motion profiles for the Warming Case, Cooling Case, and Rainfall Case (0-2.00° radius in the B-array). In each case, all 3 time stratifications have been averaged together. (Values must be considered only as approximate. Warming ω is believed to be too large.)

in a relative sense, there appears to be evidence in support of subsidence associated with the warming events.

Summary. Sounding data indicates that small time (< 3-6 hours) and space scale (< 100 km) upper level temperature changes occurred during GATE. Warming and cooling cases were chosen based on the threshold values of $\geq .7^{\circ}$C warming/3-6 hour, and $\geq 1.0^{\circ}$C cooling/3-6 hour, after GATE mean diurnal temperature deviations were subtracted out. The average magnitude of these changes, as measured from one sounding to the subsequent sounding launched 3-6 hours later, was $1^{\circ}$-$2^{\circ}$ through the vertical layer 500-200 mb. Since upper level temperature changes seldom exceeded $2.0^{\circ}$C/3-6 hour, cases were restricted to the largest 3-6 hour temperature changes. This resulted in anomalously warm

temperature deviations preceeded by anomalously cool temperature deviations, or vice versa. It is suspected (based on modelling results of W. Fingerhut (Chapter 7) that the temporal scale of warming and cooling events is less than the 3-6 hour rawinsonde interval, and that one event does not lead directly into the other. For the Warming Case, the first sounding likely ascends through a cool area, which lasts on the order of an hour or so, followed by a period of a few hours with no distinct temperature character, and the next sounding ascends through a particularly warm air mass. This causes a reversal of the temperature change pattern. Thus, the measured values of $\frac{\partial T}{\partial t}$ may be slight overestimates of actual temperature deviation values. Cloud scale (10-100 km) maximum temperature deviations of $.5^{o}$-$1.5^{o}$C are likely more accurate of what is possible in the cloud scale (10-100 km) convective environment.

Regardless of how these events are interpreted, the fact remains that warming and cooling events take place within the same environment, and even simultaneously at different locations within the B-array. Given the B-scale ship separation, this suggests that concentrated upper level temperature changes occur on a space scale of less than 100 km. Although the cloud time scale cannot be well resolved by the B-array rawinsonde data set, the data does show that convective temperature changes occur on a time scale less than 3-6 hours. Furthermore, since radiation and temperature advection terms are too small to account for the observed convective temperature changes, the warming events appear to be primarily produced by concentrated cloud scale (10-100 km) upper level sinking, and the cooling events by cloud scale (10-100 km) enhanced evaporation. Some upper level cooling may also result from cloud scale (10-100 km) layer uplifting.

# 5. AREAL PORTRAYAL OF CONVECTIVE EVENTS AS DETERMINED BY RADAR COMPOSITES

Radar Composite Technique. To obtain a picture of the average radar echo distribution around Warming, Cooling and Rainfall occurrences, digital radar data of hourly rainfall accumulations were composited. The procedure was to spatially average the various radar images using square areas 168 x 168 km centered on the sounding locations, which have been altered to account for balloon drift (Fig. 32). An example of a radar composite is shown in Fig. 33, which is the Rainfall Case composite. Each grid point represents an area 4 x 4 km. The numbers followed by periods are average hourly rainfall values (mm), multiplied by a scaling factor of 5. The numbers below each rainfall value indicate case counts or the number of individual radar measurements at that location. Radar averaging was done for each of the Rainfall, Warming and Cooling Cases. For the Rainfall Case, the radar data were selected to include the hours when rain was reported falling on a ship. To arrive at the hour most closely corresponding to an upper level 3-6 hour warming or cooling event, time for balloon ascent to 300 mb was added onto the actual Pre-warming and Pre-cooling sounding times, and a time midway through the 3-6 hour time interval was chosen as representative.

Composite Results. The resulting composite echo patterns for various convective classes are presented in Figs. 33, and 34-37. The Rainfall Case (Fig. 33) was presented first in describing the radar composite product.

The Rainfall Composite shows a heavy concentration of rainfall centered around the middle of the composite and tapering off with distance. Since the composites were made around specific locations where

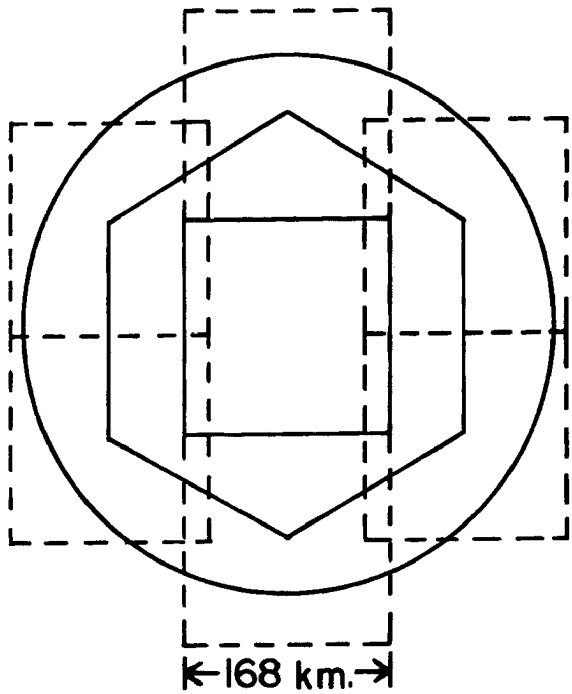


Fig. 32. Area coverage of boxes used for radar composites. Each box is centered on a ship in the B-array.

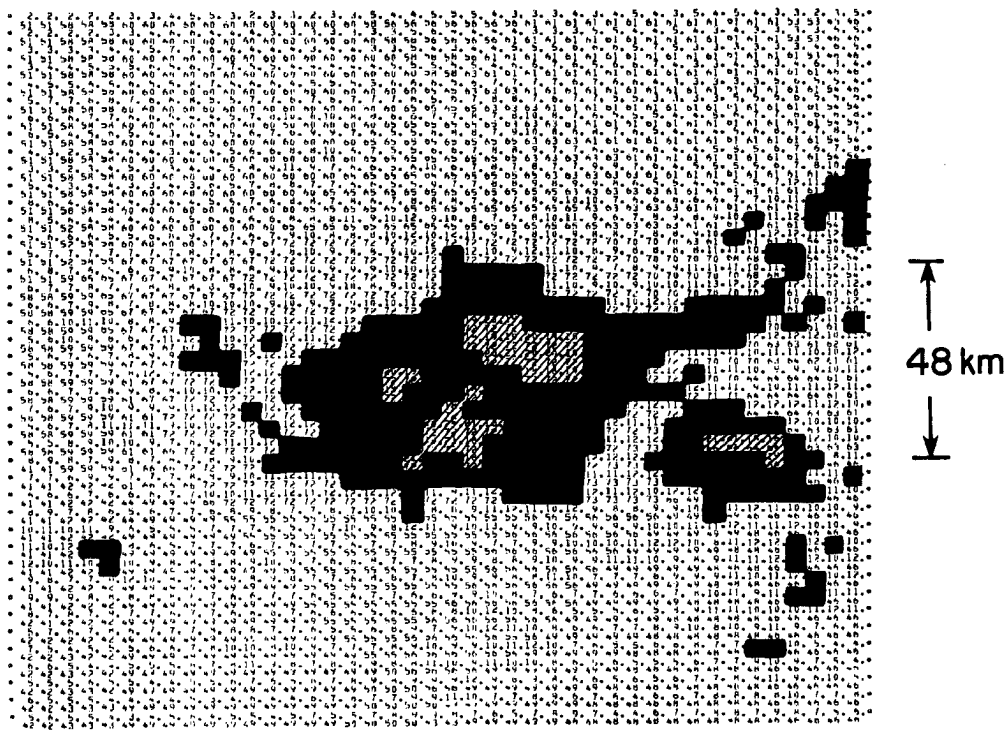


Fig. 33. Rainfall Case radar composite. Numbers with periods represent average hourly rainfall accumulations (mm). These numbers have been multiplied by a scaling factor of 5. Numbers without periods represent case counts. Outer contour represents 2.6 mm/hr, and the second contour 3.6 mm/hr.

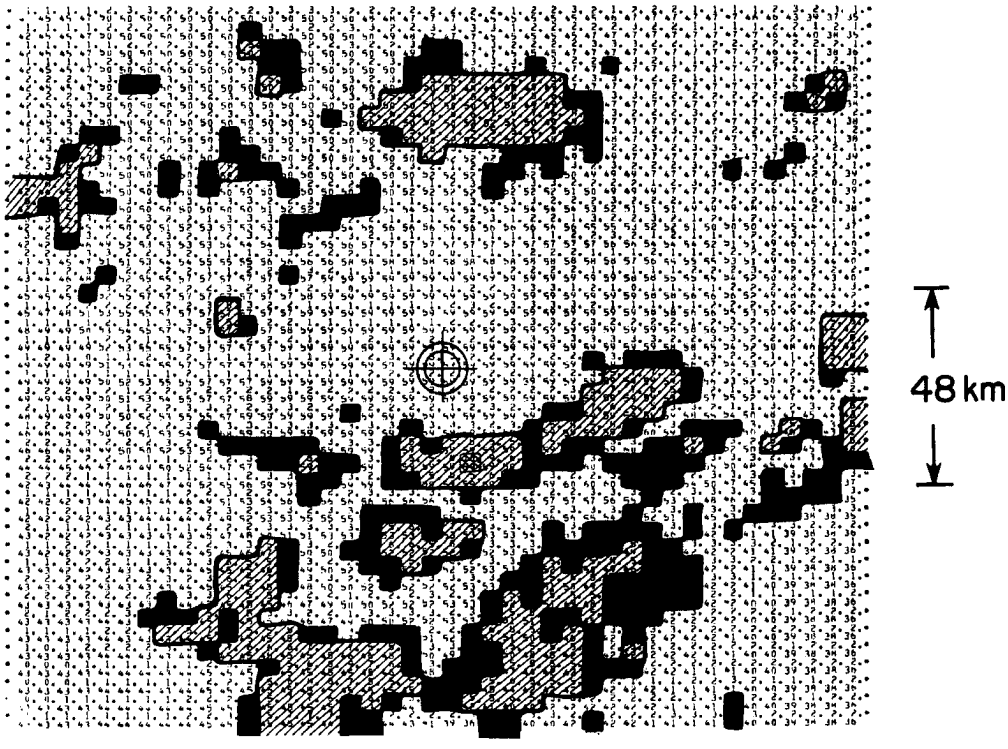


Fig. 34. Warming Case; Non-squall. Outer contour (black) represents .8 mm/hr, the next contour (hashed) represents 1.0 mm/hr and the innermost contour (cross-hashed) represents 2.0 mm/hr.

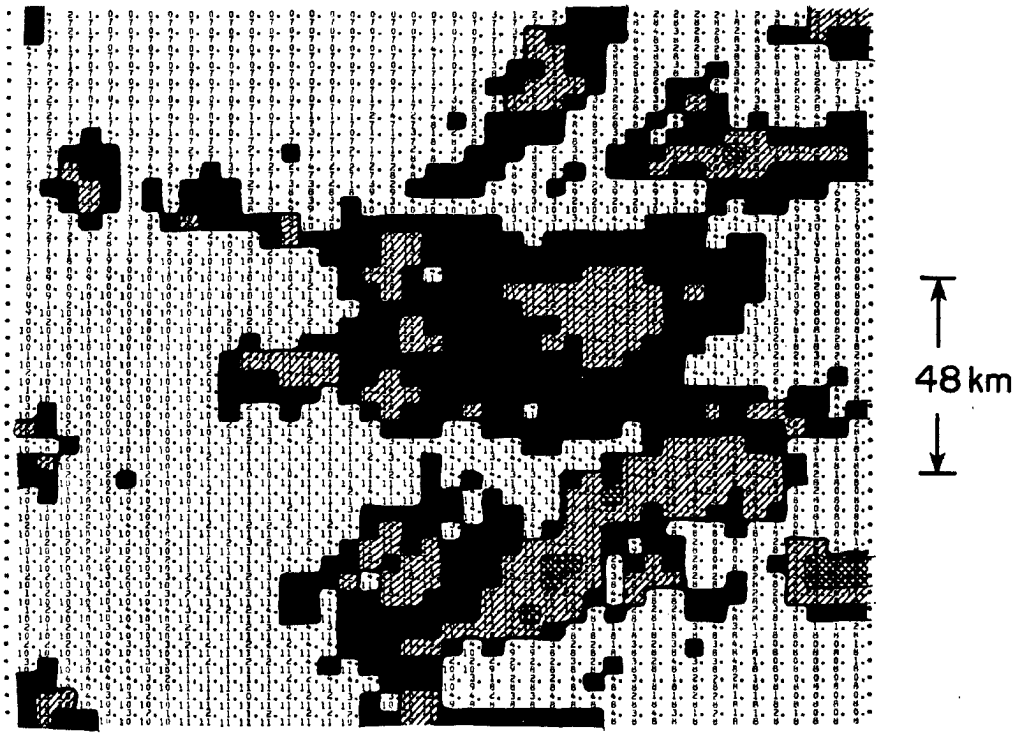


Fig. 35. Warming Case; Squall. Outer contour represents 1.0 mm/hr, the next contour represents 2.0 mm/hr and the innermost contour represents 6.0 mm/hr.

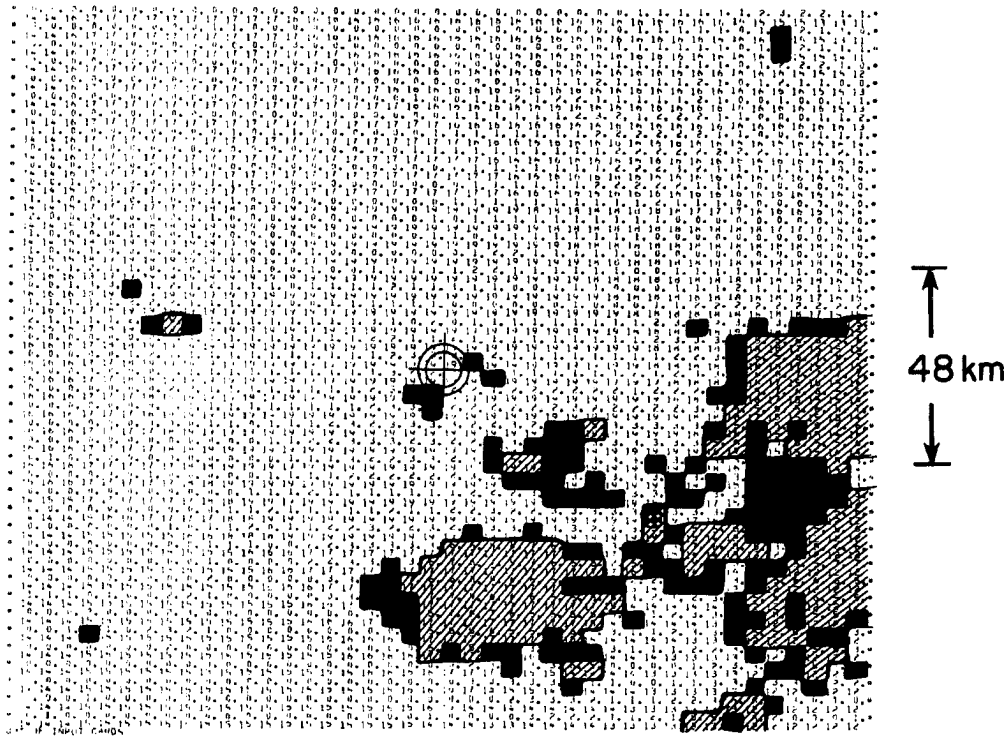


Fig. 36. Cooling Case - Non-squall. Outer contour represents .8 mm/hr, the next contour represents 1.0 mm/hr and the innermost contour represents 2.0 mm/hr.

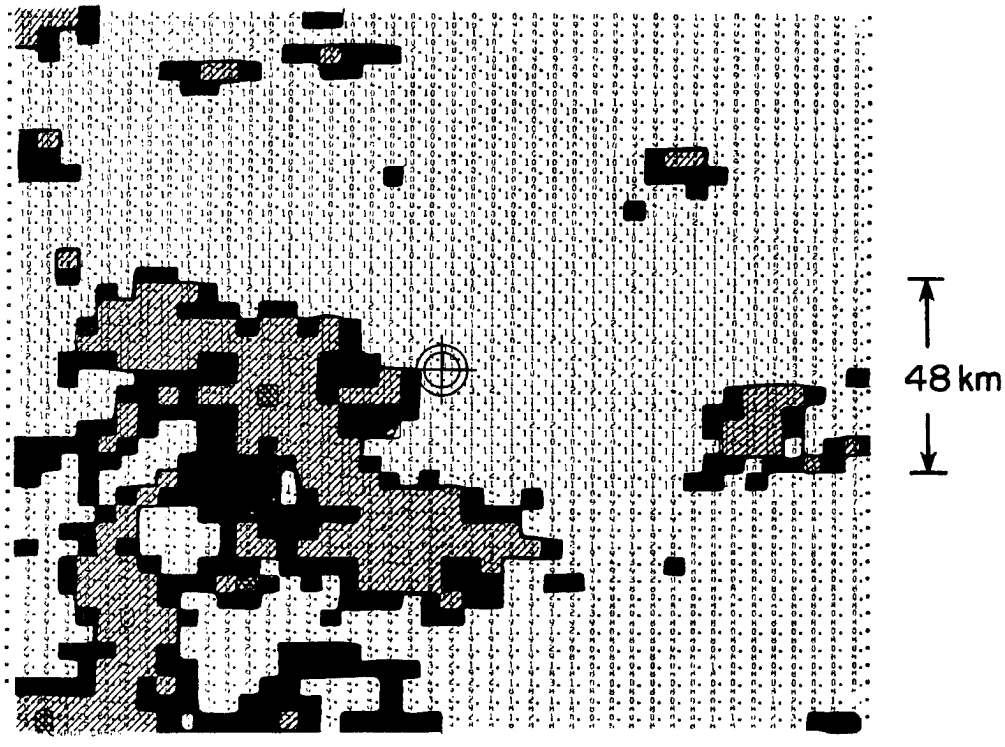


Fig. 37. Cooling Case - Squall. Outer contour represents 1.0 mm/hr, the next contour represents 2.0 mm/hr and the innermost contour represents 6.0 mm/hr.

it was known to be raining, this result was expected, and the Rainfall Composite can be used as a basis for comparison with the other radar case composites. By stratifying the Warming and Cooling Cases into Squall and Non-squall Cases, several interesting features were brought to light. When comparing Figs. 34 and 35, it can be seen that the Non-squall Warming Case does not have convection at the center (Fig. 34) while the Squall Case composite pattern (Fig. 35) shows a good deal of echo coverage in the center of the grid. It was concluded that for the rapidly traversing squall systems, the 3-6 hour time interval between soundings and consequently between sounding cases, is too large to accurately determine which rainfall picture best represents the convective pattern responsible for the upper level warming. The Non-squall Warming Case echo pattern (Fig. 34) should be carefully noted as it is of key interest to the topic of this paper - specifically the subject of how convection warms the atmosphere. It can be seen that the average rainfall pattern resulting from a composite around anomalous upper level warming cases is one of echo ringing the center of the composite at an average radius of about 30 km. Thus, warming rarely occurs within the echo itself, but rather is displaced to one side by 10-50 km. Figure 37 is a composite of only Squall Case cooling events, and this composite pattern reflects the fact that squall systems during GATE generally moved across the B-array from the NE to the SW. The measured anomalous upper level cooling is thus likely due to evaporative cooling which occurs after the squall has passed over the cooling site, or meso-scale layer uplifting occurring behind the squall line (Houze, 1977). By contrast, Fig. 36 depicts the average of only Non-squall Cooling Cases, and shows the echo to be concentrated in the SE corner. The reason for the preferential distribution of echo is likely due to the strong

easterly winds blowing from the rain area to the east and advecting the evaporation cooled air to the observation location.

Figures 38a and b show differences between 3-hourly warming events and a combination of 3 and 6 hourly events. Values do not significantly differ. Therefore, the 6 hourly time interval is not too large a time step to resolve the non-squall warming events. By combining the 3-hourly and 6-hourly events, a higher case count can be achieved.

The grid overlay shown in Fig. 39 was used to obtain the plotted values of composite echo distributions represented graphically in Figs. 40-42. These are plots of percent of area covered by echo at and above a given threshold contour vs. radius out from the center of the composite. The echo information for each of the four quadrants is presented separately because there is such a high degree of azimuthal asymmetry to the echo distribution. Note how asymmetrical the echo distributions are and how convection with the Non-squall Warming events is further removed than that for the cooling events.

Figure 43 is a graphical plot comparing the results of the Rainfall Case and Non-squall Warming Case composites. All four quadrants have been averaged. This graph further demonstrates that warming does not occur concurrent with rainfall at a station, and thus is not produced by direct latent heat of condensation. According to the physical model forwarded to interpret the results of this graph, warming is brought about by subsidence resulting from upper level convergence; this convergence is produced by the merging of Cb outflow (see sketch in Fig. 44). As the model is conceptualized, this outflow is prevented by the convective orientation from being exported to large distances and thus is forced to sink locally. Subsidence takes place in an area relatively clear of convection, and partially ringed by the Cb convective elements producing the outflow.

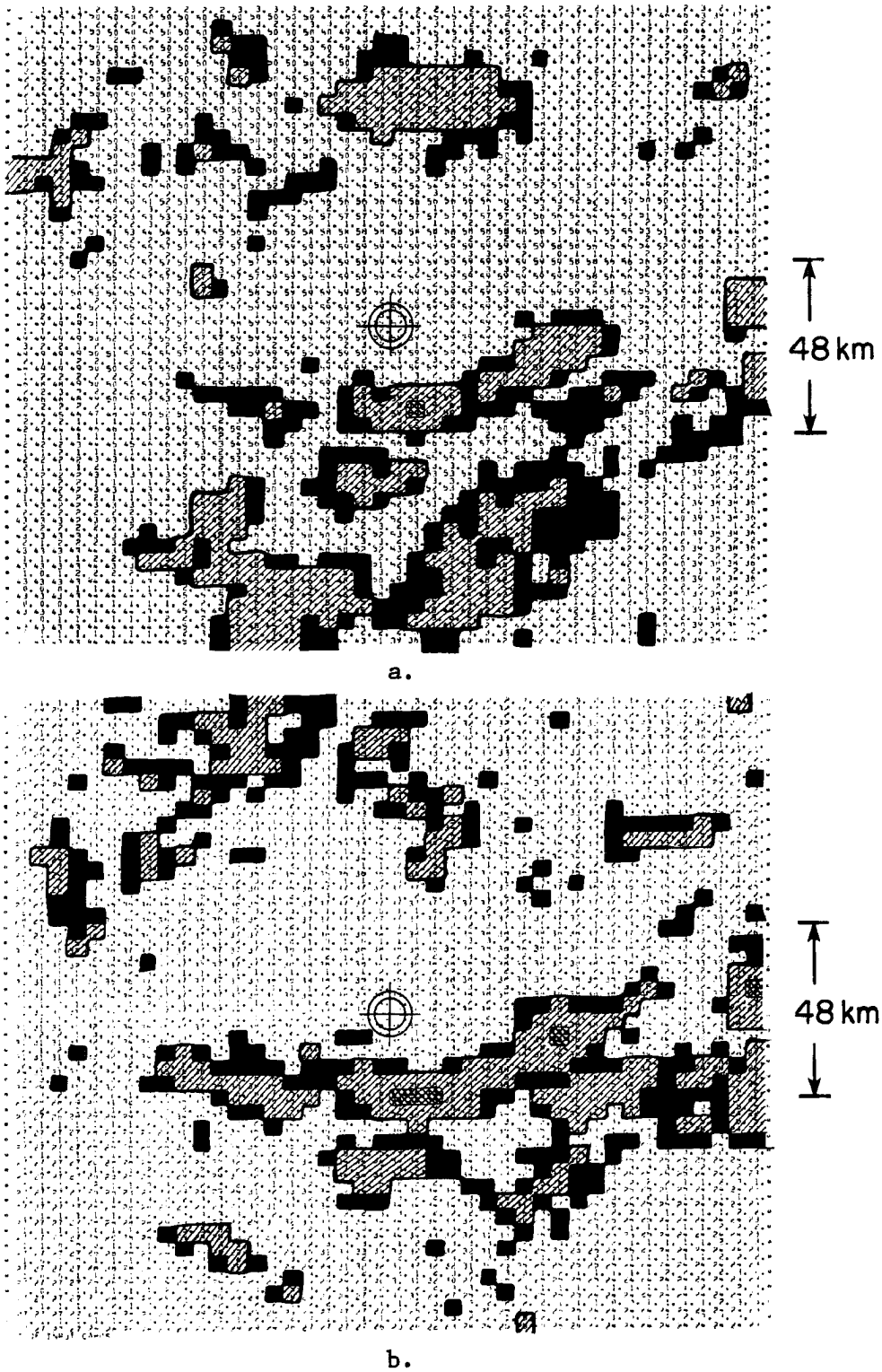


Fig. 38a-b. a) Warming Case - Non-squall; 3+6 hourly events. b) Warming Case - Non-squall; only 3 hourly events. Outer contour represents .8 mm/hr, the next contour represents 1.0 mm/hr and the innermost contour represents 2.0 mm/hr.

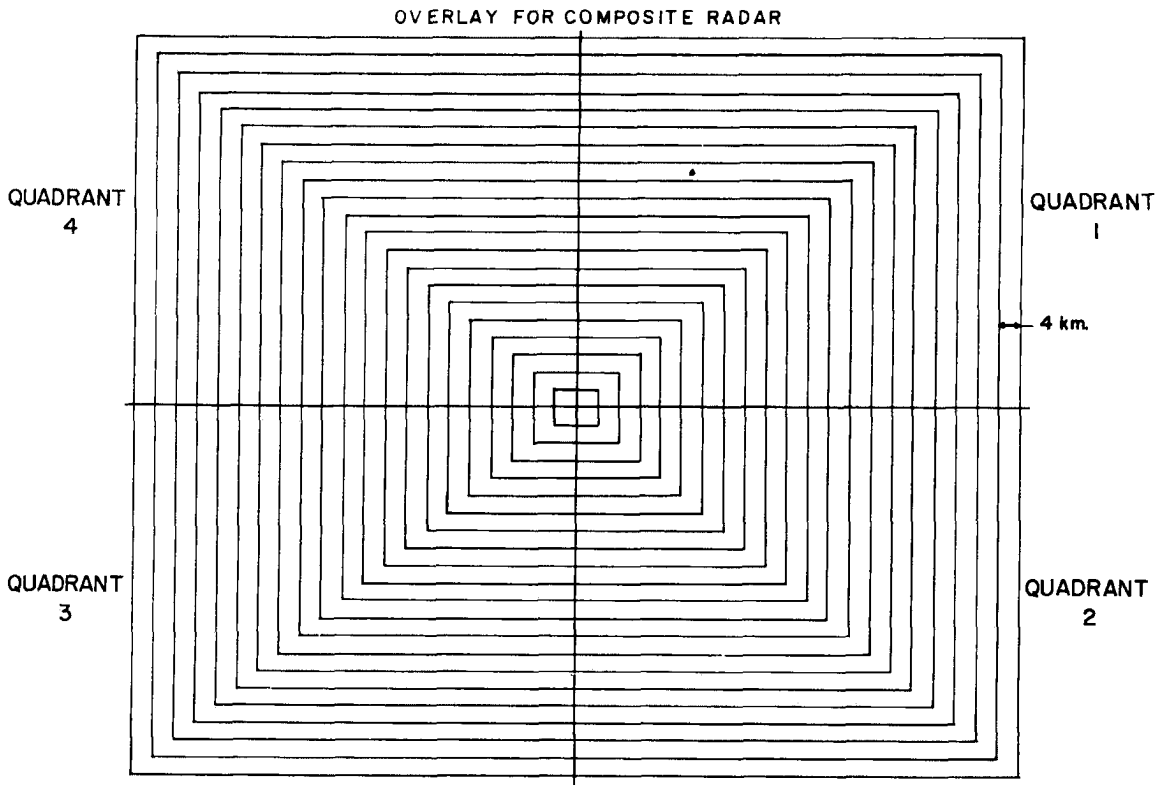


Fig. 39. Grid overlay used for obtaining values in Figs. 40-42.

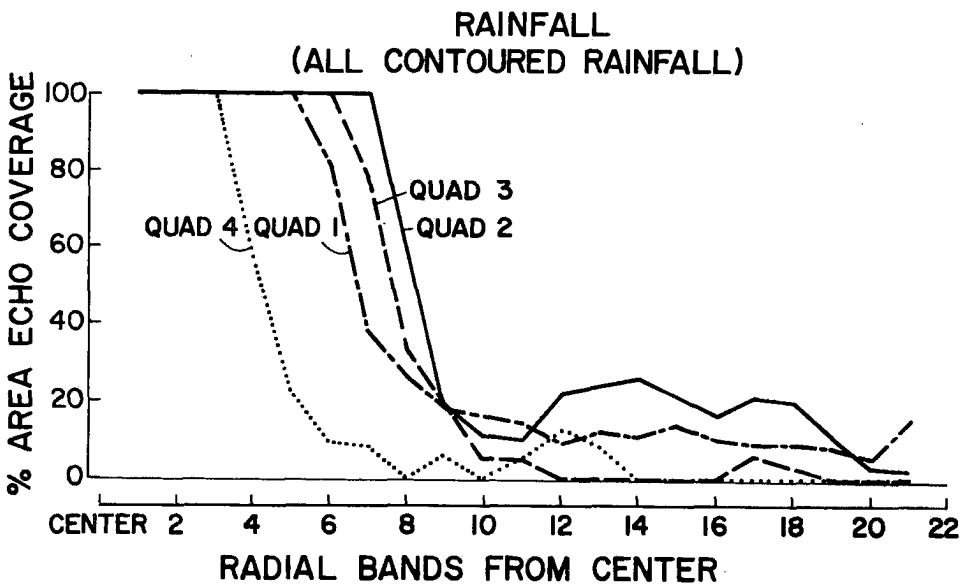


Fig. 40. Graphical representation of Rainfall Case radar composite. For location of quadrants see grid overlay in Fig. 39 above. Each radial band = 4 km.

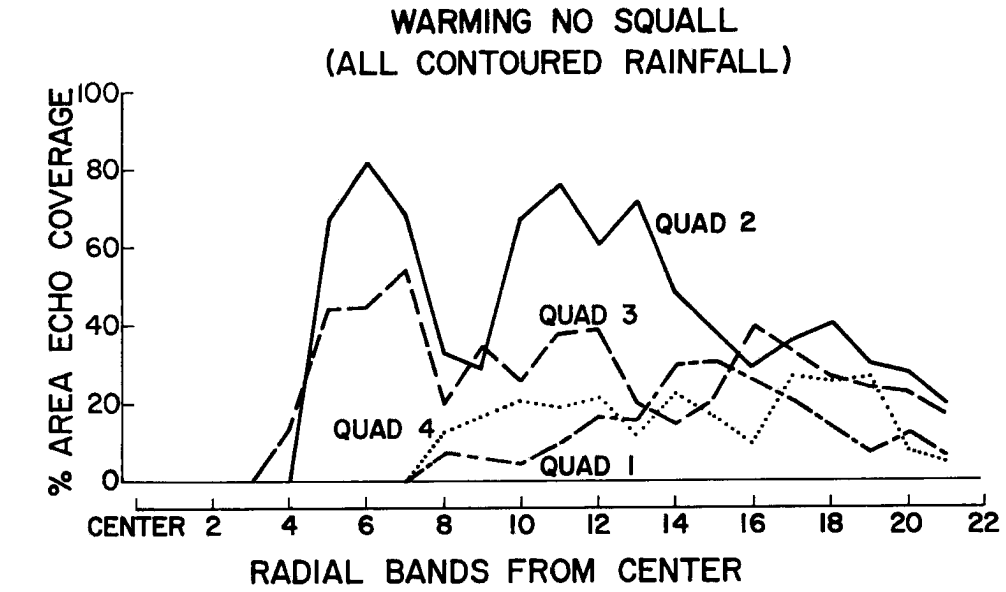


a.

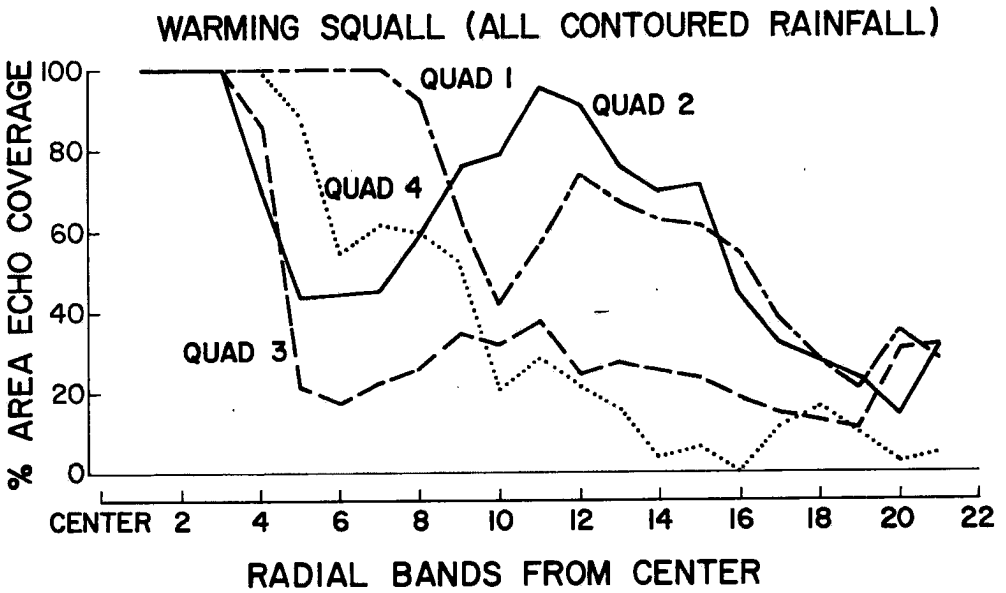


b.

Fig. 41a-b. Graphical representation of Warming Case radar composites. Each radial band is equivalent to 4 km.

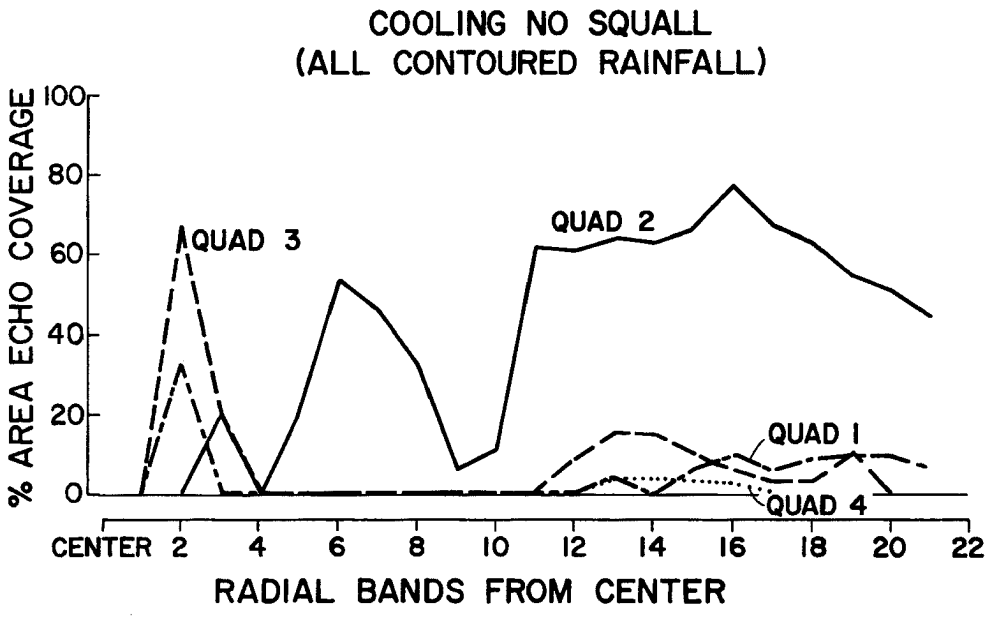


a.

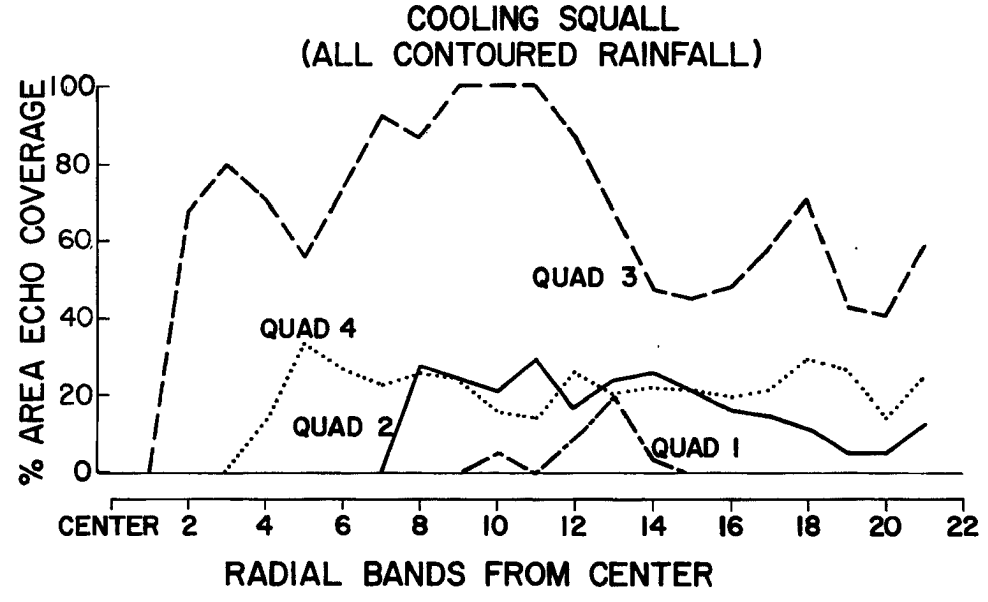


b.

Fig. 42a-b. Graphical representations of Cooling Case radar composites. Each radial band is equivalent to 4 km.

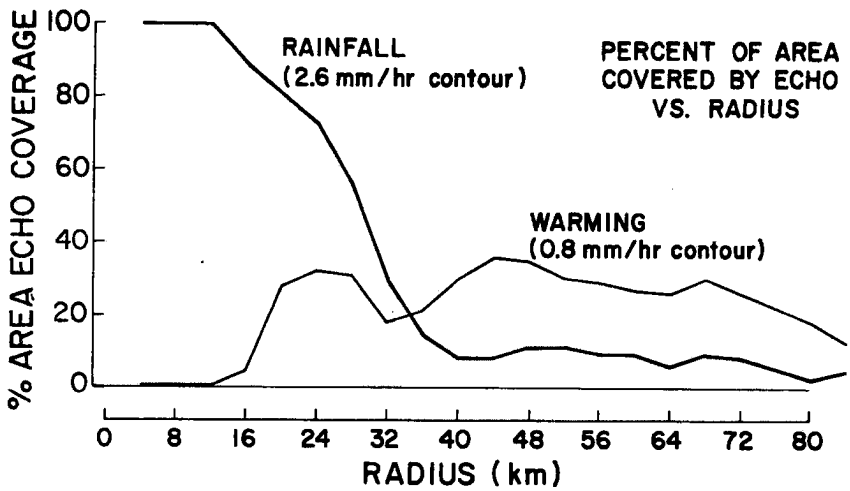


Fig. 43. Graphical plot comparing radar composites for Rainfall and Non-squall Warming Cases.

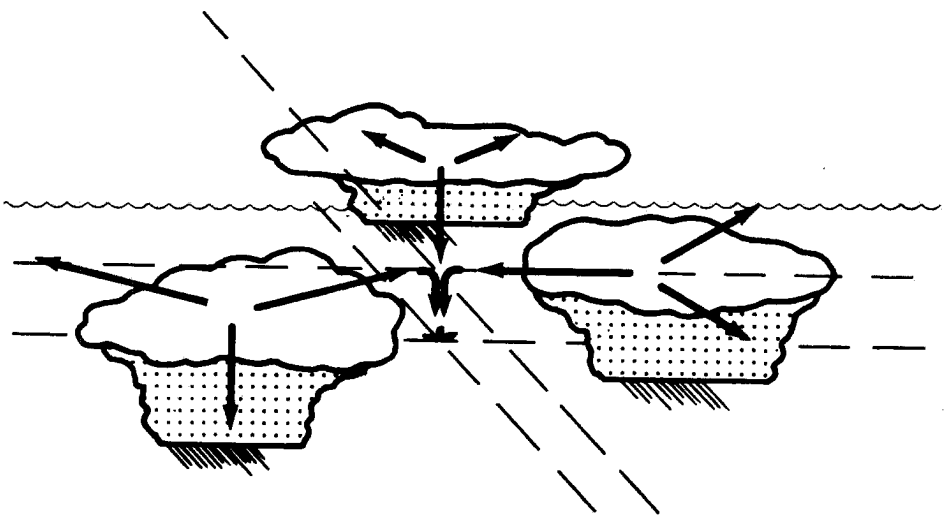

Fig. 44. Schematic demonstrating local occurrence of enhanced return-flow subsidence in upper levels resulting from the convergence of cumulus outflow in areas adjacent to the cumulus convection.

In order to investigate the warming and cooling temperature changes in more detail, individual warming and cooling events were examined. What sort of individual cases comprise the final composites? To acquire more than an instantaneous picture of echo distribution, time sequences of radar echo distribution in the 3 to 6 hours preceeding each event were produced. Statistics based on these time sequences are shown in terms of echo trend in Table 13. While the values in this table do not permit strongly definitive conclusions to be drawn, the following should be noted:

a) 60% of the Cooling Cases show a trend of decreasing echo coverage. This suggests either a dissipating system or one moving out of the region; in either case, evaporating cloud matter is likely present. Moreover, of the 8 Cooling Cases showing an increase in echo amount over the 168 x 168 sq mi box, all but 2 show echo nearest to the cooling site to be moving off or disspating.

b) 59% (48% + 11%) of the Warming Cases indicate a trend toward either increasing, or in a few cases, no change in echo coverage. This is consistent with the view that the warming is brought about by a local upper level subsidence mechanism which occurs as a compensating return flow from the surrounding active Cb elements. The large spread in echo amount associated with warming events indicates that their occurrence is much more dependent on convective orientation than on intensity of rainfall.

Summary. Radar composites based on square areas 168 x 168 km show that the average echo distribution centered on Non-squall Warming Cases is one of echo partially ringing an area relatively clear of echo. The average radial distance of the active convection is $\sim$ 30 km. This demonstrates that the warming events are associated with raining convection, and suggests that the spatial extent of warming events is even less than the B-scale ship separation.

A graphical representation of this composite in comparison with a composite centered on rain shows clearly that the warming is occurring

TABLE 14

Change of rainfall amount in time preceeding individual warming and cooling events.

| | Warming | | Cooling | |
|---|---|---|---|---|
| Classification | No. of Cases | % of Cases | No. of Cases | % of Cases |
| Increasing Rain Amount | 35 | 48 | 8 | 27 |
| Decreasing Rain Amount | 21 | 29 | 18 | 60 |
| Very Little Change | 8 | 11 | 2 | 7 |
| Insufficient Echo | 9 | 12 | 2 | 7 |
| TOTAL | 73 | | 30 | |

not within raining echo but adjacent to it. According to the proposed model, Warming events are likely brought about by an enhanced subsidence mechanism, where the convective organization prevents a portion of the surrounding Cb mass outflow from being exported to large distances and causes it to converge and sink locally.

Squall lines apparently moved through the B-array too quickly to permit an accurate echo representation of squall case warming events. Cooling Case radar composites do not show echo distribution patterns similar to the Non-squall Warming Case, in that their average echo distributions are much more non-symmetric and directional. The Squall Cooling Case echo is concentrated in the southwest quadrant of the composite box, while the average Non-squall Cooling Case rain is clustered mainly in the southeast corner. Cooling events appear to result primarily from evaporation but may sometimes also occur from forced layer uplifting. The evaporative cooling may occur in the wake of swift moving squall lines or be advected from the more steady-state non-squall systems.

An examination of the individual radar images comprising the Warming and Cooling Cases shows that only 11% of these indicated no associated echo coverage or too little echo to be significant.

# 6. CONCLUSIONS

This paper has presented and discussed two types of convection related upper level (500-200 mb) warm temperature anomalies which were observed during GATE using B-scale rawinsonde data. Averaged over the B-scale, raining environments are warmer than non-raining environments at upper levels. This is a general characteristic of the convective environment. Another type of positive temperature anomaly occurs on a smaller time and space scale, and is of greater magnitude. These more concentrated warming events are observed at individual ship locations, and take place on a time scale less than 3-6 hours. They contribute to maintaining the broader-scale disturbance positive anomaly. Numerical modeling evidence (see Chapter 7) indicates that the upper tropospheric positive temperature anomalies over the rain areas are a result of the spreading out of the many smaller cloud-scale (10-100 km) warming events. Evidence presented here indicates that smaller scale warming events result from local return flow subsidence from penetrative convection.

Large diurnal temperature changes occur in both convective and non-convective regions. They are the dominant time changes in temperature; thus it is important to account for the diurnal effects when working with GATE temperature data. Rain regions do not experience larger time changes of temperature than do non-raining regions.

A slight local cooling results when the influence of convection or B-scale temperature is integrated through the troposphere. Warming occurs only in upper levels. When compared to a non-raining environment, a raining area is significantly cooler in low levels because of downdraft evaporation effects, and is also cooler above 200 mb, due to Cb

overshoot and radiational cooling off of the cloud tops. A number of researchers have previously observed a similar vertical temperature structure for tropical disturbances. The temperature structure of the GATE disturbances thus appears to be rather typical of other tropical disturbance systems.

When one speaks of warm or cold core tropical disturbances it is necessary to distinguish between the upper and lower troposphere. The upper layers are distinctly warm, and the lower layers distinctly cool. In a vertically integrated sense, the raining systems are not clearly warm or cold core, as no appreciable tropospheric thickness differences are observed. With no large thickness change, there can be no accompanying pressure drop to enhance the circulation and intensify the system.

The net vertically integrated kinetic energy generation by B-scale vertical motion is (averaged over one day) nearly negligible. The B-array scale vertical circulation is indirect in the lower half of the troposphere, and direct in the upper layers. It appears that disturbance intensification cannot thus result from such meso-scale vertical motion.

Large 3-6 hour upper level temperature changes in excess of diurnal amounts were observed during GATE at individual ship locations. These warming and cooling events were measured as the temperature differences from one sounding to the next. Radar composites indicate that both warming and cooling temperature changes occurred in association with raining convection, on a space scale smaller than the B-scale ship separation distance ($\sim$ 100 km), and possibly as small as $\sim$ 30 km. The Warming Sounding Cases were preceeded by anomalously cool soundings, while for the Cooling Sounding Cases, this trend was reversed. This is likely a function of the case selection procedure, according to

which only the largest temperature changes were chosen. The differences between anomalously cool and anomalously warm soundings would constitute the largest observed 3-6 hourly changes.

Observed magnitudes of 200-500 mb mean temperature change were $1^{o}$-$2^{o}$C/3-6 hours, although actual temperature anomaly is slightly smaller. These temperature tendencies may be considerably greater if (as the numerical modelling results of Chapter 7 indicate) these warming and cooling events were actually to occur over a 1-2 hour or less time period. 200-500 mb temperature changes greater than $2^{o}$C/3-6 hours are seldom observed, indicating an upper limit to convectively produced cloud scale (10-100 km) temperature change.

It is concluded that Cb convection is not causing a local upper level warm temperature at the location of the rain event. The rawinsonde-radar observations indicate that the warming events occur on the side of or between the convective elements. This supports the argument that Cb produced tropospheric warming is the result of cloud return flow subsidence. The Warming Case radar composite echo distribution shows that, on the average, warming takes place in an area relatively free of echo, but partially ringed by convection. Since this pattern would be conducive to upper level convergence of the surrounding Cb outflow and enhanced upper level subsidence, it is likely that convective produced temperature increase is primarily related to the positioning of penetrative convective elements.

Radiation is too small to account for the observed magnitudes of small scale temperature changes, and there appears to be no way for advection to create such temperature anomalies, although horizontal advection may be a factor once these convectively produced cloud scale (10-100 km)

temperature anomalies have been established. (No systematic temperature gradient across the B-array has been discerned.)

# 7. NUMERICAL MODELING EXPERIMENTS

By

William A. Fingerhut

Atmospheric response to cloud-scale temperature anomalies and forced subsidence on the cloud-and meso-scale has been investigated with a numerical model. A general description of the model is given below; a detailed description is given by Fingerhut (1978). The model equations are the primitive equations in axisymmetric form with a non-dimensional pressure as vertical co-ordinate. Thus, the ocean surface, the top of the boundary layer and the tropopause are model surfaces (see Fig. 45). The boundary layer consists of only one layer which is assumed to be well mixed. Only one layer exists above the tropopause (i.e., the model stratosphere) where the flow is pure adiabatic. The troposphere is divided into five layers each initially 168 mb thick.

Physical processes that are parameterized include radiation, condensation heating and surface fluxes of momentum, heat, and moisture. Surface fluxes are given by the bulk aerodynamic formulation and the total condensation heating in a column is obtained from the vertically integrated moisture convergence.

Radiative heating in a vertical column is determined by the large-scale vertical motion ($\omega$) at 372 mb. When $\omega$ is more negative than -50 mb/d a "cloudy" profile is used; a "clear" profile is used when $\omega$ is more positive than -25 mb/d. When $\omega$ is between -25 and -50 mb/d, the radiative heating profile is interpolated from the "clear" and "cloudy" profiles. The only other significant change in the model is that the lateral boundary is open.

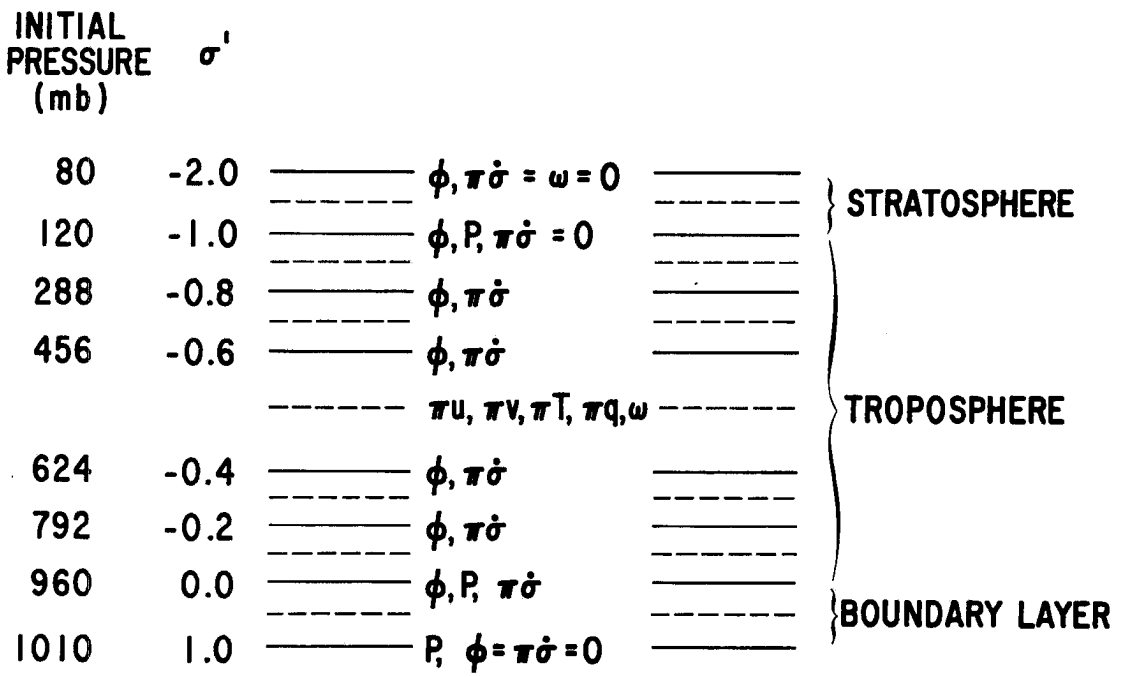


Fig. 45. Vertical structure of Fingerhut's (1978) numerical model.

The objective of the numerical experiments is to investigate the atmospheric response to:

A) forced subsidence associated with upper-tropospheric mass convergence on the cloud-scale (10-100 km) and meso-scale (100-500 km), and

B) cloud-scale (10-100 km) positive and negative temperature anomalies.

Conditions A) may occur when the outflow from two or more cumulonimbus (Cb) clouds meet, the outflow from a ring of Cb clouds converges in the center of the ring, the outflow from convective weather systems (such as tropical cloud clusters) meet, or when the outflow of a cloud cluster is blocked by another feature of the synoptic flow (see Fig. 50-Chapter 8). Cloud-scale (10-100 km) temperature anomalies, condition B), may result from local evaporation of cloud water or from local regions of upward or downward vertical motion.

Each numerical experiment was first initialized with no flow and horizontally homogeneous temperature and moisture fields. Then, either the vertical motion (class A) or the temperature (class B) fields were perturbed. Each numerical experiment in class A was initialized with a circulation similar to that depicted in Fig. 46. The initial subsidence extends from the center of the cylindrical grid outward to a radius $r_o$. Beyond $r_o$ the subsidence warms by approximately the same rate as the "clear" radiative heating cools. The subsidence outside $r_o$ is much less than that inside $r_o$ and is not shown. Quantitatively, the initial circulation is defined by specifying $r_o$ and the radial wind at $r_o$ for each model layer. The radial wind at all other radii inside $r_o$ are obtained from the assumption that the mass flux varies linearly with r from 0 to $r_o$.

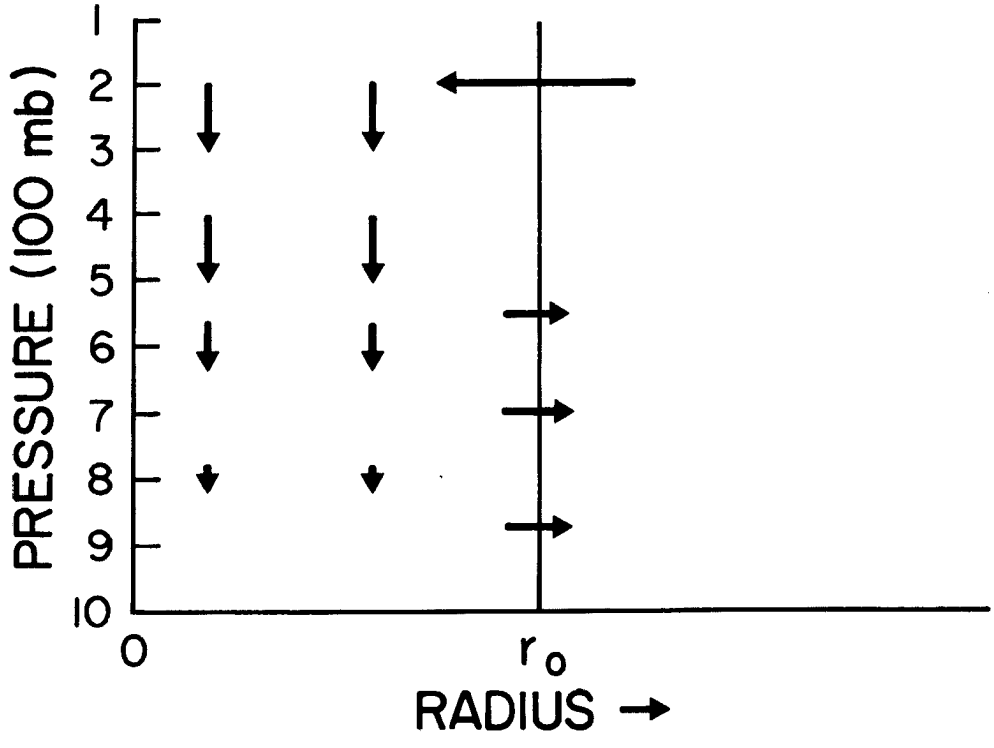


Fig. 46. Schematic of initial model circulation in class A experiments.

For the B class of experiments the initial temperature perturbation is fully defined by specifying the temperature perturbation at r = 0 for each model layer and assuming that this perturbation decreases linearly with r from 0 to 160 km.

The initial conditions for all experiments are summarized in Table 15. When condensation heating was not permitted in an experiment, the surface fluxes of heat and moisture and radiative heating were neglected. Each experiment is identified with a letter, A for class A and B for class B and a number. Only A3 and A4 are meso-scale experiments; the others are all cloud-scale. The initial radial winds in A4 are twice those in A3.

Experiment A1 began with cloud-scale subsidence and did not include any diabatic heating. The central area with large initial subsidence warmed due to compressional heating and the central surface pressure decreased accordingly. The inward surface pressure gradient increased and the low-level flow changed direction from outflow to inflow in less than 5 minutes. The depth of the low-level inflow and accompanying ascending motion grew rapidly. After just 15 minutes, the center of the grid contained only upward vertical motion. As the integration progressed, the initial subsidence propagated outward at 30 m/s.

The temperature changes in experiment A1 are strongly linked to the vertical motion; the subsidence warmed and the ascent cooled. Initially, the central part of the grid became anomalously warm. The largest temperature increase was $0.65^{o}C$ in 15 minutes at both 372 and 540 mb. As the subsidence and warming propagated outward, ascent and cooling appeared in the center area. The cooling started to reduce the warm anomaly while the subsidence warmed on the side of the anomaly. Thus,

TABLE 15

Initial conditions used in the numerical experiments.

| | Forced Subsidence Experiments (A) | | | |
|---|---|---|---|---|
| | A1 | A2 | A3 | A4 |
| Condensation heating | NO | YES | YES | YES |
| $r_o$ (km) | 40 | 40 | 280 | 280 |
| Radial wind (m/s) at $r_o$ by level | | | | |
| 204 (mb) | -3 | -3 | -1.5 | -3 |
| 372 | 0 | 0 | -.5 | -1 |
| 540 | 1 | 1 | 1.0 | 2 |
| 708 | 1 | 1 | 1.0 | 2 |
| 876 | 1 | 1 | .0 | 0 |

| | Temperature Anomaly Experiments (B) | |
|---|---|---|
| | B1 | B2 |
| Condensation Heating | NO | NO |
| Temperature perturbation($^{o}$C) at r = 0 by level | | |
| 204 (mb) | -0.25 | 0.75 |
| 372 | -0.75 | 0.75 |
| 540 | -0.25 | 0.10 |
| 708 | .00 | 0.10 |
| 876 | .00 | 0.10 |

the warm anomaly formed by the initial subsidence appeared to spread out and weaken.

The response described above is a pure gravitational oscillation. Since the initial temperature structure was stable, all vertical displacements were opposed by the natural (buoyancy) restoring force of the atmosphere. A stable atmosphere will, therefore, oppose any vertical motion and spread out and eliminate all temperature gradients.

Experiment A2 is the same as A1 except that condensation heating was allowed to occur. When the ascending motion appeared in the center of the grid, moisture was converged and condensation heating occurred. Thus, the cooling that took place in the center of the grid in A1 was mostly off-set by the condensation heating in A2. In terms of temperature, the warm anomaly created by the initial subsidence was more slowly weakened than in experiment A1. During the 10 minutes after the central ascent first appeared the warm anomaly weakened by only $0.03^{o}C$; after 30 minutes the anomaly had weakened by only $0.37^{o}C$. The occurrence of condensation heating also affected the oscillatory nature of the vertical motion in the center of the grid. After 40 minutes of simulation the vertical motion in the center of the grid had returned to subsidence in A1 while strong ascent persisted in A2. The strong ascent was just as large at 40 as at 20 minutes. Thus, condensation heating offsets the natural response of the atmosphere and permits the warm temperature anomaly, low surface pressure and ascent to persist.

In experiment A3, the subsidence initially in the center of the grid propagated outward at 30 m/s and ascending motion appeared in the center of the grid similar to experiment A2. However, the central warm anomaly reached a maximum much later in the simulation, $0.47^{o}C$ at 3 hours. The

subsequent spreading out of the warm anomaly in percentage area change was also much slower in A3 than A2. Six hours into the simulation the warm anomaly was 0.35°C.

The A4 simulation was the same as A3 except the initial magnitude of the subsidence was twice that of A3. The maximum magnitude of the developed central warm anomaly was 1.7 times larger in A4 than in A3. It should be noted that although the initial subsidence in A4 was twice as large as that in A3, only 1.7 times as much warming occurred. Apparently, the atmosphere responds faster to larger temperature gradients.

The class B experiments were initialized with no motion and a temperature structure similar to the "pre-warming" (B1) and "pre-cooling" (B2) time stratifications discussed earlier. The initial temperatures result in initial pressure gradients that increase in absolute value with height. In B1 the pressure gradient is inward. Therefore, upper-tropospheric mass should be accelerated inward, subside, and warm. The opposite is true for B2. In both experiments, the atmospheric response should be to eliminate the initial temperature anomaly.

Experiment B1 proceeded pretty much as expected. At first subsidence did appear in the center of the grid and the temperature did warm quickly. After 45 minutes, the subsidence had propagated away from the center; ascent and cooling replaced the earlier adiabatic warming. The temperature at r = 0 warmed 0.58°C at 372 and 540 mb in those 45 minutes. In the period between 45 and 90 minutes, ascent remained in the center of the grid. However, at 204 and 372 mb the ascent was very weak and the temperature there remained nearly constant. At lower levels, the ascent was more appreciable and the temperature

cooled. Experiment B1 began with a cold temperature anomaly in the upper-troposphere which was weakened and spread out during a 2 hour numerical simulation; a warm anomaly (similar to that in the "Warming" time stratification) never occurred.

In experiment B2, the initial response to the warm temperature anomaly (as in the "pre-cooling" time stratification) was also expected. Ascending motion developed throughout the depth of the troposphere at the center of the grid and progressed outward at 30 m/s. By 45 minutes, the ascending motion had cooled 0.66 and 0.77°C at r = 0 in the 204 and 372 mb layers, almost completely eliminating the initial warm anomaly. Some cooling also occurred at and below 540 mb, but this was eliminated by low-level subsidence in the period from 45 to 90 minutes. After 90 minutes of simulation, the initial temperature anomaly had been eliminated as in experiment B1. Beyond 90 minutes, the temperature remained horizontally uniform; a cold anomaly similar to that in the "cooling" time stratification never occurred.

Discussion. All of the experiments discussed above show that if a stably stratified atmosphere is perturbed with either vertical motion or a temperature anomaly, the atmosphere responds with a gravitational oscillation that eliminates the perturbation. This in itself is not surprising. The apparent quickness of the atmospheric response is interesting though. Strong initial perturbations and small-scale perturbations produced the quickest response; large-scale perturbations showed the longest lifetimes.

The results of the numerical experiments discussed above suggest that it is very difficult for Cb clouds to warm the atmosphere. Warming by compensating subsidence around or between individual Cb clouds can be

spread out and can be eliminated very quickly due to the small horizontal scale. If Cb clouds are to be effective in warming the atmosphere, compensating subsidence must occur over a larger area. For example, if Cb clouds are organized into a band by the large-scale then the outflow from the band will converge on the inside of the band, subside, warm a meso-scale area and lower the surface pressure. If an area is large enough to persist until a meso-scale low pressure area, low-level convergence, and convection form, the meso-scale circulation can help maintain the convection and thus, establish a positive feedback.

Upper-level convergence and forced subsidence on a large-scale (hundreds of kilometers) appears to have great potential for forming convective weather systems due to the longer period of time necessary to eliminate large-scale warm temperature anomalies. A warm anomaly and lower surface pressure can persist for a sufficient time to allow a convective feedback response to occur. Once Cb convection begins, a warm upper-troposphere and a low surface pressure can be maintained for several hours. If a meso-scale convective weather system ($\sim$ 500-1000 km) can thus be formed in a favorable large-scale environment, then large-scale forced subsidence might be capable of initiating tropical cyclone genesis, a synoptic event that has been very difficult to understand. These experiments show that such a convective response is not possible on the cloud-scale (10-100 km). It should thus be expected that the cloud-scale warming and cooling events observed in GATE not persist in time.

# 8. GENERAL DISCUSSION OF CUMULUS HEATING

By

William M. Gray

Our past Colorado State University observational studies Lopez (1968, 1973a, 1973b) and Gray (1972, 1973) indicate that the latent heat released from cumulus clouds (both precipitating and non-precipitating) goes primarily into potential energy gain and increasing the temperature of the rising parcel to that of the environmental temperature. The small extra (above environment) temperature increase of 1-2$^{o}$C of the rising cumulus or Cb parcel, which is required for buoyancy, does not warm the environment unless it directly mixes out from the cloud at a higher temperature. It appears that the rising cumulus parcel typically continues rising until it loses its buoyancy and temperature excess. It then mixes with its environment at a temperature little different to (or even lower) than that of the environment. This does not directly warm the environment. Any heat transports out from the rising cloud are overcome by evaporation of the residual liquid-water particles as the clouds die. Although heavy rainfall may have occurred, there is typically no local region warming; instead, there is often a local cooling of the immediate environment. The observations of this paper support this assessment. As far as direct temperature change is concerned, Cb convection appears to act as a direct cooling influence. Kininmonth (1970) has also presented evidence for Cb clouds acting as direct cooling agents.

As previously discussed by Gray (1977, 1979) and Lopez (1973b) cumulus induced temperature increase is not directly related to the

amount or intensity of the cumulus convection but rather to the positioning of the penetrative convective elements in relation to each other and in relation to the surrounding upper level flow fields. The data of this paper substantiate this. When such positioning of Cb elements allows the mass from their outflows to diverge to great distances, little local warming results. On the other hand, if the mass from the Cb outflows is constricted in some way and forced to locally subside, then local upper-level warming can result.

This view of how convection acts to warm the troposphere is now accepted by many scientists but is not consistent with the view held by a number of meteorologists during the 1960's who believed that the higher cloud temperatures required for buoyancy resulted in a positive temperature advection or diffusion of energy from the sides of the individual convective elements and that cumulus warming occurred from such diffusion.

The observational evidence of this paper and W. Fingerhut's modeling results (Chapter 7) support the idea that upper tropospheric cumulus induced temperature increase results from Cb outflow subsidence brought about by a favorable arrangement of convective elements or larger scale surrounding flow patterns. The modeling results indicate that cloud scale (10-100 km) upper level positive and negative temperature deviations resulting from subsidence warming or evaporation quickly dissipate themselves. According to the modeling results, the evaporation cooling resulting from the drying Cb at location B in Fig. 47 typically establishes a sinking response which wipes away the negative temperature in an hour or less. The modeling results also indicate a similar rapid response to wipe away and spread out most of the warming occurring on

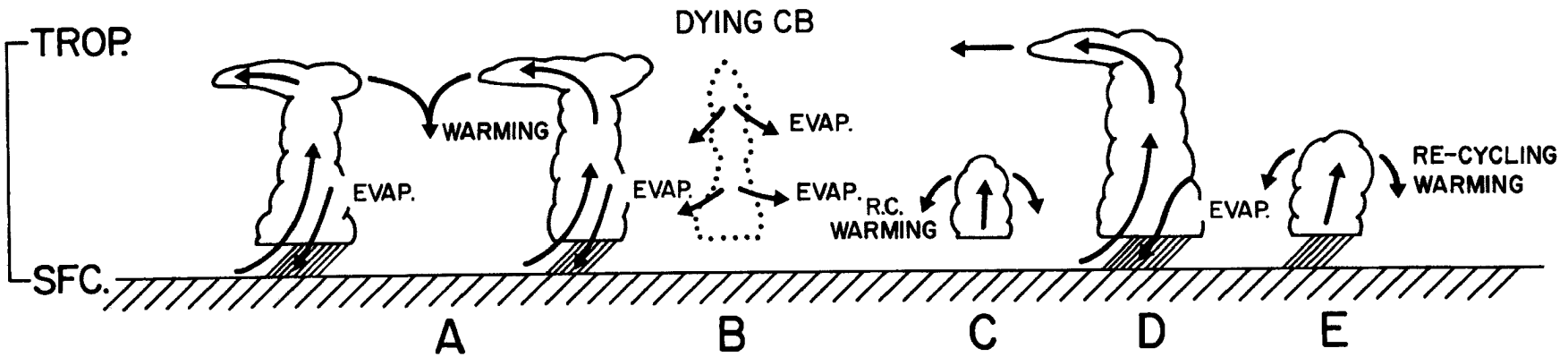


Fig. 47. Idealized view of the various cloud induced warming and cooling processes. Cb return flow subsidence warming can occur at location A but not at location D. Evaporation induced subsidence is occurring at location B and on the sides of the Cb elements around location A and D. Up-moist and down-dry mass recycling (R.C.) warming is occurring at locations C and E.

this scale. Region A shows a typical location for upper level mechanically forced subsidence between Cb elements. By contrast, the isolated Cb element at location D does not have its outflow restricted as the Cb clouds surrounding point A do, and little or no local warming can result. Evaporation cooling is responsible for most of the low level cooling which occurs in the rain areas. There can also be substantial middle and lower level warming due to local up-moist and down-dry mass recycling associated with towering cumulus and cumulus clouds as seen at locations E and C. Such recycling vertical motion is not detected in meso scale (100-500 km) mass budgets. This type of condensation warming cannot thus be related to the mean meso-scale vertical motion field.

## 8.1 Scale of GATE Warming Events

The upper level warming and lower level cooling of the GATE tropical disturbance may be thought of as resulting from the outward spreading of many different cloud scale (10-100 km) wide areas of concentrated subsidence warming and evaporation cooling. These concentrated areas of warming and cooling result in local region (10-100 km) upper tropospheric (200-500 mb) temperature changes of about ½ to 1½°C per hour. These warming events last only an hour or less (as determined by the modeling results) and cannot be resolved by the 3 and 6 hour GATE rawinsonde network.

It is to be noted that these warming and cooling events are not simultaneously observed at other B-array ships. The cloud scale (10-100 km) nature of these local warming and cooling events is to be emphasized.

Fingerhut's modeling results indicate that 10-100 km scale temperature warming and cooling events rapidly dissipate and spreads out at

gravity wave velocities over a larger space domain of 300-500 km in just a few hours. This rapid spreading out and dissipation of 10-100 km scale temperature deviation events prevents a local concentration of warming and cooling and inhibits small scale instability. An idealized warming event is portrayed in Fig. 48. Here the subsidence warming occurring at time (3) is rapidly cancelled out by a compensating cooling response as shown at time intervals (3) to (4) and (4). (1) and (2) denote conditions before convection and before warming. Note how the magnitude of the warming event is completely dissipated at its place of occurrence at time (4) and that the warming energy has been spread (through gravity wave initiated oscillation) over a much broader area. Warming events can often be preceeded by cooling and vice versa. The modeling results indicate that the time interval between the numbered temperature change events of Fig. 48 is only about an hour or less. The upper level positive temperature deviations observed in the rain areas (100-500 km scale) are believed due to the outward spreading of many of the local (10-100 km) warming events. Observational and modeling results indicate an upper limit on 10-100 km scale temperature anomaly of about $1\frac{1}{2}^{o}C$ or so.

## 8.2 Inability of the Troposphere to Warm and Cool on a Small Scale

The observation and modeling evidence of this report helps to demonstrate the general inability of the troposphere to sustain cloud scale (10-100 km) temperature deviations. Any warming or cooling event on this scale will cause a rapid alteration of pressure-thickness values and cause a compensating divergence and vertical motion response which will rapidly dissipate such an anomaly. Thus, speculation on the mechanism of the so-called short-wave cutoff of instability by the CISK

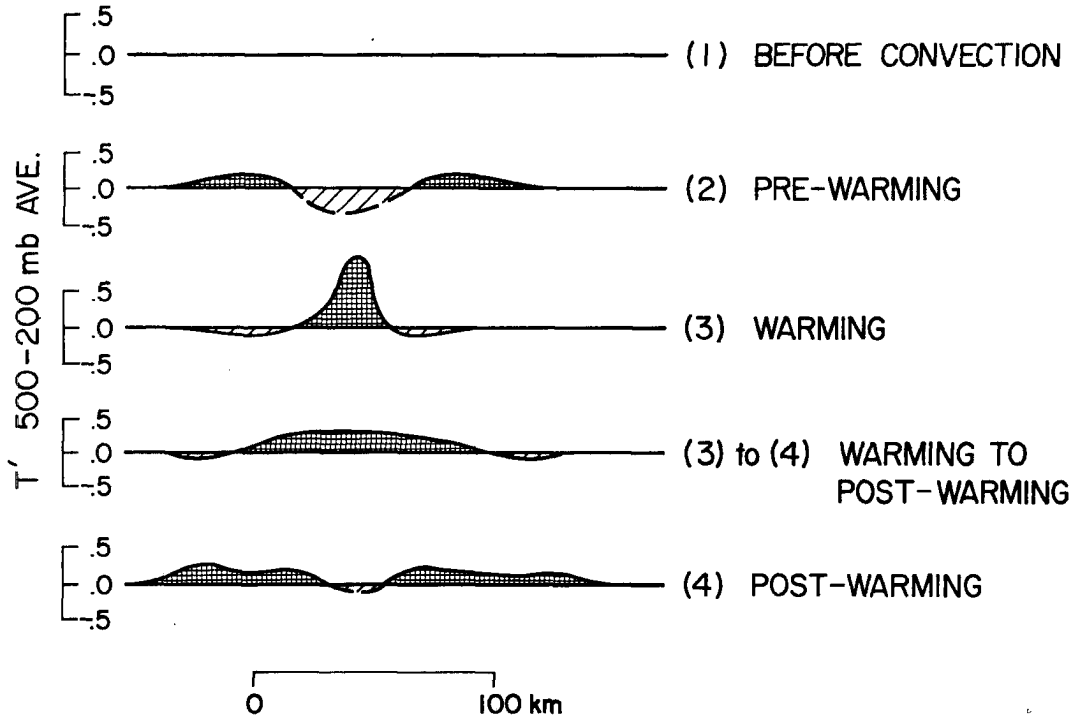


Fig. 48. Idealized view of the occurrence and spread out of an upper-tropospheric cloud scale (10-100 km) subsidence warming event between time periods (1) to (4).

or wave-CISK models does not appear very relevant. The tropical troposphere is inherently incapable of sustaining a significant small scale (10-100 km) temperature-pressure deviation. Small scale instability is thus physically impossible. The early tropical cyclone model difficulties experienced by Kasahara (1961) due to small scale instability are likely a result of an unrealistic formulation of the atmosphere's response to cumulus heating. The modeling success of Yamasaki (1977) and Rosenthal (1978) in directly solving for cumulus convection elements at individual grid points is possible only because of the strong small scale (or short-wave) stability of the troposphere to cloud induced temperature change.

## 8.3 Tropospheric Warming Mechanisms

There appears to be three primary types of upper level warming mechanisms. All result from subsidence. These are:

1) Subsidence in response to tropospheric radiational cooling as typically occurs in clear regions and anticyclones. These warming rates are only about 0.1-0.2°C/3 hr and require but 20-30 mb/d subsidence. This type of subsidence warming typically occurs on a large scale of 500-5000 km and is not relevant to the discussion of this paper.

2) Upper level warming on a scale of 10-100 km from the concentration of Cb outflows as indicated at Point A in Fig. 47. This results from a favorable meso-scale arrangement of Cb cloud elements as discussed. A second type of cloud scale (10-100 km) subsidence occurs as a result of upper tropospheric evaporation cooling. These cloud scale (10-100 km) upper level warming and cooling events quickly spread out and weaken. They are, nevertheless, believed to be responsible for most of the upper tropospheric warming occurring in the usual tropical disturbance. This is the type of subsidence warming that has been treated in this paper.

3) Upper level warming due to a dynamically forced subsidence mechanism occurring on the meso-scale (100-1000km results) from a combination of tropical disturbance Cb outflow and a special arrangement of the surrounding disturbance upper-level meso-scale (100-1000km) flow convergence. Such a dynamically forced subsidence is required for tropical cyclone genesis. The time (1-6 hours) and space scale (100-1000km) are significantly larger than that of the Cb outflow subsidence discussed in 2). Large scale rates of upper level positive temperature increase (0.1-0.3°C/hr) and corresponding surface pressure decrease (0.3-1.0 mb/hr) over regions of 100-500 km diameter can result for short periods of a few hours. This is a rare type of subsidence warming which typically occurs only with tropical cyclone genesis. It exists long enough and over a large enough area as to allow a convective heating response which is able to sustain and further intensify the initial warming. Such a sustaining warming response is not possible for mechanism 2).

   Dynamically forced subsidence requires a favorable positioning of the convection with the surrounding upper level wind systems as would result when the outflow from a cloud cluster interacts with an upper tropospheric trough. Other examples of this type of dynamically driven subsidence are that of the hurricane eye (Gray and Shea, 1973) or the mechanically forced subsidence in advance of middle latitude squall lines as discussed by Hoxit et al. (1976). This type of sustained meso-scale convective induced subsidence warming did not occur in GATE.

## 8.4 Absence of Tropical Cyclone Genesis During GATE

A general discussion of cumulus warming as related to tropical cyclone genesis may shed some light on the interpretation of the GATE cumulus warming mechanisms and why the GATE area, despite its intense ITCZ convective activity, is, nevertheless, incapable of producing tropical cyclones.

To understand tropical cyclone genesis it is necessary to understand the pre-cyclone disturbance's energy budget and the conditions which produce dynamically forced subsidence.

Tropical Disturbance Energy Budget. Moist-static energy (h) can increase or decrease in the tropical pre-cyclone disturbance through transfer from the sea by latent and sensible exchange ($E_o$), by radiation (R), or through horizontal transports on the boundaries ($\nabla \cdot \mathbb{V}h$). This energy balance may be expressed as:

$$\frac{\partial h}{\partial t} = (E_o + R) - (\nabla \cdot \mathbb{V}h) \qquad (4)$$

$$\text{where } h = gz + C_p T + Lq$$

Each term has been integrated through the depth of the troposphere. Estimates of $E_o$ and R for the inner $4^o$ radius of tropical systems indicate that $(E_o + R)$ is positive in most tropical disturbances in the western oceans because sea surface energy flux in these areas is larger than tropospheric radiational cooling. Steady state conditions ($\frac{\partial h}{\partial t} = 0$) are accomplished only through a higher radial export of energy in the upper level outflow than that imported at lower levels. An idealized h-budget for the summertime pre-cyclone disturbance (diagram a) and the

average GATE disturbance (diagram b) is portrayed in Fig. 49.

It can be seen that the usual vertical circulations through the pre-cyclone disturbance of the western oceans produce an energy depletion of the system. The pre-cyclone disturbance maintains itself only through energy received from the ocean. It is observed that most tropical systems weaken or die when their ocean energy source is reduced. Energy received from low-level inflow goes to enhance deep Cb convection. These Cbs rise to great heights and induce outflow at levels ($\sim$ 12-14 km) where h is larger than that of the inflowing air. Thus, the transverse circulation of the tropical disturbance is typically acting to decrease the energy of the system. Any process which acts to reduce this mean circulation will lead to an energy accumulation within the system and intensity increase. Conversely, any process leading to an enhancement of the disturbance's transverse circulation will lead to energy loss and a system weakening. This idea is quite at variance with the long held and prevailing view that intensity and transverse circulation are positively related. Our project's many data sets (McBride, 1979) show that this is definitely not the case. Intensifying disturbances do not have stronger transverse circulations than weak or filling systems. It should be realized that frictional dissipation is a slowly acting process and that the momentum field of the tropical system will be only slowly influenced by a lessening of transverse circulation. Tropical disturbances export large amounts of kinetic energy in their outflows (McBride, 1979). Reduction of the tropical disturbance's mass circulation should not appreciably reduce the disturbance's momentum field.

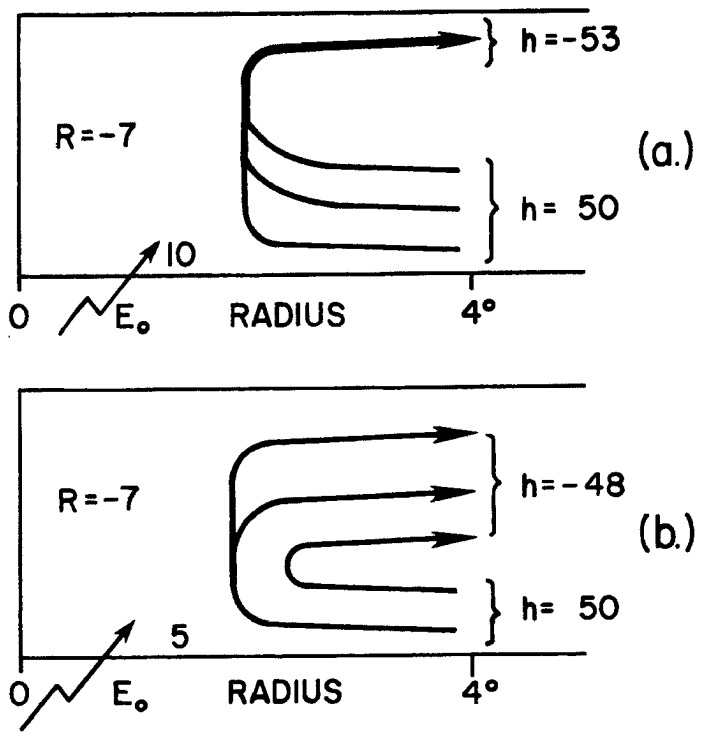


Fig. 49. Schematic representation of the typical h-budget within $4^{o}$ radius of the pre-cyclone cloud cluster in the western tropical oceans (diagram a) and a similar h-budget for the average GATE cloud cluster (diagram b). Units are arbitrary.

The GATE disturbance systems are, energywise, different than disturbance systems of the western oceans which spawn tropical cyclones. Evaporation rates (0.25-0.4 cm/d) are only half to two-thirds of those occurring within the western ocean systems. Surface energy fluxes in GATE systems, unlike conditions for disturbances in the western oceans, are not sufficient to balance tropospheric radiation energy loss of 1.1-1.4°C/d and $(E_o + R)$ for the GATE disturbances is negative (Fig. 49). GATE disturbances maintain themselves only through horizontal import of energy. This is accomplished partly through the special middle level divergence pattern (with export of low values of h) occurring in GATE which are not present in western ocean systems. (See reports of Frank, 1978; McBride and Gray, 1978; Dewart, 1978; McBride, 1979 for more

discussion). Thus, GATE disturbances import energy, most western ocean disturbances export energy. It is only when GATE disturbances advect westward to longitudes > 40-50$^{o}$ (where ocean energy fluxes are larger) that intensification is possible.

It is interesting to note that the low level vertical motion in the GATE disturbances is 2-4 times larger than that of western ocean disturbances undergoing transformation to tropical cyclones.

In the western oceans this excess internal energy of the disturbance manifests itself in a greater local up-moist and down-dry mass recycling which the author believes is fundamental to the tropical cyclone genesis process. It is hypothesized that if the in-and-out transverse circulation of the western ocean disturbances is reduced, then energy would accumulate in these systems. This is not true with GATE disturbances. Any reduction in GATE disturbance transverse circulation acts to weaken rather than strengthen the disturbance.

Thus, the primary factor in specifying tropical disturbance cumulus heating is not the magnitude of the disturbance's meso-scale upward motion (in GATE this was large) but rather the magnitude of the disturbance's surface energy flux in comparison with its outer radii horizontal energy flux (assuming that the radiational characterization of any disturbance is about the same).

Cumulus heating schemes which show disturbance energy gain to be directly related to the magnitude of the disturbance's upward circulation appear to be quite invalid. Disturbance energy gain can occur only if $(E_o + R) > (\nabla \cdot \mathbb{V})$. This inequality is quite independent of the disturbance's vertical circulation and magnitude of condensation energy release.

Our project's research is indicating that once the conditions of $(E_o + R) > 0$ are satisfied as they are for most western ocean systems, then the primary factor determing cyclone genesis is whether a mechanism exists to reduce the disturbance's outward horizontal energy flux. Our observational analyses indicate that this requires a special arrangement of the disturbance's surrounding flow fields which allows for the onset of dynamically forced subsidence.

Dynamically Forced Subsidence as Related to Tropical Cyclone Genesis. As discussed by Gray (1979) and McBride (1977, 1979) tropical cyclone genesis potential is primarily related to differences in the upper and lower troposphere surrounding ($\sim 6^o$ radius) wind field patterns. If these are favorable, then dynamic subsidence and cyclone genesis can occur. This means that the upper level flow fields surrounding the pre-cyclone disturbance must act to reduce or inhibit the increase of the transverse circulation through these systems. Gray (1979) has discussed a physical mechanism by which a favorable outer disturbance flow environment and rainband activity can act to reduce or retard a disturbance's transverse circulation.

The operation of such an inhibiting transverse circulation in the GATE region would, because of its negative $(E_o + R)$ as previously discussed, not lead to an enhancement of a disturbance's internal energy. Tropical cyclone genesis was thus quite impossible within the GATE A/B-array.

A large body of satellite information is now available in both the Western Atlantic and Pacific to indicate that the location of the center of newly forming tropical cyclones (and thus the center of the initial warming of these systems) is not typically within the disturbance's

active convective region (Oliver and Anderson, 1969; Dvorak, 1975; Wright, 1976; Arnold, 1977; Erickson, 1977; plus other data). Instead the center occurs within the clear region just to the west or northwest of the cloud cluster (as seen in Fig. 50a),in the clear region between two different clusters (as in Fig. 50b), or between active convective regions in the same cluster (as in Fig. 50c). These locations are places where the disturbance's upper-level outflow impinges upon the circulation of an upper level trough, the outflow from another cluster, or the outflow from different cloud groups within the disturbance.

It appears that only at locations where such a dynamically forced subsidence occurs, can significant and sustained temperature increase occur such that a sustained surface pressure drop can occur over a broad enough region (100-500 km) sufficient to allow tropical cyclogenesis to take place.

Lopez (1973b) has also discussed this probable mode of tropical cyclone genesis.

> "The interactions between a disturbance and the surrounding flow can be viewed in the following way: A tropical disturbance as a whole takes in environmental mass at low and middle levels and exports mass at high altitudes. A compensatory sinking motion is induced in the air surrounding the disturbance to satisfy the synoptic upward mass transport of the disturbance as a whole. In this way, the potential energy produced by the cloud cluster as a whole is converted into sensible energy outside the cluster. The degree of the resultant warming depends, however, on the scale on which the compensatory sinking occurs. If the subsidence takes place over a broad region, a slight warming is experienced, which is probably used to compensate for the radiational cooling of the area. If the compensatory subsidence occurs over a small region near the disturbance, however, enough compressional warming could take place to explain hurricane development. In fact, Oliver and Anderson (1969) have found from satellite observations that the majority of hurricanes form around a circulation center that develops in the clear area ahead

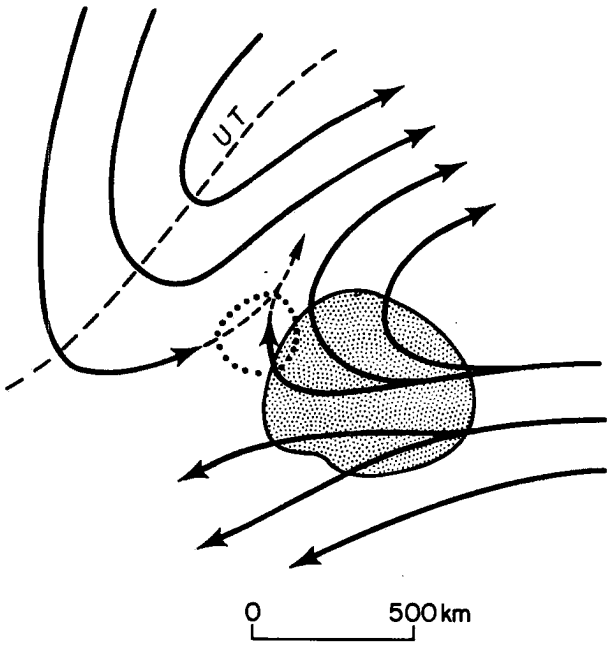


Fig. 50a. Idealized portrayal of 200 mb flow features associated with intensifying tropical disturbance where the initial cyclone center occurs in the dotted region adjacent to the cloud area (shaded) and an Upper Trough (UT) is present to the northwest.

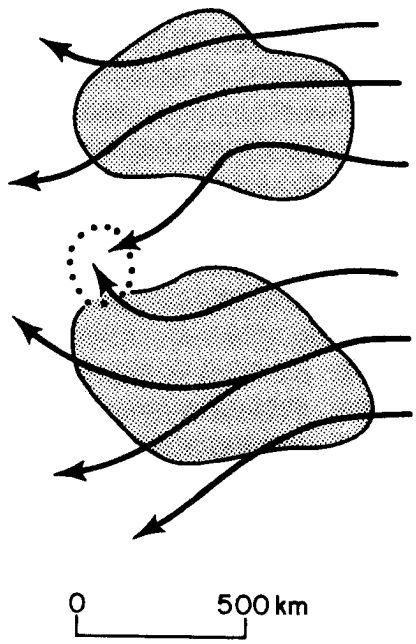


Fig. 50b. Schematic of how the outflow from two disturbances could produce large flow convergence in the dotted region between the disturbances.

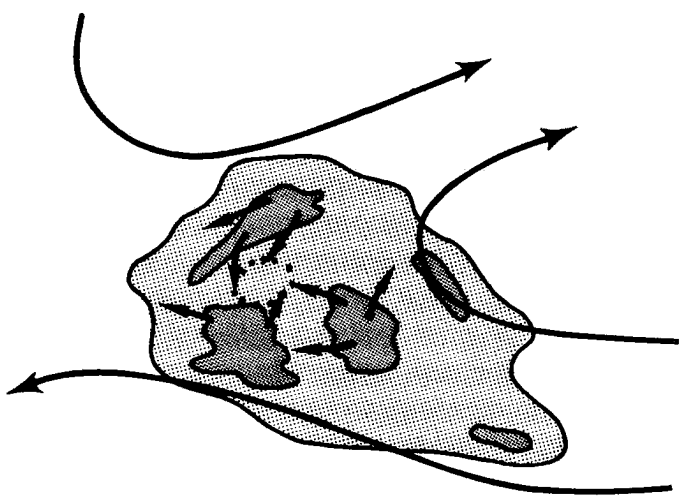

Fig. 50c. Conditions where dynamically forced subsidence occurs within the disturbance cirrus shield (light shading) but between active convective disturbance areas (heavy shading). The cirrus level outflow from the convective areas meet in the dotted circle region.

> of the convective region. There are reasons to believe that the broadscale flow at the level of the disturbance's outflow (approx. 200 mb) might be the controlling factor. Thus, if the wind pattern at that level allows the outflow from the disturbance to be spread over a broad region, only gentle subsidence and warming will occur. However, if the upper-air wind pattern blocks somewhat the outflow, strong local subsidence and considerable warming might develop near the disturbance. The convective activity would then organize itself around the resulting warm-core low-pressure region.

The implications of this physical view on meso-scale convection warming indicate that cloud warming processes do not well relate to the vertical motion at the top of the boundary layer or to boundary layer moisture convergence (as assumed by the many CISK and wave-CISK modelers). The large diurnal variations in weather systems mean upward vertical motion as reported by Ruprecht and Gray (1976) and McBride and Gray (1978) without similar weather system intensity variations is further evidence for the lack of $\frac{\partial T}{\partial t}$ change being directly associated with the magnitude of condensation energy release.

Condensation heating appears not to be directly related to temperature adjustments needed to maintain lapse rates; to cumulus parcel minus environmental temperature differences; or to total disturbance moisture convergence. A number of cloud heating schemes have assumed that the tropical disturbance's temperature change can be related to the magnitude of the disturbance's upward vertical motion or to the disturbance's moisture convergence. These schemes do not take into consideration the required upper level surrounding wind and cloud configurations which are necessary to concentrate and enhance the convection's return flow subsidence.

It is not surprising that tropical cyclone genesis (as opposed to cyclone intensification) has yet to be satisfactorily modeled. No cumulus

heating scheme so far proposed appears to be able to realistically model the cumulus convective processes which bring the positive tropospheric temperature increases necessary for tropical cyclogenesis.

The observations of this paper have hopefully drawn attention to the complexity of the cumulus convective warming processes and the necessity for more observational analysis before realistic schemes to treat cumulus heating can be developed.

## ACKNOWLEDGEMENTS

The author wishes to acknowledge the guidance and continued encouragement by Professor William M. Gray during the course of this research endeavor. Invaluable assistance was provided by Mr. Edwin Buzzell, Mr. Charles Solomon and Ms. Elizabeth Keim in the computer processing of various GATE data products, and the development of their output format. I would like to express my gratitude to Ms. Barbara Brumit for her assistance in manuscript preparation. The author would also like to acknowledge the constructive discussions on this topic with Dr. William M. Frank, Dr. John McBride and Dr. Alan Betts.

This research has been primarily supported by the National Science Foundation Grant No. ATM 78-01640 with supplementary support by the National Science Foundation (RANN) Grant No. ENV 77-10229.

# BIBLIOGRAPHY

Arnold, C. P., 1977: Tropical cyclone cloud and intensity relationships. Dept. of Atmos. Sci. Paper No. 277, Colo. State Univ., Ft. Collins, CO, 155 pp.

Betts, A. K., 1973: A composite mesoscale cumulonimbus budget. J. Atmos. Sci., 30, 4, 597-610.

Brown, J. M., 1974: Mesoscale motions induced by cumulus convection: a numerical study. Ph.D. Dissertation, M.I.T. Cambridge, MA, 206 pp.

Cox, S. K. and K. T. Griffith, 1978: Tropospheric radiative divergence during Phase III of the GARP Atlantic Tropical Experiment (GATE). Dept. of Atmos. Sci. Paper No. 291, Colo. State Univ., Ft. Collins, CO, 166 pp.

Dewart, J. M., 1978: Diurnal variability in the GATE region. Dept. of Atmos. Sci. Paper No. 298, Colo. State Univ., Ft. Collins, CO, 76 pp.

Dvorak, V. F., 1975: Tropical cyclone intensity analysis and forecasting from satellite imagery. Mon. Wea. Rev., 103, 420-430.

Erickson, S. L., 1977: Comparison of developing vs. non-developing tropical disturbances. Dept. of Atmos. Sci. Paper No. 274, Colo. State Univ., Ft. Collins, CO, 81 pp.

Esbensen, S. and V. Ooyama, 1977: Informal report on GATE Phase III rawinsonde data quality. Article appearing within "Information on Upper Air Data Quality and Comparisons of Different Types of Radiosondes in use During GATE", Report compiled and edited by Bob Burpee, U.S. GATE Central Program Workshop, 25 July-12 Aug., NCAR, Boulder, CO, 12 pp.

Fingerhut, W. A., 1978: A numerical model of a diurnally varying tropical cloud cluster disturbance. Mon. Wea. Rev., 106, 2, 255-264.

Foltz, G. S., 1976: Diurnal variation of the tropospheric energy budget. Dept. of Atmos. Sci. Paper No. 262, Colo. State Univ., Ft. Collins, CO, 141 pp.

Frank, W. M., 1976: The structure and energetics of the tropical cyclone. Dept. of Atmos. Sci. Paper No. 258, Colo. State Univ., Ft. Collins, CO, 180 pp.

Frank, W. M., 1978: The life cycles of GATE convective systems. J. Atmos. Sci., 35, 1256-1264.

BIBLIOGRAPHY (cont'd)

GATE Convection Subprogram Data Center - Analysis of Rawinsonde Intercomparison Data, 1976: NOAA Technical Report EDS 20, U.S. Dept. of Commerce, NOAA, Environmental Data Service, Washington, DC, 75 pp.

George, J. E. and W. M. Gray, 1976: Tropical cyclone motion and surrounding parameter relationships. J. Appl. Meteor., 15, 1252-1264.

Global Atmospheric Research Programme, 1975: Report on the field phase of the GARP Atlantic Tropical Experiment. Paper prepared by the International Scientific and Management Group (ISMG), Edited by J. P. Kuettner and R. F. Long, GATE Report No. 16, WMO, Case postale No. 5, CH-1211, Geneva 20, Switzerland, 524 pp.

Gray, W. M., 1972: A diagnostic study of the planetary boundary layer over the oceans. Dept. of Atmos. Sci. Paper No. 179, Colo. State Univ., Ft. Collins, CO, 95 pp.

Gray, W. M., 1973: Cumulus convection and large-scale circulations, Part I: Broadscale and meso-scale interactions. Mon. Wea. Rev., 101, 839-855.

Gray, W. M., 1975: Preliminary analysis of a selective sample of GATE ship and aircraft data. Preliminary Scientific Results (Vol. II) of the GARP Atlantic Tropical Experiment, GATE Report No. 14, World Meteorological Organization, ISMG, 188-190.

Gray, W. M., 1977: Cyclone intensity determination through upper tropospheric aircraft reconnaissance. Paper prepared for the 11th Technical Conference on Hurricanes and Tropical Meteorology, Dec. 13-16, Miami Beach, FL, 288-293.

Gray, W. M., 1979: Hurricanes/their formation, structure and likely role in the tropical circulation. Quart. J. Roy. Meteor. Soc., 105, 155-218.

Gray, W. M. and R. Jacobson, Jr., 1977: Diurnal variation of deep cumulus convection. Mon. Wea. Rev., 105, 9, 1171-1188.

Gray, W. M. and D. J. Shea, 1973: The hurricane's inner core region. II: Thermal stability and dynamic characteristics. J. Atmos. Sci., 8, 1565-1576.

Houze, R. A., Jr., 1977: Structure and dynamics of a tropical squall-line system. Mon. Wea. Rev., 105, 12, 1540-1567.

Hoxit, L. R., C. Chappell and M. Fritsch, 1976: Formation or pressure troughs in advance of cumulonimbus clouds. Mon. Wea. Rev., 104, 11, 1419-1428.

BIBLIOGRAPHY (cont'd)

Kasahara, A., 1961: A numerical experiment on the development of a tropical cyclone. J. Meteor., 18, 259-282.

Kininmonth, W. R., 1970: Thermal modification of the troposphere due to convective interaction. Dept. of Atmos. Sci. Paper No. 167, Colo. State Univ., Ft. Collins, 36 pp.

Lopez, R. E., 1968: Investigation of the importance of cumulus convection and ventilation in early tropical storm development. Dept. of Atmos. Sci. Paper No. 124, Colo. State Univ., Ft. Collins, CO, 86 pp.

Lopez, R. E., 1973a: A parametric model of cumulus convection. J. Atmos. Sci., 30, 1345-1373.

Lopez, R. E., 1973b: Cumulus convection and larger-scale circulations, Part II: Cumulus and mesoscale interactions. Mon. Wea. Rev., 101, 856-870.

McBride, J. L., 1977: Observational analysis of the differences between developing and non-developing tropical disturbances. Paper prepared for the 11th Technical Conference on Hurricanes and Tropical Meteorology, Dec. 13-16, Miami Beach, FL, 260-267.

McBride, J. L., 1979: Observational analysis of tropical cyclone formation. Ph.D. Thesis, Dept. of Atmos. Sci., Colo. State Univ., Ft. Collins, CO.

McBride, J. L. and W. M. Gray, 1978: Mass divergence in tropical weather systems, Paper I: Diurnal variation, Paper II: Large scale controls on convection. Dept. of Atmos. Sci. Paper No. 299, Colo. State Univ., Ft. Collins, CO, 109 pp.

O'Brien, J. J., 1970: Alternative solutions to the classical vertical velocity problem. J. Appl. Meteor., 9, 2, 197-203.

Oliver, V. J. and R. K. Anderson, 1969: Circulation in the tropics as revealed by satellite data. Bull. Amer. Meteor. Soc., 50, 702-706.

Reeves, R. W., 1977: Rawinsonde data quality. Article appearing within "Information on Upper Air Data Quality and Comparisons of Different Types of Radiosondes in use During GATE", Report compiled and edited by Bob Burpee, U.S. GATE Central Program Workshop, 25 July-12 Aug., NCAR, Boulder, CO, 13 pp.

Reeves, R. W. and S. Esbensen, 1977: GATE workshop recommendations for integrating U.S.S.R. RKZ and VIZ rawinsonde thermodynamic observations. Paper prepared for the U.S. GATE Central Program Workshop, 25 July - 12 Aug., NCAR, Boulder, CO, 4 pp.

BIBLIOGRAPHY (cont'd)

Reeves, R., S. Williams, E. Rasmussen, D. Acheson, T. Carpenter and J. Rasmussen, 1976: GATE convection subprogram data center - analysis of rawinsonde intercomparison data. NOAA Tech. Report, EDS 20, 75 pp.

Reynolds, R., 1977: Selected comments from MET 0 20 technical note no II/105 (draft version) Large-scale (A-scale) mean features of the GATE atmosphere during Phase III. Article appearing within "Information on Upper Air Data Quality and Comparisons of Different Types of Radiosondes in use During GATE", Report compiled and edited by Bob Burpee, U.S. GATE Central Program Workshop, 25 July-12 Aug., NCAR, Boulder, CO, 12 pp.

Rosenthal, S. L., 1978: Numerical simulation of tropical cyclone development with latent heat release by the resolvable scales I: model description and preliminary results. J. Atmos. Sci., 35, 258-271.

Ruprecht, E. and W. M. Gray, 1976: Analysis of satellite-observed tropical cloud clusters, Part I: Wind and dynamic fields, Part II: Thermal, moisture and precipitation. Tellus, 28, 391-426.

Smith, E. A. and T. H. Vonder Haar, 1976: Hourly synchronous meteorological satellite-1 (SMS-1) data collected during the GARP Atlantic tropical experiment (GATE): Earth located, Edited data set. Dept. of Atmos. Sci. Paper, Colo. State Univ., Ft. Collins, CO, 180 pp.

Williams, K. T. and W. M. Gray, 1973: Statistical analysis of satellite-observed cloud clusters in the western Pacific. Tellus, 21, 313-336.

Wright, S., 1976: The comparable development of tropical storm Holly with a gulf tropical disturbance. Mon. Wea. Rev., 104, 1451-1454.

Yamasaki, M., 1977: A preliminary experiment of the tropical cyclone without parameterizing the effects of cumulus convection. J. Meteor. Soc. Japan, 55, 1, 11-31.

Yanai, M., S. Esbensen and J. H. Chu, 1973: Determination of bulk properties of tropical cloud clusters from large-scale heat and moisture budgets. J. Atmos. Sci., 30, 611-627.

Zehr, R., 1976: Tropical disturbance intensification. Dept. of Atmos. Sci. Paper No. 259, Colo. State Univ., Ft. Collins, CO, 91 pp.

# APPENDIX A

## UPPER-AIR DATA: DESCRIPTIONS AND COMPARISONS

Several different upper-air sounding systems were employed during GATE by the various participating nations, with the result that significant biases exist in the data profiles thus measured. Also, there were problems with the performance of the shipborne upper-air wind-finding system using Omega or VLF navigation and navaid signals.

This appendix attempts to highlight the conclusions which have been drawn regarding the characteristics and differences of the various rawinsonde systems. Table 16 describes the upper-air systems employed within the B and A/B-scale arrays. Table 17 details some particular problems encountered during data analysis, while Table 18 discusses instrumental biases and their effect on subsequent data reduction.

TABLE 16

Description of Upper-air Systems Employed Within the B and A/B-scales

LOCATE W-3 SYSTEM — GATE Report No. 16 Page 11-4

Description:

The LOCATE W-3 system, built by Beukers Laboratories Incorporated (BLI), was the most widely deployed, being used by three US ships, as well as ships from France, Britain, the Federal Republic of Germany, and Canada. This system is software controlled, centered around a minicomputer. It is designed to determine winds by measuring changes in sonde position derived from phase changes in signals received from either Omega navaid transmitters (North Dakota-Trinidad-Norway) or communication transmitters in the Very Low Frequency (VLF) band, (Cutler, Maine-Balboa, Canal Zone-Rugby, England). The Omega capability of this system received little use throughout the field phase, mostly because of noisy and weak Omega signals received through the sonde.

The sonde used with this system was the VIZ model 1232-300 (1224 on the French ships) which was capable of receiving and retransmitting signals from 10 to 28 KHz. It also measures and transmits thermodynamic parameters.

NOAA Technical Report EDS 20 Pages 2 and 3

Description:

A timelag correction was applied to the US thermistor measurements, and timelag and temperature corrections were applied to the hygristor readings.

The US recorded specific humidity to the nearest 0.01 g/kg, Canada reported relative humidity to the nearest 1%, and the FRG reported dewpoint to the nearest 0.1 C. Relative humidities were recomputed for the analysis.

MTF SYSTEM — GATE Report No. 16 Page 11-6

Description:

The USA ship Researcher used a system which totally depended on Omega navaid signals for windfinding. This system was designed and built by the General Electric Company for the National Aeronautics and Space Administration (NASA) Mississippi Test Facility (MTF). It employs a Beukers 403 MHz receiver and Beukers RF heads designed to pass the 13.6 KHz Omega signal, but uses hardwired logic as opposed to the software-controlled computer of the Beukers systems.

The sonde used was the hi-resolution VIZ Model 1224-300, which was capable of tracking with Omega navaids. It employed a navaid receiver similar to the Model 1232 sonde, but incorporated an additional narrow-band frontend filter designed to pass 13.6 KHz Omega signals. The

TABLE 16 (cont'd)

MTF SYSTEM — GATE Report No. 16 Page 11-6

performance of this system, over the Beukers W-3/VIZ 1232 combination in the Omega mode, was somewhat better because of the use of this narrow band filter on the sonde, which reduced background noise.

VANGUARD SYSTEM — NOAA Technical Report EDS 20 Appendix B Page 20

Description:

The bulk of the Vanguard data acquired during GATE consisted of FPS-16 (C-band) radar tracking data recorded on magnetic tape and met data (pressure, temperature, humidity) from a VIZ Model 1298 radiosonde, recorded on a strip chart.

USSR UPPER-AIR SYSTEM — GATE Report No. 16 Page 11-7

Description:

The system employed by the USSR is of the transponder type, employing radio direction finding techniques for winds with assistance of an onboard computer. In general, data from this equipment were very consistent and reliable.

NOAA Technical Report EDS 20
Appendix A Page 17
Page 3
Page 2-3

Description:

Radiosonde temperatures were routinely corrected for insolation error by an amount dependent on sonde altitude and solar elevation angle.

Moisture was reported as relative humidity to the nearest 1%.

The USSR data were determined for mandatory and significant levels. The Canadian and US systems employed the VIZ radiosonde, the soundings being processed and archived with 5 mb resolution. Thus, further processing of the National Processing Center (NPC) archived products was required in order to produce comparable data sets. Since the USSR temperature and humidity were reported at significant levels only (with heights to the nearest 10 m), 5 mb data points had to be obtained by linear interpolation. Concurrently, the heights were recomputed hydrostatically to the nearest meter using pressure, temperature and humidity.

See Appendix A of Reeves et al. (1976) for detailed information regarding the USSR upper-air system, including documentation of the mandatory levels used, and a summary of the criteria utilized for selection of significant levels.

TABLE 17

Difficulties with the Upper-Air Systems

GATE Report No. 16 Page 11-9

Description:

Most of the problems associated with upper-air data for the B and A/B-scales of GATE were with the ships using the LOCATE W-3 systems with Omega or VLF navigation and navaid signals. These systems had difficulties in deriving reliable winds because of the following problems:

Weak or Missing Signal Strength GATE Report No. 16 Page 11-9

Description:

The Omega/VLF ships in the B-array using mostly LOCATE W-3 could partially circumvent this problem by using VLF signals instead of the weaker Omega signals. However, even VLF windfinding met problems because the VLF transmitting stations had regular scheduled stand-downs. To avoid this, ascent times were adjusted slightly.

Technical Problems GATE Report No. 16 Page 11-10

Description:

There was 'cross-talk' between the temperature/humidity circuit and the VLF/Omega windfinding circuit in the high resolution sonde used in the LOCATE W-3 system.

There were software problems with the LOCATE W-3 system.

There was a drifting of the transmitter frequency of the sonde and consequently interference could arise between sondes in the B and C-scale arrays.

NOAA Technical Report EDS 20
Pages 20 and 21

Description:

The 403-MHz telemetry link was the cause of considerable difficulty in both the acquisition and processing of data. Frequency drift during flights was a common complaint of operators. One result of the drift was radio interference at high altitudes, apparently from nearby sondes. Careful monitoring and adjustment of the receiver coupled with frequent changes in the antenna direction helped minimize this problem but did not eliminate it.

A second problem was cross-talk between the meteorological and VLF or Omega transmissions from the sonde. This problem was partially corrected during the in-port period prior to Phase III by alterations to the electronic circuitry on each sonde and has been treated with some success during the processing of the data.

TABLE 17 (cont'd)

Overall Evaluation — GATE Report No. 16 Page 11-16

Description:

Thus VLF/Omega wind performance was poor during the first phase of GATE, but improved during the second and third phases.

For B-scale ships, which most studies dealt with, it was noticed that the lower tropospheric VLF winds were not reliable during all phases. In general, radar winds were more reliable than VLF winds. This was not always true for the upper troposphere. The MTF-Omega system of the Researcher operated reliably during Phases II and III.

GATE Report No. 16 Page 11-3

Description:

It should be pointed out that the experiment design was based on navaid windfinding systems because the number of vessels available in the world equipped with radar windfinding systems is quite small and the installation of stabilized radars on nearly 20 ships would have been prohibitively expensive. In addition, shipborne weather radar systems were badly needed for other purposes, especially quantitative or qualitative precipitation measurement in convective clouds.

TABLE 18

Instrumental Biases

Contained in the NOAA Technical Report EDS 20, are results from various intercomparison analyses. Within this documentation can be found descriptions of intercomparison procedures, as well as lists of formal intercomparison flights, and periods used in the investigation. Data from the formal Intercomparison Periods and Phases I and III from the United States, the Federal Republic of Germany, Canada, and the Union of Soviet Socialist Republics were used in the intercomparison analysis of GATE rawinsonde temperature, humidity and winds. Only highlights from this and other pertinent reports are included here.

---

Thermodynamic Data Comparisons NOAA Technical Report EDS 20 Page 4

Systematic biases exist in temperature and humidity data between VIZ and USSR systems.

---

1) Mean USSR vs. VIZ Temperature Differences

Description:

The mean temperature differences vs. height for the USSR comparisons are shown in Fig. 51. The difference profiles are similar for all comparative sets, i.e., the USSR temperatures are cooler in the lower troposphere and warmer above relative to the other three nations. Most of the differences at individual levels are not significantly different from zero by Student's test. However, when the entire profile is viewed, there can be no question that the differences display a strong height dependence.

The observed tropospheric height-dependence in temperatures cannot be attributed to USSR solar radiation corrections, which reduce the temperatures at all levels by an amount that increases with height. Figure 52 compares day and night USSR-VIZ mean temperature differences, which are on the order of 1 K. That comparison is consistent in the upper levels with the expected change, i.e., lowering of USSR-VIZ differences from night to day, but inconclusive in the lowest 200 mb where radiation corrections are small. These results must be considered tentative, since only 8 sounding pairs were available for computing the nighttime average. Lag corrections applied to the US temperature data account for only a small part of the differences, since they typically lower the US values by about .1-.2 C near the surface and about .3-.4 C in the upper troposphere.

---

Esbensen and Ooyama (1977) Page 1-2

2) Temperature Differences Among Individual Ship Observations

Description:

TABLE 18 (cont'd)

Not only are there discrepancies between the USSR and VIZ soundings, but there also exist similar discrepancies between individual observing platforms. Bidassoa standard deviation values for surface specific humidity and upper level temperatures depart markedly from other VIZ systems near the same latitude. Vize and Zubov have serious biases in temperature and humidity with respect to other USSR platforms.

NOAA Technical Report EDS 20 Page 6

3) Height/Pressure Differences

Description:

Intercomparisons between the VIZ-sondes used by the US, Canada, France and Germany and the USSR RKZ-sonde system show a discrepancy in the heights reported for various thermodynamic features. The tropopause pressure reported by the VIZ soundings was consistently higher (from 5-15 mb) than that reported by the USSR soundings. This suggests a systematic difference between USSR and VIZ height or pressure measurements.

Reeves and Esbensen (1977) Page 1

Description:

The systematic height/pressure differences were large enough (up to 15 mb at tropopause pressure) to warrant a separate study at CEDDA to try to determine the cause. A number of possible causes investigated were: a) temperature biases, b) VIZ baroswitch accuracies, c) USSR earth curvature and refractive index corrections, d) hydrostatic computations, and e) geometric to geopotential height computations. None of these could account for the rather large pressure biases found. In addition, the FRG comparison of German M-60 and VIZ sondes showed no height or pressure bias. While we do not know, at the time of the GATE '77 workshop, the reason for the pressure/height bias, we strongly suspect the height measurement for the RKZ soundings. Analysis of intercomparison data and observational Phase III data indicate that this problem is also ship-dependent.

NOAA Technical Report EDS 20 Page 6

Description:

A possible ship-dependency was identified from the series of Intercomparison Period I soundings taken through the trade inversion. The Professor Zubov soundings reported the trade inversion base consistently 5 to 15 mb lower than either the corresponding VIZ soundings or soundings from the other Intercomparison Period I USSR ship, Ernst Krenkel.

TABLE 18 (cont'd)

Reeves (1977) Page 3

4) Humidity Comparison

Description:

The formal intercomparison data reveal height-dependent relative humidity differences. Figure 53 shows the USSR sondes relatively drier than the VIZ-sondes in the boundary layer, but wetter in the middle and upper troposphere.

NOAA Technical Report EDS 20 Page 5

Description:

The dryness of the USSR soundings in the 950-1000 mb layer appears to be caused in part by inability to resolve the humidity profile from the significant level values.

NOAA Technical Report EDS 20
Pages 6-7

Description:

Above 500 mb, the USSR humidity values are 10% to 20% higher than the VIZ humidities. However, since these differences occurred at specific humidities of less than 1 g/kg, they are of lesser importance for budget studies than would be the case for a 10% difference in the lower layers.

Wind Data Comparisons

NOAA Technical Report EDS 20
Pages 13-14

Description:

Wind comparisons were made between the USSR winds derived from radar tracking, and the US winds derived from radar, VLF, and Omega tracking.

1) Over 50 mb layers, differences between VLF wind components and those determined by radar tracking have standard deviations of about 1.5 m/sec. This result, obtained from the most sophisticated processing strategy available, approaches the requirement for the GATE B-scale analysis.

2) For smaller vertical layers the result is less satisfactory. In 5 mb layers the standard deviations of the differences between VLF and radar wind components are about 2.5 m/sec. This result will not be adequate for all C- and D-scale objectives of GATE.

TABLE 18 (cont'd)

3) The winds from the MTF-Omega (Researcher) appear to compare less favorably with radar tracking than do the VLF winds. The data recorded on the Omega system are not compatible with the most sophisticated processing strategy, i.e., the multisolution technique being used for the VLF data from the Oceanographer, Dallas, and Gilliss.

4) Comparisons to date of Omega and VLF data with the USSR ship winds have not included the multisolution strategy. The results on only nine flights indicate that the USSR wind data compare favorably with that obtained by the Vanguard system. The MTF Omega-USSR comparisons produce a standard deviation of differences somewhat larger than the VLF-USSR comparisons.

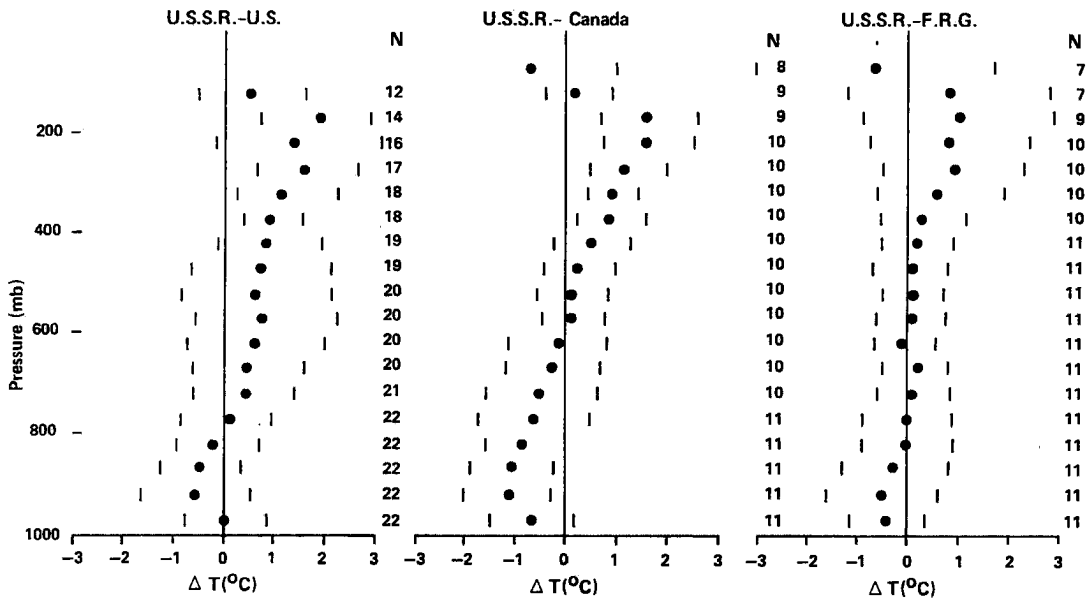


Fig. 51. Means and standard deviations of the temperature differences vs. pressure for the USSR-US, USSR-Canada, and USSR-FRG comparisons (from NOAA Technical Report EDS 20, p. 43).

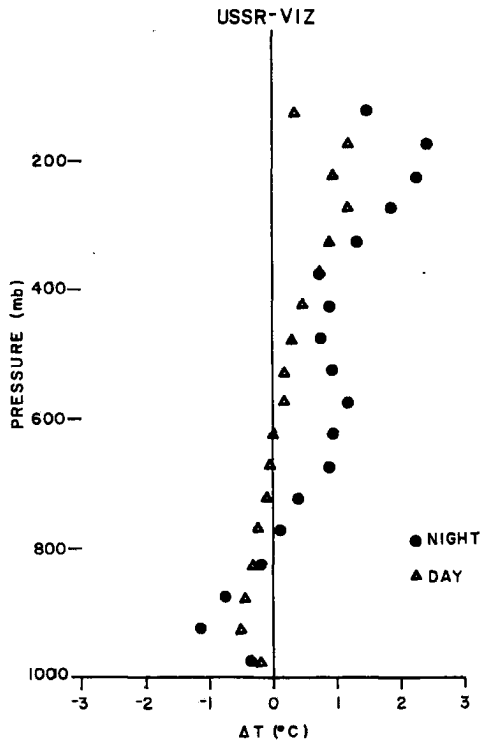


Fig. 52. Comparison of day (29 pairs) and night (9 pairs) mean temperature differences vs. pressure for the USSR-VIZ comparisons. Soundings from the US, Canada and FRG were combined (from NOAA Technical Report EDS 20, p. 45).

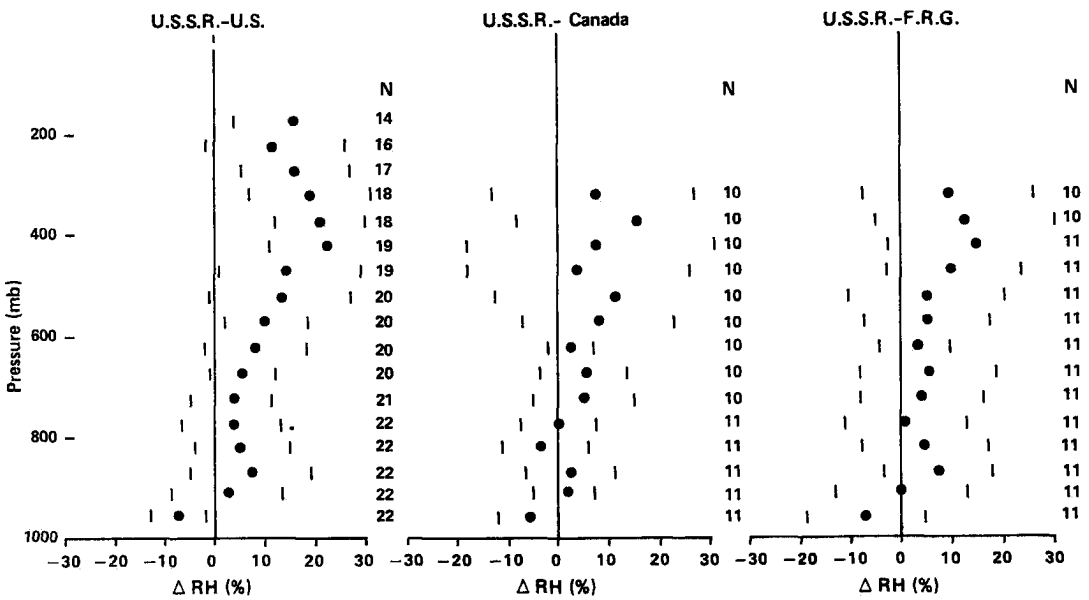


Fig. 53. Means and standard deviations of the relative humidity differences vs. pressure for the USSR-US, USSR-Canada, and USSR-FRG comparisons (from NOAA Technical Report EDS 20, p. 43).

# APPENDIX B

## AREA COVERAGE OF SATELLITE DATA COLLECTED IN SUPPORT OF GATE

During GATE, two GCF sectorizers were dedicated to the acquisition and recording of digital VISSR data from the SMS. Because of the tremendous volume of high resolution digital visible data available for a single image, the sectorizers were able to record visible data for only two smaller subsets of the full image area, while all of the lower resolution IR data were collected. Thus, during daylight (0800-1900 GMT), each image consisted of infrared data for the full disk and visible data for two sectors, a small sector with ½ mi resolution covering the A/B-scale array, and a larger sector with a 2 mi resolution. From the 4-25 July, a sector with 1 mi rather than ½ mi resolution was taken (to reduce the effect of satellite motions). See Fig. 54 for areal coverage of the various sectors.

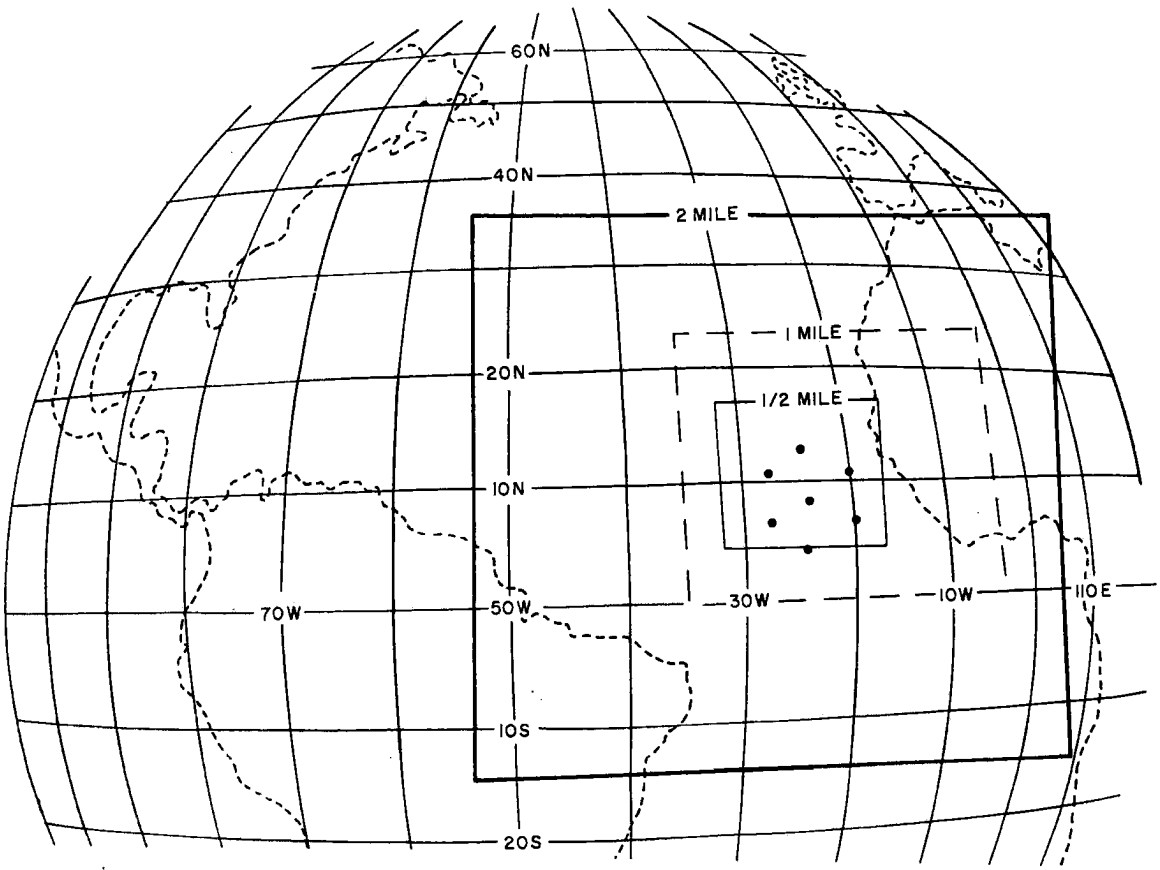


Fig. 54. Approximate area covered by SMS ½ mi, 1 mi and 2 mi resolution visible pictures, superimposed on sketch of full disc infrared picture. The A/B-scale hexagon is shown. (From Field Phase Report for GATE Convection Subprogramme.)

# APPENDIX C

## MASS-BALANCING OF WIND DATA

Mass-balancing is a procedure undertaken when working with wind data to ensure conservation of mass in a vertical column; the same amount of mass flowing into a volume must also flow out. This means that the vertical velocities at the surface ($\omega_o$) and at the upper boundary of the column ($\omega_t$) should both be 0. When vertical velocities are computed kinematically using rawinsonde wind data, this condition is usually not quite satisfied; a vertical integration up from the surface will show a residual vertical velocity amount at the top. Therefore, this excess vertical motion must be distributed in some fashion over the vertical column, and corresponding adjustments made to the wind values.

Various schemes may be employed to achieve mass-balance. Quite frequently a correction value constant with height is applied. Thus, all the vertical wind values will be either reduced or increased by a constant amount. Another technique commonly used is one where the correction value varies linearly with height. See Fig. 55 for an example of the linear correction scheme applied to the B-scale winds in this study. This technique is best applied where wind measurement errors likely increase as a linear function of height. A scheme of this sort is described in more detail in O'Brien (1970).

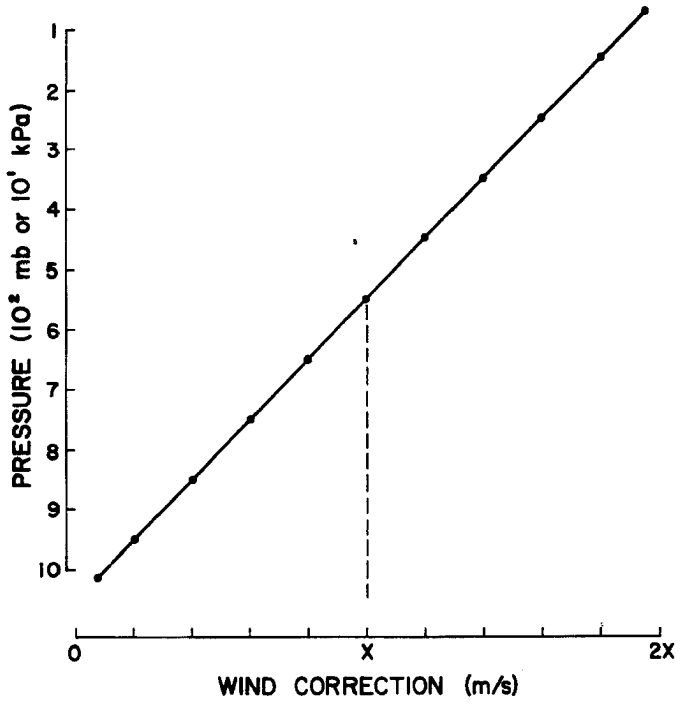


Fig. 55. Magnitude of correction added to the B-scale radial winds at each vertical level. The magnitude of X is such that the resultant vertical velocity equals zero at the surface and at 100 mb.

W. M. GRAY'S FEDERALLY SUPPORTED RESEARCH PROJECT REPORTS SINCE 1967 (cont'd)

| CSU Dept. of Atmos. Sci. Report No. | Report Title, Author, Date, Agency Support |
|---|---|
| - - | Tropical Cyclone Genesis in the Western North Pacific (66 pp). W. M. Gray. March 1975. U.S. Navy Environmental Prediction Research Facility Report. Technical Paper No. 16-75. (Available from the US Navy, Monterey, CA). Navy Support. |
| 241 | Tropical Cyclone Motion and Surrounding Parameter Relationships (105 pp). J. E. George. December 1975. NOAA Support. |
| 243 | Diurnal Variation of Oceanic Deep Cumulus Convection, Paper I: Observational Evidence, Paper II: Physical Hypothesis (106 pp). R. W. Jacobson, Jr. and W. M. Gray. February 1976. NOAA-NESS Support. |
| 257 | Data Summary of NOAA's Hurricane Inner-Core Radial Leg Flight Penetrations 1957-1967, 1969 (245 pp). W. M. Gray and D. J. Shea. October 1976. NSF and NOAA Support. |
| 258 | The Structure and Energetics of the Tropical Cyclone (180 pp). W. M. Frank. October 1976. NOAA-NHEML and NOAA-NESS and NSF Support. |
| Unnumbered | Severe Thunderstorm Wind Gusts (81 pp). G. W. Walters. December 1976. NSF Support. |
| 262 | Diurnal Variation of the Tropospheric Energy Budget (141 pp). G. S. Foltz. November 1976. NSF Support. |
| - - | Tropical Cyclone Research by Data Compositing (70 pp). W. M. Gray and W. M. Frank. July 1977. Naval Environmental Prediction Research Facility, Monterey, CA. NEPRF Technical Report TR-77-01. Navy Support. |
| 274 | Comparison of Developing vs. Non-developing Tropical Disturbances (81 pp). S. L. Erickson. July 1977. U. S. Army Support. |
| 277 | Tropical Cyclone Cloud and Intensity Relationships (154 pp). C. P. Arnold. November 1977. U.S. Army and NHEML Support. |
| - - | New Results of Tropical Cyclone Research from Observational Analysis (106 pp). W. M. Gray and W. M. Frank. June 1978. Naval Environmental Prediction Research Facility, Monterey, CA. NEPRF Technical Report TR-78-01. Navy Support. |

W. M. GRAY'S FEDERALLY SUPPORTED RESEARCH PROJECT REPORTS SINCE 1967 (cont'd)

| CSU Dept. of Atmos. Sci. Report No. | Report Title, Author, Date, Agency Support |
|---|---|
| 188 | Cumulus Convection and Larger-Scale Circulation, Part I: A Parametric Model of Cumulus Convection (100 pp). R. E. Lopez. June 1972. NSF Support. |
| 189 | Cumulus Convection and Larger-Scale Circulations, Part II: Cumulus and Meso-scale Interactions (63 pp). R. E. Lopez. June 1972. NSF Support. |
| 190 | Cumulus Convection and Larger-Scale Circulations, Part III: Broadscale and Meso-scale Considerations (80 pp). W. M. Gray. July 1972. NOAA-NESS Support. |
| 195 | Characteristics of Carbon Black Dust as a Tropospheric Heat Source for Weather Modification (55 pp). W. M. Frank. January 1973. NSF Support. |
| 196 | Feasibility of Beneficial Hurricane Modification by Carbon Black Seeding (130 pp). W. M. Gray. April 1973. NOAA Support. |
| 199 | Variability of Planetary Boundary Layer Winds (157 pp). L. R. Hoxit. May 1973. NSF Support. |
| 200 | Hurricane Spawned Tornadoes (57 pp). D. J. Novlan. May 1973. NOAA and NSF Support. |
| 212 | A Study of Tornado Proximity Data and an Observationally Derived Model of Tornado Genesis (101 pp). R. Maddox. November 1973. NOAA Support. |
| 219 | Analysis of Satellite Observed Tropical Cloud Clusters (91 pp). E. Ruprecht and W. M. Gray. May 1974. NOAA-NESS Support. |
| 224 | Precipitation Characteristics in the Northeast Brazil Dry Region (56 pp). R. P. L. Ramos. May 1974. NSF Support. |
| 225 | Weather Modification through Carbon Dust Absorption of Solar Energy (190 pp). W. M. Gray, W. M. Frank, M. L. Corrin and C. A. Stokes. July 1974. |
| 234 | Tropical Cyclone Genesis (121 pp). W. M. Gray. March 1975. NSF Support. |

W. M. GRAY'S FEDERALLY SUPPORTED RESEARCH PROJECT REPORTS SINCE 1967

| CSU Dept. of Atmos Sci. Report No. | Report Title, Author, Date, Agency Support |
|---|---|
| 104 | The Mutual Variation of Wind, Shear, and Baroclinicity in the Cumulus Convective Atmosphere of the Hurricane (69 pp). W. M. Gray. February 1967. NSF Support. |
| 114 | Global View of the Origin of Tropical Disturbances and Storms (105 pp). W. M. Gray. October 1967. NSF Support. |
| 116 | A Statistical Study of the Frictional Wind Veering in the Planetary Boundary Layer (57 pp). B. Mendenhall. December 1967. NSF and ESSA Support. |
| 124 | Investigation of the Importance of Cumulus Convection and Ventilation in Early Tropical Storm Development (88 pp). R. Lopez. June 1968. ESSA Satellite Laboratory Support. |
| Unnumbered | Role of Angular Momentum Transports in Tropical Storm Dissipation over Tropical Oceans (46 pp). R. F. Wachtmann. December 1968. NSF and ESSA Support. |
| Unnumbered | Monthly Climatological Wind Fields Associated with Tropical Storm Genesis in the West Indies (34 pp). J. W. Sartor. December 1968. NSF Support. |
| 140 | Characteristics of the Tornado Environment as Deduced from Proximity Soundings (55 pp). T. G. Wills. June 1969. NOAA and NSF Support. |
| 161 | Statistical Analysis of Trade Wind Cloud Clusters of the Western North Pacific (80 pp). K. Williams. June 1970. ESSA Satellite Laboratory Support. |
| - - | A Climatology of Tropical Cyclones and Disturbances of the Western Pacific with a Suggested Theory for Their Genesis/Maintenance (225 pp). W. M. Gray. NAVWEARSCHFAC Technical Paper No. 19-70. November 1970. (Available from US Navy, Monterey, CA). U.S. Navy Support. |
| 179 | A Diagnostic Study of the Planetary Boundary Layer over the Oceans (95 pp). W. M. Gray. February 1972. Navy and NSF Support. |
| 182 | The Structure and Dynamics of the Hurricane's Inner Core Area (105 pp). D. J. Shea. April 1972. NOAA and NSF Support. |